Development of biochar based electrode for enhanced removal of Chemical Oxygen Demand (COD) from synthetic wastewater using electrochemical treatment

Awet Hadish Gediwon

A Thesis Submitted to Chemical Engineering Department,

School of Mechanical, Chemical and Materials Engineering

Presented to Partial Fulfillment of the Requirement for the Degree of Masters of Science in Chemical Engineering (Specialization in Process Engineering)

Office of Graduate Studies

Adama Science and Technology University

November 2021

Adama, Ethiopia

Development of biochar based electrode for enhanced removal of Chemical Oxygen Demand (COD) from synthetic wastewater using electrochemical treatment

Awet Hadish Gediwon

Advisors:

Dr. Tatek Temesgen

Dr. Selvakumar Periyasamy

Thesis Submitted to Chemical Engineering,

School of Mechanical, Chemical and Materials Engineering

Presented to Partial Fulfillment of the Requirement for the Degree of Masters of Science in Chemical Engineering (Specialization in Process Engineering)

Office of Graduate Studies

Adama Science and Technology University

November 2021

Adama, Ethiopia

APPROVAL PAGE

We, the advisors of the thesis entitled “Development of biochar based electrode for enhanced removal of Chemical Oxygen Demand (COD) from synthetic wastewater using electrochemical treatment” and developed by Awet Hadish Gediwon, hereby certify that the recommendation and suggestions made by the board of examiners are appropriately incorporated into the final version of the thesis.

Major Advisor	Signature	Date
Co-advisor	Signature	Date

We, the undersigned, members of the Board of Examiners of the thesis by Awet Hadish Gediwon have read and evaluated the thesis entitled “Development of biochar based electrode for enhanced removal of Chemical Oxygen Demand (COD) from synthetic wastewater using electrochemical treatment” and examined the candidate during the open defense. This is, therefore, to certify that the thesis is accepted for partial fulfillment of the requirement of the degree of Master of Science in Chemical Engineering

Chairperson	Signature	Date
Internal Examiner	Signature	Date
External Examiner	Signature	Date

Finally, approval and acceptance of the thesis is contingent upon submission of its final Copy to the Office of Postgraduate Studies (OPGS) through the Department Graduate Council (DGC) and School Graduate Committee (SGC).

Department Head	Signature	Date
School Dean	Signature	Date
Office of Postgraduate Studies, Dean	Signature	Date

DECLARATION

I hereby declare that this Master Thesis entitled “Development of biochar based electrode for enhanced removal of Chemical Oxygen Demand (COD) from synthetic wastewater using electrochemical treatment” is my original work. That is, it has not been submitted for the award of any academic degree, diploma, or certificate in any other university. All sources of materials that are used for this thesis have been duly acknowledged through citation.

_____	_____	_____
Name of the student	Signature	Date

RECOMMENDATION

We, the advisors of this thesis, hereby certify that we have read the revised version of the thesis entitled Development of biochar based electrode for enhanced removal of Chemical Oxygen Demand (COD) from synthetic wastewater using electrochemical treatment" prepared under our guidance by Awet Hadish Gediwon, submitted in partial fulfillment of the requirements for the degree of Masters of Science in Chemical Engineering. Therefore, we recommend the submission of the revised version of the thesis to the department following the applicable procedures.

_____	_____	_____
Major advisor	Signature	Date
_____	_____	_____
Co-advisor	Signature	Date

ACKNOWLEDGMENT

First of all, I would like to thank and praise my GOD for completing my thesis research work. I am heartily thankful to my advisor Dr. Tatek Temesgen, for his valuable support, giving intellectual freedom in my work, tireless advising, engaging me in new ideas and demanding a high quality of work, kindness, positive criticism, advising throughout the present research work, continuous encouragement and guidance. I am also very grateful to my co-advisor, Dr. Selvakumar Periyasamy, for his encouragement, endless help, and valuable guidance throughout this research.

I also extend my sincere thankfulness to the laboratory technicians of the School of Mechanical, Chemical and Materials Engineering at the Department of Chemical Engineering to Mr. Bundi Roba, at the Department of Material Engineering to Demeke Tesfaye and Mr. Ermiyas, and Department of Biology to Mr. Eticha Abdisa and Mr. Yonas at Addis Ababa University for their support to experimental works. I would also like to express my deepest gratitude towards my family and parents for their unstoppable support and offer help to attain this thesis that they stay in my side. My honest thankfulness also goes to my classmates for their encouragement, motivation in discussions and ideas throughout my research work.

I am also grateful to Adama Science and Technology University (ASTU) for providing me with this chance as well as financial help for my Master's Thesis.

ABSTRACT

Wastewater generated from industrial activities and municipals contains a variety of hazardous chemicals dumped to open land and water bodies. These chemicals are just a major source of pollution. Wastewater contains a large amount of COD, which is an organic and inorganic component. This research focuses on the electrochemical elimination of COD from synthetic wastewater utilizing a biochar-based electrode. The bamboo biochar (BBC) production parameters such as chemical activator (KOH, NaOH, H_2SO_4, and H_3PO_4), the percentage composition of activators (30%, 35%, and 40%), carbonization temperature (400, 600, and 900 ^oC) and carbonization time (30, 60, and 90 minutes) were optimized to improve the yield. In the study, 35% KOH/BBC and 30% KOH BBC yielded maximum biochar 29.28% and 27.51%, respectively, at 600 ^oC for 1-hour pyrolysis. MnO_2 coating brings significant changes in the biochar as per FTIR, XRD, and SEM results. Electrode prepared from 35% KOH/BBC with and without coating 0.01, 0.1, and 0.2 M MnO_2 was characterized by cyclic voltammetry. 0.01 M MnO_2/35% KOH BBC prepared electrode brings rectangular like CV profile, mostly seen in ideal electrodes. Additionally, 75 F/g specific capacitance and higher surface area are indications of good electrode performance features also occur. A high energy density of 5.1266 Wh/kg and power density of 615.192 W/kg was also achieved in 0.01 M MnO_2/35% KOH BBC-based electrode. The reason for maximum electrode performance at lower MnO_2 is that excess manganese lowers the conductivity due to its low conductivity nature. Electrochemical synthetic wastewater treatment was investigated with a series of batch experiments at NaCl electrolyte concentration (1–2 g/L); current densities (7.06-11.76 mA/cm^2) and 10 V for 2 hour contact time were performed for the effective treatment using the prepared electrode. A higher removal of COD 76.57% was achieved at 2 g/L NaCl and 11.76 mA/cm^2 of current density. Here, 3.76 kWh/kg COD of minimum energy consumption at 2 g/L NaCl salt and current density of 7.06 mA/cm^2 resulted. The use of an electrochemical treatment that combined biochar with a manganese oxide electrode resulted in improved electrochemical properties, which aided in reducing COD from glucose synthetic wastewater.

***Keywords**: Synthetic wastewater, bamboo, MnO_2, biochar electrode, cyclic voltammetry, electrochemical treatment.*

TABLE OF CONTENTS

LIST OF TABLES

LIST OF FIGURES

ACRONYMS AND ABBRIVATIONS

AOP- Advanced oxidation process

BBC- Bamboo biochar

BOD- Biological Oxygen Demand

CDI- Capacitive deionization

COD- Chemical Oxygen Demand

CV- Cyclic Voltammetry

EAOP- Electrochemical Advanced Oxidation Process

EDLC- Electrochemical double layer capacitor

FTIR- Fourier transform infrared spectroscopy

MnO_2- Manganese dioxide

MnO_2/KOH BBC- Manganese oxide coated on activated bamboo biochar

SEM- Scanning electron microscope

TDS- Total Dissolved Solids

TMO- Transitional metal oxide

XRD- X-ray Diffraction

CHAPTER ONE

1. INTRODUCTION

1.1. Background of the study

A constant supply of clean water is necessary to build and implement a wide range of human activities (Seow et al., 2012). Even though it is easy to guess that industries are the leading economic sectors in many countries, due to the hazardous effluents generation, consider them source of pollution to the ecosystem (Yaqub et al., 2012; Bakhtiari et al., 2017). Because these effluents cannot be completely degraded, they are dumped on the ground and poured into surface water, where they eventually leak into ground water, infecting it. Water is used in a variety of ways, including agriculture, household, industrial and recreational activities. The naturally available water is misused and poisoned by these operations' effluents (Bhagawan et al., 2018). The substances that cause pathogenic and hazardous compounds are found in massive quantities in wastewater (Ashish Chauhan, 2015; Bakhtiari et al., 2017). In humans, exposure to industrial chemicals has the potential to cause disability, cancer, and death (H. Jiang et al., 2016). Toxics damage human health when pesticides handled in an unprofessional and unprotected way (Seow et al., 2012; Yaqub et al., 2012; Nur-E-Alam et al., 2017). Variable pH, high suspended particle concentrations, BOD, COD, and other components distinguish wastewater generated by industrial activity, households, and other sources (Ashish Chauhan, 2015; Birhanie et al., 2017; Bhagawan et al., 2018). These contaminants cause a huge problem due to incomplete or partial treatment.

Wastewater contains a high COD concentration that reflects the total organic content of wastewater (Ashish Chauhan, 2015; Bakhtiari et al., 2017; Nur-E-Alam et al., 2017). It has inherent deficiencies because it covers biodegradable organics and biologically resistant and refractory compounds, i.e., it provides no information on significant organic fractions with different biodegradation kinetics. Effluent is composed of biodegradable sections made up of various fractions with different biodegradation rates, as well as inert COD fractions that have a significant impact on treatment efficiency (Ashish Chauhan, 2015; Sivagami et al., 2018). A significant decontamination method for COD could enhance the availability of fresh water and

solve environmental problems associated with wastewater. Especially in developing countries, due to the lack of awareness and advanced technologies, wastewater has a significant impact on humans' lives and environmental concerns because of the large volume of wastewater discharged. The production process creates a major environmental burden (Seow et al., 2012; Yaqub et al., 2012). Thus, for developing countries like Ethiopia development of new efficient and sustainable technologies is expected to be critical in resolving the issues.

Wastewater treatment is becoming an essential part of industrial manufacturing operations in the production process (Nur-E-Alam et al., 2017; Bhagawan et al., 2018). Various physical, chemical, and biological techniques were applied to treat water effluents. Chemical precipitation, filtration, biological mechanism, ion exchange, electrocoagulation, and membrane separation are generally used. Cost, practicability, sludge production, the extent of organic matter removal, and potentially harmful byproducts formation are all limits that each process faces. Because of the wide range of biocides used in industries to combat fungal attacks, biological treatment of wastewater may be problematic (Yaqub et al., 2012; Bakhtiari et al., 2017). Due to the complicated composition of effluents produced from different sides and the major environmental and technological issues that this industry poses, the development of appropriate treatment solutions for these effluents is critical.

The oxidation process generates hydroxyl radical, a powerful and non - selective oxidant for mineralization or degradation of these recalcitrant organic pollutants present in effluent (Ashish Chauhan, 2015). O_3, H_2O_2, UV-radiation, hydroxyl radicals are the most popular in hunting pollutants. The high energy consumption and requirement of chemicals producing undesired ion formation make to find other effective methods. The electrochemical mineralization of organic pollutants is a relatively new technology consisting of electrolytic cells having two electrodes; anode and cathode, immersed in an electrically conducting solution and connected via an electrical circuit. The cathode and anode configuration and materials redox reaction is the mechanism to remove pollutants with low power and energy demands (Bhagawan et al., 2018). Electrochemical shows incredible decontaminating pollutants from wastewater which can be used as a significant method of treatment electrode materials used as anode and cathode form mineral ore have some limitations like toxicity, high cost, non-renewable which needs to be solved to sustain the environment and resources (Chaplin, 2014).

Biomass resources are the best alternatives to non-renewable energy sources (Fujishige et al., 2017). Biochar is a carbon-rich solid substance obtained from biomass via pyrolysis, a thermochemical process (Sahoo et al., 2021). Biochar owns the high surface area, physicochemical stability, high energy and power density, high porosity, and catalytic activity due to the increase of micro-pore volume caused by the removal of volatile organic compounds at high temperature, high content of organic carbon, and low susceptibility to degradation (Qu et al., 2015; C. Liu et al., 2020). Chemical activation increases the property of biochar in creating pores, increasing surface area, increasing yield, and other significant factors. Chemical activators such as KOH (Qu et al., 2015; N. Zhao et al., 2017; Sajjadi et al., 2019; Qanytah et al., 2020; W. Chen et al., 2020), NaOH (Q. S. Liu et al., 2010; Sajjadi et al., 2019), H_2SO_4 (Ahmad & Hameed, 2009; Qu et al., 2015), H_3PO_4 (J. Jiang et al., 201; Ji Zhang et al., 2017; F. Cheng & Li, 2018), $ZnCl_2$ (C. Liu et al., 2020), Fe_3O_4 (Du et al., 2020) and others (Ahmad & Hameed, 2009; Y. Cheng et al., 2019), have been widely used in many biochar activations. Biochar has been applied in soil amendment products, climate change mitigation, wastewater treatment, energy storage, catalyst degradation (Qu et al., 2015; Yuan et al., 2016). Various biomasses used in biochar production for different applications are like rice husk (Yuan et al., 2016), coconut shell (Frolova & Kharytonov, 2019; Elisadiki & King'ondu, 2020), bamboo (Qu et al., 2015; Yuan et al., 2016; W. Chen et al., 2020; Rafique et al., 2021), coniferous wood (Frolova & Kharytonov, 2019), corncob (Ghani et al., 2016; Qanytah et al., 2020), corn straw (N. Zhao et al., 2017), infested ash tree (Kouchachvili & Entchev, 2017), Jackfruit peel waste (Jothi Ramalingam et al., 2020), jujube wood waste (Rafique et al., 2021), pea protein (Demir et al., 2018), palm kernel shell (Ghani et al., 2016), walnut shell (C. Liu et al., 2020), red cedar (J. Jiang et al., 2013) and red oak (Du et al., 2020) are the few. Bamboo made up of chemical components such as hemicellulose, cellulose, and lignin, making up more than 90% of total mass, shows incredible biochar properties. The bamboo fibers own unique ultra-hierarchical structures (Gezahegn, 2020). Bamboo is among the fastest-growing plants, with most species reaching maturity within five years growing in various climates.

Biochar has been used for electrode purposes because of its attractive characteristics (Fujishige et al., 2017). These electrode materials are referred to as ideal electrodes because they have virtually perfect catalytic activity, thermal and mechanical stability, and electrical conductivity

(H. Lyu et al., 2019). Energy storage, capacitance deionization (CDI), and other applications have all made use of biochar electrode materials. CDI uses a biochar electrode with a capacitance storing property to adsorb ions from a water sample by providing an electric potential to the electrodes' surface during the adsorption/desorption process. Adsorption examines the connection between positive and negative ions. At the same time, desorption describes how ions near the surface (before applying the charge) begin to be ejected due to the same charge sign as the surface charge grows up (Hashem et al., 2020). CDI in most studies has been applied mostly in desalinating salty water solutions (Zhuang et al., 2020).

EDLC, a substitute name for CDI, is an energy-storing supercapacitor technique that improves capacitance by accumulating charges or ions at the electrode/electrolyte interface (Yong Zhang et al., 2015). While most biochar-based electrodes have a lower capacitance, they are less effective in CDI. Most studies indicate transitional metal oxide (TMO) as a source to compensate for bio char electrodes' low specific capacitance (Karnan et al., 2017; G/cherkos, 2019). When coupled with carbon-based materials, TMOs produced from reversible and quick faradaic processes improve electrochemical performance synergistically (Elisadiki & King'ondu, 2020). Oxidation of organic pollutants is done by intermediacy of hydroxyl radicals electro-generated from water on high oxidation power anode and active ions from the biochar adsorption when potential is applied (Agnieszka Kapałka, Helmut Baltruschat, 2011). Hydroxyl radical can also be generated by applying electrolysis process electrochemically. It is done by electrolytic discharge of water at potential. The electrochemical oxidation of organic compound by electrogenerated OH radical then takes place near anode surface (C. Zhang et al., 2018).

Low conductivity and specific surface area, as well as poor intrinsic conductivity, describe TMO. As an electrode material, a hybrid of TMO and bio chars affords excellent electrochemical performance (Karnan et al., 2017; Gezahegn, 2020). MnO_2 has emerged as an excellent faradaic material. It can be used as an alternative TMO due to its good environmental compatibility, high theoretical specific capacity of 1370 F/g, extended operating potential, and cost-effectiveness (B. H. Cheng et al., 2017). When MnO_2 is used in a CDI, its high capacitance helps with charge transfer (Zhuang et al., 2020).

There is no work reported on treatment of synthetic wastewater containing COD using biochar composite with MnO_2 based working electrodes. Thus, the research focuses on the development of working electrodes from bamboo biochar to treat synthetic wastewater. For this, bamboo

biochar was produced by activating KOH, H_2SO_4, NaOH, and H_3PO_4 at different chemical compositions, carbonization temperatures, and times. Then, the biochar with high yield was coated with MnO_2 to prepare the working electrode. The electrode was prepared by making with a mold having a conical shape in the presence of chlorinated rubber as binder and toluene solvent. The function of MnO_2 was to increase the charge storing capacity of the electrode. COD containing synthetic wastewater was treated using prepared electrode in electrochemical setup.

1.2. Statement of Problems

The importance of water to life on earth cannot be underestimated. Because sufficient water is required for agriculture, human consumption, and industry, urban and industrial activities have polluted the environment that should be treated or at least minimized. Chemicals used in different processing activities pollute the environment when discharged with wastewater that has not been treated or only partially treated. The reduction of available freshwater has harmed one-sixth of the world's population (Saad et al., 2020). Wastewater dumped into water bodies offers significant health concerns to downstream consumers and causes ecological degradation in water bodies. This results in a lack of clean water, decreased soil fertility, water pollution, and damage to the lives of aquatic living animals, among other things, making it a serious problem. All these problems are more obvious in developing nations, such as Ethiopia.

In addition to suspended particles, SO_4^{2-}, Cl^-, BOD, and COD, which contains both organic and inorganic waste, is the most polluting component in effluents from different sources. COD contains biodegradable and non-biodegradable components that will be oxidized chemically, which overestimates the biodegradable demand. A high COD value implies that the wastewater is poisonous and that biologically resistant organic compounds are found (Ashish Chauhan, 2015). Numerous treatment procedures were tested to mitigate the dangers, including biological treatment, chemical precipitation, filtration, ion exchange, electrocoagulation, membrane separation, and adsorption. They were not completely utilized because of constraints such as cost, practicability, dependability, stability, environmental impact, sludge formation, operating difficulty, pretreatment requirements, and potentially harmful byproducts release (Chaplin, 2014; Sivagami et al., 2018). Therefore, it is urgently needed to develop cost-effective by determining the energy consumed for each process and efficient treatment technology by increasing research interest using alternative low-cost and effective methods for wastewater treatment.

Biochars inherent properties make it a good electrode material for the electrochemical treatment of wastewater. The rejection of fossil fuel electrodes is based on being easily unavailable and poisonous. When biomass feedstock's can replace fossil fuel bases, these issues will be resolved. Biochar-based electrodes can store energy, reducing energy consumption and making it more cost-effective. The high capacitance of the electrode is obtained when transitional metal oxides are coated with activated biochars. MnO_2 owns high capacitance with low ionic conductivity that hider's high energy storing nature which is the reverse of biochar. To own an electrode possessing high conductivity and capacitance, making biochars with MnO_2 composite would be advisable in addition to its low cost compared to other transitional TMOs. To this effect, the research examines the potential of activated bamboo biochar coated with MnO_2 to be prepared as an electrode material to remove COD from synthetic wastewater.

1.3. Objective

1.3.1. General Objective

The general objective of the research is to develop a bamboo biochar-based anode electrode for enhanced removal of Chemical Oxygen Demand (COD) in synthetic wastewater using electrochemical treatment.

1.3.2. Specific Objectives

- To produce biochar from bamboo biomass under different effects such as chemical activator type, percentage of activators, carbonization temperature and time, and its characterization
- To prepare anode electrode using MnO_2 coated on activated bamboo biochar and its characterization
- To treat synthetic wastewater by electrochemical treatment using the prepared MnO_2/biochar electrode as anode material

1.4. Research Questions

1. At what parameter combination can maximum biochar yield be achieved?
2. Can electrode prepare from MnO_2 coated on activated biochar show better electrochemical property?

3. Is it possible to treat synthetic wastewaters through electrochemical methods using biochar based as an anode electrode?

1.5. Significance of the Study

This research aims to lower the high COD concentration in effluents using a biochar-based electrode from locally accessible bamboo as biochar in an electrochemical process. Environmentally sustainable, low cost, and energy consumption electrochemical approach using bio based electrode is the aim of this study. Biochars are chosen as electrode materials because of their unique properties, such as cost-effectiveness, ease of availability, high porosity, and catalytic activity. Biochars are also non-polluting materials, enabling them to be both ecologically beneficial and cost-effective. The study will assist industries in increasing their interest in using low-cost biomass-based electrodes to reduce pollutants in wastewater discharge to open lands or water bodies, which harms public health and the ecosystem. This research will be used by a variety of organizations, including governmental and nongovernmental groups and researchers working on pollution prevention. As a result, this research will add to the existing understanding of wastewater treatment with biochar-based electrode materials. This treatment technique demonstrates the viability of capacitive electrode materials in lowering energy usage.

1.6. Scope of the Study

This research was based on a laboratory experiment that used an electrochemical treatment with a bamboo-activated biochar-based electrode to minimize COD from synthetic wastewater. First, the effect of four variables was studied for bamboo biochar production: chemical activator, chemical activator percentage, carbonization temperature, and carbonization time. Following that, MnO_2 activated bamboo biochar composite with maximum yield biochar was conducted. Biochar paste working electrode was made using activated bamboo biochar/MnO_2, and its performance was examined by CV. Characterization of raw bamboo, activated bamboo biochar, and MnO_2 biochar was conducted XRD, FTIR, and SEM were studied. To test the removal effectiveness of COD, synthetic wastewater was prepared and then treated using an electrochemical mechanism with a prepared working electrode as the anode. The COD level of treated synthetic wastewater was detected using an open reflux titration method, and energy consumption for the treatments were also performed.

CHAPTER TWO

2. LITERATURE REVIEW

2.1. Introduction

Environmental contamination, which results from the expansion of modern industrial activities, is one of the continent's most pressing issues. Most industrialists attempt to discharge their wastewater effluents, which are either improperly treated or completely untreated, directly into rivers or nearby water bodies, as well as land, without regard for the potential for harm to the local community (Seow et al., 2012; Nur-E-Alam et al., 2017). Despite the importance of the world economy, the processing industry has become one of the biggest sources of environmental pollution due to wastewater discharge (Yaqub et al., 2012; Ashish Chauhan, 2015). It is also observed that wastewaters have COD and suspended solid contents approximately five times higher than municipal wastewaters (Yaqub et al., 2012). In most industrial activities high amount of fresh water used for processing is designated as water composed of toxic chemicals, chemicals applied for a specific purpose, posing major environmental issues (Ashish Chauhan, 2015; Bakhtiari et al., 2017).

2.2. Industrial and Municipal Wastewater Features

Water effluent is a severe pollutant with organic load, inorganic matter, chromium, suspended particles, ammoniacal nitrogen, sulfide, chloride, and other toxins derived from different processing activities (Seow et al., 2012; Bhagawan et al., 2018). Thus, wastewater has a profound impact on the environment because it creates a threat to the aquatic environment and human health (Bakhtiari et al., 2017; Bhagawan et al., 2018). Wastewater contains a diverse range of elements and physicochemical features (Bakhtiari et al., 2017). The wide variation of wastewater composition is presented in Table 2.1.

2.2.1. Organic Loads

wastewater contains a complex mixture of biogenic matter from the hides and a wide range of organic compounds added during the specific process, as well as high amounts of dissolved organic matter and suspended particulates (Seow et al., 2012). It contains pesticides, dung,

proteins in solution and suspension, animal fats, lipids, and other constituents are all forms of organic matter (Birhanie et al., 2017).

COD is a useful parameter that reflects the total organic content of wastewater (Haixiu Chen et al., 2019). But, it has inherent deficiencies because it covers biodegradable organics and biologically resistant and refractory compounds, i.e., it provides no information on significant organic fractions with different biodegradation kinetics. Despite this, some information about the different forms of the organic load was collected in the literature. According to studies, wastewaters contain biodegradable sections made up of various fractions with different biodegradation rates and inert COD fractions that have a significant impact on treatment efficiency (Seow et al., 2012). Thus, BOD is a controversial parameter if applied to wastewater since the wastewater contains many inhibitors. (Bhagawan et al., 2018; Moradi et al., 2020) reported the maximum discharging limit of COD is 500 mg/L in Ethiopia.

Table 2-1: Industry wastewater composition according to different literature references

pH	**BOD_5**	**COD**	**TDS**	**Cl^-**	**Ref.**
9.0	-	17600	6900	1,200	(Deepa et al., 2021)
3.4-3.7	-	5250-9600	38200-39400	26513-31103	(Genawi et al., 2020)
-	11000-25000	3000-6000	22000-33000	15000-30000	(Sundarapandiyan et al., 2010)
3.7-4.3	528	9922-10180	1800-1950	1239	(Isarain-Chávez et al., 2014)
2.4	-	2370	-	-	(Costa et al., 2010)
8.67	3120.6	7273	-	-	(Alemu et al., 2019)
7.8-8.8	150-250	1500-2500	3000-5000	1360-1740	(Sivagami et al., 2018)
12	4050	12600	-	13250	(Sawalha et al., 2020)
4.42	-	-	4831	2411	(Mani Tripathi & Chaurasia, 2020)

Note: except pH all terms are in mg/L.

2.3. Environmental Impacts

Wastewater entails that it brings unavoidable costs and challenges in terms of air and water pollution and general degradation of the natural environment. It has a significant negative influence on water, soil, and atmospheric systems. The presence of organic pollutants and increased levels of heavy metals in wastewater influences water bodies (Seow et al., 2012; Ashish Chauhan, 2015). Most of the organic matter generated from leather processing is not biodegradable (Nur-E-Alam et al., 2017)**.** These effluents are released on the land as well as dumped into surface water which ultimately leaches to ground water and leads to contamination due to the accumulation of toxic metallic components known as toxic or carcinogenic. This resulted in a series of well-documented problems in living things because they cannot be completely degraded becoming more complex and critical to the ecosystem (Seow et al., 2012; Birhanie et al., 2017).

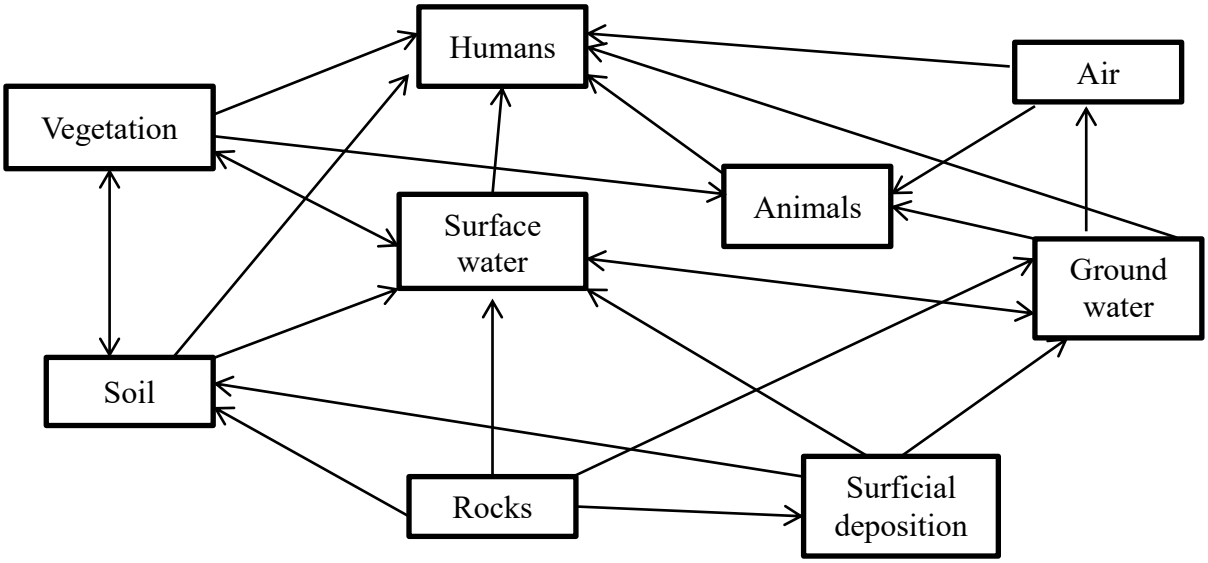

Figure 2-1: Wastewater affecting areas adapted from (Nur-E-Alam et al., 2017)

2.4 Treatment Methods

A great concern has been applied to the increasing environmental problem of tannery wastewater contaminating surface water, groundwater, and soil (Seow et al., 2012). Enormous treatment technologies have been developed for the removal of contaminants. Most of the heavy metal ions are toxic to living organisms, non-degradable, and are persistent in the environment; therefore, elimination of them from wastewater is important to protect public health (Seow et al., 2012; Kuppusamy et al., 2017)**.** Electrochemical precipitation, chemical reduction, solvent extraction,

chemical precipitation, coagulation, ion exchange, electro-dialysis, evaporation, reverse osmosis, and adsorption will be reviewed below as methods for removing pollutants from wastewater.

2.4.1 Biological Treatment

Biological treatment is commonly used to remove organics and nitrogenous matter of waste water, which contributes to high concentrations of BOD value by using microorganisms using both aerobic and anaerobic processes**.** Biological techniques are frequently utilized to reduce organic content in industrial effluents, usually following mechanical and physicochemical processing (Du et al., 2020). Even though these systems are simple, they occupy a large land area. The efficiency of the systems is affected due to; poor mixing of water and active biomass, sulfides inhibition, and low COD loading rates (Nur-E-Alam et al., 2017).

The biological process is often inefficient and inadequate to remove pollutants completely, besides being time-consuming (Du et al., 2020). It has a low biodegradability because some microorganisms' ability to break down certain pollutants is limited, preventing the complete removal of these chemicals by a conventional biological process (Bashir et al., 2009; Costa et al., 2010; Kuppusamy et al., 2017). In addition, traditional physical-chemical processes are comparatively expensive and may lead to secondary pollution. This is because it needs additional chemicals to completely treat (Seow et al., 2012). Wastewater treatment by biological processes may be difficult because of the presence of a broad spectrum of biocides used in the leather industry to prevent fungal attacks (Yaqub et al., 2012).

2.4.2 Chemical Coagulation

Electrocoagulation has shown to be an intriguing technology for turbidity removal, decolorizing colors, and breaking up emulsion-based wastes. Since it is a pretreatment rather than a final treatment, it is hugely helpful for the coarse removal of pollution (Hoislbauer & Siebenhofer, 2008). Coagulation occurs when charged particles in colloidal suspension are neutralized by counter-ions through mutual interaction, resulting in the formation of agglomerates and sedimentation (Mohammed & Dabai, 2020). Destabilization, followed by coagulation, flocculation, and sedimentation, can be achieved by cations that interact specifically with negative colloids to neutralize their charge. The process consists of rapid dispersal of a coagulant by rapid mixing, followed by slow mix and sedimentation (Mohammed & Dabai, 2020).

Due to the large organic load in the wastewater business, coagulation-flocculation is vital. Pre-treatment using coagulation, flocculation, and sedimentation remove a significant part of contaminants. The main limits of coagulation are the production of sludge, the need for continuous chemicals, and the transfer of dangerous components into the solid phase for disposal (Bashir et al., 2009; Seow et al., 2012; Nur-E-Alam et al., 2017).

2.4.3 Chemical Precipitation

Precipitation is a chemical reaction in which dissolved and suspended ions are converted into insoluble solids. This conversion from metal ions to insoluble solid is accelerated by precipitating agents such as lime and magnesia. It is a successful means of removing chromium from wastewater. It's a straightforward, low-cost, convenient, and secure solution. However, this method necessitates the use of a lot of chemicals, and it results in a lot of harmful sludge. Filtration and disposal of sludge add to the overall cost of the process (Nur-E-Alam et al., 2017).

2.4.4 Ion-exchange

Ion exchange involves substituting mobile ions from the solution of interest for electrostatically attached ions to the functional groups in a sample. Whether they exchange positive or negative charges is classed as cationic or anionic (Mohammed & Dabai, 2020). Acidic functional groups, such as sulphonic groups, are found in cation exchange resins, whereas basic functional groups, such as amine, are found in anion exchange resins. Organics and other particles in effluents often foul this mechanism, finding it incapable of handling concentrated metal solutions. Ion exchange is also nonselective and exceedingly sensitive to the pH of the solution and expensive (C. Zhao & Chen, 2019).

2.4.5 Membrane Process

The membrane can remove organic compounds and inorganic pollutants for the treatment of effluents. Reverse osmosis is an important membrane technology in the treatment of wastewater.

2.4.5.1. Reverse Osmosis (RO)

RO is the opposite of natural osmosis, and it works by forcing pressured water across a semi-permeable membrane. Water moves from a weaker saline solution to a stronger saline solution by osmosis, and a semi-permeable membrane gradually separates the two solutions until they are

equal. Water is permitted to pass through a semi-permeable membrane from a stronger saline solution to a weaker solution. Because salt molecules are bigger than water, the membrane prevents salt particles from passing through (C. Zhao & Chen, 2019). Reverse osmosis has several disadvantages, including 2-4 gallons of water flushed down the drain every gallon of filtered water produced, limited flow rates, high-pressure inflow need, membrane scaling, and high installation costs (Mohammed & Dabai, 2020).

2.4.6. Advanced Oxidation (AOP)

AOP is defined as those which involve the generation of hydroxyl radicals in sufficient quantity to affect water purification. The advanced oxidation process uses high powerful oxidants such as O_3, H_2O_2, UV radiation, hydroxyl radicals, and Fenton oxygen are generated through different techniques. The oxidant radicals (OH and H) are very reactive species and attack the organic molecules with very high rate constants to water, carbon dioxide, and salts (Mohammed & Dabai, 2020). AOP provides a variety of options for oxidant production, allowing for better compliance with treatment regulations (C. Zhao & Chen, 2019). It is efficient in treating industrial effluents that contain degradable organics and effluents that contain refractory organic pollutants, such as extremely toxic and low biodegradable organic pollutants (Chaplin, 2014). This approach has the advantage of being low-cost and requiring little floor space, but its reliability must be enhanced (Seow et al., 2012; Nur-E-Alam et al., 2017; Pokharel, 2020).

2.4.7. Electrochemical Treatment

The electrochemical method for the mineralization of organic pollutants is a relatively new technology and has recently attracted a great deal of attention (Costa et al., 2010). Anode and cathode immersed in an electrically conducting solution and connected via an electrical circuit in the electrochemical treatment method. Removing pollutants with low energy demands depends on the cathode and anode arrangement (Hashem et al., 2020). This method allows for energy recovery by producing fuels at the cathode, which can help to reduce their carbon footprint even more. Electrochemical systems provide various advantages over traditional water treatment technologies, including the capacity to handle a variety of contaminants, modular cell assembly, and energy recovery. Nowadays, it has reached such a state that they are comparable with other

technologies in terms of cost and more efficient and more effective at the industrial level (Hoislbauer & Siebenhofer, 2008).

Pollutants are transformed into non-toxic substances via decomposition into simpler compounds or oxidation form during the oxidation process of waste water, resulting in a significant reduction in BOD, COD, and others. Because it requires no auxiliary chemicals, only electrical energy (electron is the main reagent), is suitable to a wide range of contaminants, does not require high pressures or temperatures, produces no secondary pollutants, and requires little additional equipment and maintenance (Sahoo et al., 2021). The use of electrochemical technology for wastewater treatment is a reasonably easy and clean procedure. Electrochemical waste treatment can result in partial or complete pollution breakdown. The oxidation of organic matter to CO_2 is referred to as complete mineralization. During electrochemical oxidation remediation, organic contaminants are either directly oxidized at the anode or indirectly oxidized by anodically generated oxidants such as Cl_2, OH, and H_2O_2 (Bhagawan et al., 2018). Anodes with a high oxidation potential are required for direct oxidation. Pollutants are adsorbed on the anode surface before eliminating the anodic electron transfer process (Yaqub et al., 2012).

Treated tannery waste water by electrochemical oxidation using RuO_2-IrO_2-TiO_2 anode and titanium mesh electrode as cathode obtained 97% COD reduction was reported in (Kuppusamy et al., 2017). Cu electrode presented higher mineralization than Al to remove contaminants in tannery wastewater (Halilovic et al., 2017). Furthermore, the efficiency of the electrochemical process for the remediation of real effluents can be enhanced by adding ions, not only to yield better electrical current flow but also to provide the electro generation of strong oxidizing agents (electrolytes) like active chlorine species. The electrolyte has an impact on the production of oxidizing species during electrochemical reactions. Sodium sulfate (Na_2SO_4), sodium chloride (NaCl), potassium chloride (KCl), sodium nitrate ($NaNO_3$) and sodium carbonate (Na_2CO_3) are common supporting electrolytes (Sivagami et al., 2018; Abera, 2020; R. Xu et al., 2020).

Table 2-2: Works on the treatment of effluents (COD) via an electrochemical method

Sample type	Electrode	Operation conditions	Removal	Ref.
Synthetic tannery wastewater	Graphite/graphite	Current density: 0.024 A/cm^2, pH: 9 and NaCl electrolyte; 40 g/L	81.03 % COD after 2 h	(Sundarapandiyan et al., 2010)
Tannery wastewater	Ti/Ti	pH: 4, Current density: 100 mA/cm^2	41% COD after 5 h	(Bosnic, M., Buljan, J., Daniels, 2000)
Synthetic tannery wastewater	Si/BDD	0.01 M Na_2SO_4, pH: 2.4, current density: 100 mA/cm^2,	Higher COD after 4 h	(Costa et al., 2010)
Leachate wastewater	Graphite/graphite	Current density: 79.9 mA/cm^2, Na_2SO_4: 1 g/L, Voltage: 30 V	COD–68% after 4 h	(Bashir et al., 2009)
Landfill leachate	BDD/SS	Current density: 45 mA/cm^2, effluent pH, temperature: 20 ^oC	90 % COD after 4 h	(Hoislbauer & Siebenhofer, 2008)
Pulp and paper industry effluent	Fe/Fe	Current density: 4 mA/dm^2, NaCl: 4 g/L, pH: 7, initial COD: 3000 mg/L, inter-electrode distance: 2 cm	95 % COD after 4 h	(Moradi et al., 2020)

Note BDD- boron-doped diamond, SS- stainless steel, COD- chemical oxygen demand, Ti- Titanium, Si- silicon, Fe- iron.

2.4.7.1. Working Principle of Electrochemical Oxidation

In direct oxidation, contaminants in the majority of the wastewater must reach the electrode surface, where the oxidation reaction takes place once they have been adsorbed. The nature of the electrode materials influences the selectivity and efficiency of the oxidation process, and mass transfer becomes an important process. Bulk oxidation includes indirect oxidation methods that necessitate the electrochemical production of a mediator that can then react in the bulk

solution. This mediator is produced at the anode/cathode and is responsible for the oxidation of impurities.

The most common electrochemical indirect agents are Cl_2 and H_2O_2. However, practically any salt in a waste can form oxidants that function in the bulk, so Cl^-, SO_4^{2-}, PO_4^{3-}, and a variety of other salt anions play a part in the electrochemical destruction of organics (Hoislbauer & Siebenhofer, 2008). The production and activity of oxidants is a series of events that occur in all electrolysis and that can be aided by the presence of reagents (Cl_2, O_2) that increase oxidant generation. There is no pure bulk electrochemical process, only an electrochemical process in which the contribution of the bulk process is greater than the contribution of surface processes in the oxidation of organics (Korpe et al., 2019). In bulk operations, one thing to keep in mind is that oxidants created during electrochemical treatments must be considered (Hoislbauer & Siebenhofer, 2008).

At the anode in electrochemical oxidation, there are two types of oxidative mechanisms. For anodes with strong electro catalytic activity, oxidation happens at the electrode surface, which is known as direct electrolysis. On the other hand, oxidation occurs on a metal oxide electrode via a surface mediator on the anodic surface, where they are continually created, and a process known as indirect electrolysis. In indirect electro-oxidation, NaCl or KCl salts are added to the electrolyte to improve conductivity and produce hypochlorite ions. The anodic oxidation is described as follows:

$$2Cl^- \longrightarrow Cl_2 + 2e^- \quad \text{……2.1}$$

$$Cl_2 + H_2O \longrightarrow H^+ + Cl^- + HOCl \quad \text{…….2.2}$$

$$HOCl \longleftarrow H^+ + OCl^- \quad \text{……..2.3}$$

The chlorine that has been freed generates hypochlorous acid, which then dissociates to form a hypochlorite ion. The following is an explanation of the electrochemical conversion/combustion of organics on a noble oxide coated catalytic anode (MOx). With H_2O released at the anode, adsorbed hydroxide radicals are produced.

$$MO_x + H_2O \longrightarrow MO_x(^{\cdot}OH) + H^+ + e^- \quad \text{……2.4}$$

The adsorbed hydroxyl radicals interact with the oxygen already present in the oxide anode, potentially causing oxygen to transfer from the adsorbed hydroxyl radical to the oxide, leading to the formation of the higher oxide MOx+1.

$$MO_x(\cdot OH) \longrightarrow MO_{x+1} + H^+ + e^- \quad \text{.....2.5}$$

Active oxygen can exist at the anode surface in two forms: physisorbed adsorbed hydroxyl radicals (•OH) or chemisorbed (oxygen in the lattice, MOx+1). Cl^- ion combines with MO (•OH) to create adsorbed OCl^- radicals when NaCl is used as a supporting electrolyte, as shown below.

$$MO_x(\cdot OH) + Cl^- \longrightarrow MO_x(\cdot OCl) + H^+ + 2e^- \quad \text{.....2.6}$$

The MOx (•OCl) interacts with the Cl ion to produce active oxygen (dioxide) and chlorine in the reactions below:

$$MO_x(\cdot OCl) + Cl^- \longrightarrow MO_{x+1} + Cl_2 + e^- \quad \text{.....2.7}$$

$$MO_x(\cdot OCl) + Cl^- \longrightarrow MO_x + \tfrac{1}{2} O_2 + Cl_2 + e^- \quad \text{.....2.8}$$

In the pollutant degradation process, the produced hypochlorite ions serve as a primary oxidizing agent. The organic matter in the effluent reacts with OCl^- to produce CO_2 and water, i.e.

$$\text{Organics} + OCl^- \longrightarrow CO_2 + H_2O + Cl^- \quad \text{.....2.9}$$

The rate of electro-oxidation of organic pollutants is determined by the anode's catalytic activity, the diffusion rate of organic compounds in the active sites of the anode, and the applied current density. The following side reactions can take place during the electrochemical production of hypochlorite ions. When hypochlorite ions reach a saturation level, chlorate can be produced chemically or electrochemically.

$$2HClO + ClO^- \longrightarrow ClO_3 + 2H^+ + 2Cl^- \quad \text{..... 2.10}$$

$$6ClO^- + 2H_2O \longrightarrow 2ClO_3 + 6H^+ + 4Cl^- + \tfrac{1}{2} O_2 + 6e^- \quad \text{.....2.11}$$

To improve oxidation efficiency, side reactions should be controlled. The pseudo-steady-state theory can be applied to each of the intermediate products in the bulk solution (HOCl and OCl) (Abera, 2020). Even though electrochemical show incredible decontaminating pollutants from

wastewater and can be used as a significant treatment method, there are limitations such as toxicity, high cost, and non-renewable materials that must be resolved to sustain the environment and resources. Biomass-based resources are the best alternatives to non-renewable energy sources (Hoislbauer & Siebenhofer, 2008).

2.5. Biochars and Their Applications

2.5.1. Introduction to Biochar

Biochar is a carbon-rich solid material produced from biomass through a thermochemical process called pyrolysis (Y. Cheng et al., 2019; W. Chen et al., 2020). It has high organic carbon content and has poor susceptibility to disintegration. Because of the increase in micro-pore volume produced by the evacuation of volatile organic compounds at high temperatures, biochar has a large surface area, physicochemical stability, high carbon content, high porosity, and catalytic activity (Sahoo et al., 2021)**.** The feedstock's lignin, cellulose, hemicellulose, fat, and starch are thermally broken down during pyrolysis, generating three products: bio char (solid), bio-oil (partly condensed volatile matter), and non-condensable gases. Bio-oil and combustible gases are used to make energy, such as power/heat generation and transportation fuel, as well as bio-based products like wood preservatives, food flavoring, adhesive, and biochemical components (Fujishige et al., 2017).

Biomass is an alternative carbon source to fossil fuels since it is renewable, non-edible, broad, and inexpensive. Biomasses are the most widely used renewable materials on the planet, and they are reportedly the most suitable and favorable materials for producing biochar and other platform compounds used in the food, textile, and biodiesel industries. Biodiesel has huge environmental, economic, and contextual relevance (N. Zhao et al., 2017; Y. Cheng et al., 2019). The three basic components of a biomass material have distinct characteristics. These components make up about 90% of the dry weight basis in lignocellulosic biomass, occurring in complex structures with each other (Zhuang et al., 2020).

2.5.2. Applications of Biochar

Biochars ' characteristics are high surface area, adsorption capacity, micro-porosity, magnetism, nuclear ratio, ion exchange capacity, and elemental composition. Biochars effect in wastewater

treatment is dictated by these distinguishing criteria (R. Xu et al., 2020). In recent years, agrochemicals, antimicrobials, polyaromatic, volatile organic substances, or cationic aromatic dyes have all been studied using biochar to remove them from wastewater (Pokharel, 2020). The removal mechanisms of different pollutants are governed by their interactions with various attributes of biochar. Biochar often compromises both positively and negatively charged surfaces. The negatively charged functional groups contribute to cation exchange capacity whereas O-containing functional groups in biochar exhibit anion exchange capacity. O-containing alcohol, carbonyl, and carboxylate functional groups are generally believed to contribute to biochar cation exchange capacity because they carry a negative charge and serve as lewis bases for the sorption of cations (Sahoo et al., 2021).

Biochar can help improve water treatment and sludge settling by trapping inhibitors and harmful chemicals or offering a surface for microbial immobilization in the activated sludge treatment process. The chemical makeup and morphological structure of biochar significantly influence the sorption of pollutants that constitute a serious threat to public health and the environment (Nur-E-Alam et al., 2017; Lam et al., 2019). Bamboo biochar is a promising alternative because of its porous structure, abundant raw materials, and environmental friendliness (Zhuang et al., 2020). Biochar introduced to a biological treatment unit improved control performance by adsorbing inhibitors, enhancing the system's buffering capacity, and neutralizing microbial cells degradation (Qu et al., 2015; N. Zhao et al., 2017). Biochar may also have a role in decreasing the mobility or accessibility of inhibitors such as organic molecules by binding them in their porous structure while maintaining optimal microbial activity for digestion (W. Chen et al., 2020). By most findings, biochar adsorbs more cations than anions.

Figure 2-2: Biochar characteristics and suitability for specific applications adapted from (Ambaye et al., 2021)

Biochar production and land application have been suggested as a potential climate change mitigation strategy (Sahoo et al., 2021). When biomass is processed into biochar, CO_2 that is generated during photosynthesis is bound to the biochar, resulting in reduced CO_2 emissions. Carbon storage in biochar is anticipated to decrease the emission of 0.1-0.3 billion tons of CO_2 each year degradation (Qu et al., 2015; Halilovic et al., 2017).

Table 2-3: Biochar based COD containing wastewater treatment from previous studies

Biochar	**COD removal (%)**	**Reference**
Bamboo	42% after 2 hours	(Hata et al., 2015)
Bamboo	75.21% after 10 hours	(Ahmad & Hameed, 2010)
Coconut shell	60-70% after 5 hours	(Sudarsan & Srihari, 2019)

Wastes from anaerobic digestion of sewage sludge, manure, and residues from food, beverages, or agricultural industry usually contain high levels of nutrients, making them suitable for utilization as an organic soil fertilizer (W. Chen et al., 2020). In the soil, biochar exhibits adaptive modifications that influence microbial abundance and activity. Microbes that acquire their metabolic demands from these micro-habitats use the pores of biochar as a residence.

Because of its distinctive property, biochar has a higher capacity to accumulate cations per unit carbon than soil nutrients (Norakmalah Mohd Zawawi et al., 2017). This enhances the carbon exchange capacity of the soil, preventing ammonium leaching and allowing it to be stored in plant-available form for a long time. Microbial uptake can also keep the nutrient in the soil. Similarly, the features of biochar and soil management measures may reduce NO_2 emissions connected with nitrogen fertilizer use (Halilovic et al., 2017; N. Zhao et al., 2017). The application of biochars as electrode material for energy is detailed below.

2.5.3. Bamboo Biochar

Bamboo is a taxonomic category of perennial evergreen grasses with about 1,450 species (family Poaceae). It is a natural fiber plant because of its rapid growth rate (it matures in five years) and homogeneity: Bamboo flourishes in a wide range of temperatures, including both cold mountains and hot tropical climates degradation (Qu et al., 2015; W. Chen et al., 2020)**.** Chemical components such as hemicellulose, cellulose, and lignin make up more than 90% of the total mass of bamboo. Bamboo strands feature a variety of ultra-hierarchical structures with varying length scales, thus lending to the specificity (W. Chen et al., 2020).

The cellulose fibril orientation variation within distinct cell wall layers is essential for bamboo cell wall ultrastructure. In contrast to wood, bamboo fiber lamellation is made up of distinct fibrillar orientations inside alternating narrow and broad layers along the longitudinal cell axis. Bamboo has stable chemical components and a three-dimensional microtextured that is well-connected degradation (Qu et al., 2015; Guoxiong Zhang et al., 2018).

Figure 2-3: Mature bamboo biomass

Bamboo can be carbonized under a nitrogen atmosphere at high temperatures to make low-cost carbon materials with interconnected, multichannel, and porous geometries (F. Cheng & Li, 2018; Sofyan et al., 2018) can provide a microtexture with a wide surface area, good conductivity, and a well-ordered microstructure (Qanytah et al., 2020), which increase ion transport by providing low-resistance channels, potentially improving in supercapacitor electrodes, high electrochemical activity, soil fertilizer, green gas emission, and other fields (F. Cheng & Li, 2018; W. Chen et al., 2020). For example, The surface area and average pore diameter of bamboo biochar activated by H_3PO_4 have measured 988.23 m^2/g and 2.82 nm, respectively, with a color and COD of 91.84% 75.21% reduction from real textile mill effluent was observed by (Ahmad & Hameed, 2009). At 350 °C, Indian bamboo lost more than 70% of its weight, whereas Moso-bamboo lost 68-72% of its weight between 600 and 1000 °C. This means that biochar can be made at a relatively low temperature, such as 600 °C. The aromatization of residual carbon is seen to be completed at 600 °C for bamboo carbonization (Fujishige et al., 2017). Bamboo has been carbonized under different temperatures and activators, as shown in the table below.

Table 2-4: Bamboo chemical activation and carbonization temperatures from different sources

Activator/biomass ratio	**Carbonization condition**	**Reference**
KOH/bamboo = 3:1	800 ^oC for 1 h	(W. Chen et al., 2016)
H_3PO_4/bamboo = 2:1	400 ^oC for 2 h	(Shrestha et al., 2016)
KOH/bamboo = 4:1	800 ^oC for 1 h	(Guoxiang Zhang et al., 2016)
KOH/bamboo = 4:1	750 ^oC for 1 h	(Hao Chen et al., 2015)
KOH/bamboo = 3:1	900 ^oC for 3 h	(Guoxiong Zhang et al., 2018)
H_3PO_4/bamboo = 4:1	500 ^oC for 1 h	(Sofyan et al., 2018)
KOH/bamboo = 2:1	800 ^oC for 6 h	(Li & Wu, 2015)

2.5.4. Biochar Activation

Biochar is activated to extend biochar application (Yuan et al., 2016; Chen et al., 2020). Activation is an important process for increasing the specific surface area of carbon materials and adjusting the pore structure. Physical and chemical activation of biomass is the two types of activation.

2.5.4.1. Physical Activation

Physical activation is a two-step process that involves pyrolysis carbonization of raw materials followed by a controlled gasification process at higher temperatures (> 875 ^{o}C) in the presence of oxidizing gases such as CO_2, steam, air, or their combinations (Ahmad & Hameed, 2009; W. Chen et al., 2020). As a result, the porosity and the surface area of biochar are increased. Porosity growth is said to be aided by greater activation temperatures and longer activation times. A broadening of the pore size distribution is frequently associated with increased porosity.

2.5.4.2. Chemical Activation

Chemical activation is typically accomplished by adding activators to biomass sources and then carbonizing. Chemical activation's precise mechanism isn't well defined. To develop porosity, the general reaction (with alkalis) combines hydroxide reduction and carbon oxidation. CO, CO_2, and H_2 are produced during the reaction, and the chemically activating substance is removed by washing with acid/base and water (Li & Wu, 2015; Y. Cheng et al., 2019). It has a lot of benefits to physical activation, including a higher activation efficiency and lower energy usage. It's done by soaking or suspending biomass or biochar in the suitable concentration of an alkaline solution at temperatures ranging from 25 - 100 ^{o}C. Depending on the materials used for modification, soaking and stirring can take 6 – 24 hours (Ahmad & Hameed, 2009; Y. Cheng et al., 2019). The most common basic and acid chemical activating agents are here:

Potassium Hydroxide (KOH)

Because of its lower activation temperature and maximum yield, KOH is a well-known activator for creating pore structures in carbon materials with well-defined pore size distribution and super-high specific surface area. Positive surface charges are formed by KOH, which assist in the adsorption of negatively charged species. The H_2O and CO_2 created during the activation process help promote porosity development by allowing carbon to be gasified. During thermal treatment, produced K and K_2CO_3 easily intercalate into the carbon lattices of the carbon matrix, inducing the carbon lattices to expand and stabilize the voids between the carbon atomic layers (Sajjadi et al., 2019; W. Chen et al., 2020). When intercalated K compounds are removed by acid washing, carbon lattices expand and cannot return to their prior structure, resulting in micro-porosity. High O-containing functional groups and surface area were found in comparison to sulfuric acid, phosphoric acid, and potassium hydroxide (W. Chen et al., 2020).

Phosphoric Acid (H_3PO_4)

H_3PO_4 is great for building ester bonds with -OH groups to cross-link polymer chains. Extending the biomass structure improves the separation of cellulose microfibers and P-O-C linkages at high temperatures, leading to the creation of open pores (Qanytah et al., 2020). The development of porosity with phosphoric acid begins at a low temperature, rapidly increases to a broad maximum, and then diminishes at a higher temperature. At the same time, the temperature range is dependent on the biomass source (J. Jiang et al., 2013; F. Cheng & Li, 2018).

Sulfuric Acid (H_2SO_4)

H_2SO_4 modification has also successfully expanded surface area and porosity by bearing SO_3H into the precursor surface. The results showed that SO_3^- sulfonation produced greater $–SO_3H$ densities, but H_2SO_4 sulfonation significantly increased the surface area and pore volume of bio-char. The surface area of the bio-char would be reduced in both sulfonation approaches degradation (Ahmad & Hameed, 2009; Qu et al., 2015).

Sodium Hydroxide (NaOH)

Carbon properties can be improved by increasing the amount of NaOH in biochar, boosting the activation temperature, or prolonging the activation period. These responses result in the formation and growth of pores via four processes: the formation of new pores, the opening of previously inaccessible pores, the broadening of existing pores, and the merger of existing holes due to pore wall rupture. An increase in the NaOH/char ratio of 3:1 has been noticed an increase in the NaOH/char ratio of 3:1 has been noticed (B. Xu et al., 2010) results in a sustained increase in surface area and porosity. Excess NaOH causes a vigorous gasification reaction, which degrades the carbonaceous structure, resulting in a considerable reduction in accessible area above ideal concentration (Q. S. Liu et al., 2010; Sajjadi et al., 2019).

2.5.5. Biochar Electrodes

Ideal electrode materials for energy storage and other applications are known as supercapacitors as they have both strong catalytic activity and superior conductivity (Dehkhoda, 2016; Yuan et al., 2016). It's quite difficult to find a single material that has both features. Electrodes with diverse inorganic materials have strong thermal stability and reactivity, but their conductivity is

restricted to many grain boundaries and flaws. Furthermore, for large-scale applications, the cost of carbon and metal material electrodes is still regarded as expensive (Yong Zhang et al., 2015; Dehkhoda, 2016). Because of their desirable physicochemical qualities, such as strong electrical conductivity, high specific surface area, and outstanding chemical stability, carbon-based materials ranging from traditionally activated carbons to advanced carbons have been commonly applied for electrode uses (Yuan et al., 2016; Mohd Abdah et al., 2020).

Modern supercapacitors have great power density, high reliability, and quick charging/discharging properties. As a result, supercapacitors are employed in a wide range of applications, including electric cars. As a result, carbon is selected for electrode fabrication in supercapacitor applications (Dehkhoda, 2016; Armynah et al., 2019). Biochar is ideal for various types of rechargeable batteries because of its price and sustainable synthesis and its high specific charge storage capacity compared to standard graphite materials. Biochar generated from wheat stalks has been demonstrated to provide many lithium battery storage sites, allowing for quick electron and lithium battery ion movement, a low and smooth voltage profile, and reduced voltage fluctuation when used as an anode material in lithium batteries (Armynah et al., 2019; Rahman et al., 2020).

Several new carbon-based materials with increased conductivity have been developed. Biomass-based carbon materials are of particular interest since they are sustainable and renewable, and because of their natural porous structures, high surface area, high conductivity, heteroatom doping, various nanostructures, and physicochemical stability, they can exhibit outstanding electrochemical performance, leading to high capacitance, providing outstanding, and cycling stability (L. Lyu et al., 2019; Parthasarathy et al., 2021). The carbon materials synthesized using KOH and pre-treated carbon exhibited excellent performance with a maximum specific capacitance of 268 F/g and retained up to 222 F/g. High specific surface area and pore volume, correct pore size distribution, and certain oxygen groups could contribute to the superior electrochemical characteristics (Li & Wu, 2015). A rectangular hierarchical porous structure, activated carbon from natural bamboo has shown to have remarkable electrochemical performance. The polyaniline composites electrodeposited well into the biochar, yielding 277 and 236 F/g, revealing good rate capability (Zhou et al., 2012).

High energy and power density electrochemical energy storage devices are more important to reduce the dependency on fossil fuels and are also required for intermittent renewable energy storage (Senthil & Lee, 2021). Biochar electrode owns higher energy and power density, which indicates the amount of energy stored with the proportional weight of substrate used for electrode preparation. The porous structure is favorable for the contact between the electrode material and the electrolyte and is advantageous for the transport of ions (Demir et al., 2018; Qanytah et al., 2020). According to (Hui Chen et al., 2020), a potential electrode material made from bamboo coated with $CoMoO_4$ reveals better electrochemical features with excellent specific capacitance and a high energy density of 56.74 Wh/kg at a power density of 785.03 W/kg. (Qu et al., 2015) reported a better electrochemical performance from corncob biochar with an energy density of 5.3 Wh/Kg and high power density in 6 M KOH solution.

2.5.6. Biochars Electrode Role in Water Treatment

As stated before, an electrode from biomass-based bio char has developed as a super capacitor, rechargeable batteries material for energy storage purposes. Studies also reported that biochar electrodes applied for water treatment reported that water desalination based on electrochemical adsorption/desorption e.g. capacitive deionization (CDI), gained attention as a cost-effective and energy-efficient method (Li & Wu, 2015) (Dehkhoda, 2016). CDI device is based on electric double-layer capacitors (EDLCs). CDI, also called electro-sorption, is an electric potential induced adsorption process on the surface of electrodes. The creation of EDLCs in the region of electrodes as a result of applying an electric potential is the basis for this technology operating mechanism (Hao Chen et al., 2015). The ions bind to EDLCs electrostatically and can be desorbed by withdrawing the applied potential. The cations begin to move toward cathodes and the anions begin to move toward anodes when an electrical potential is applied between the electrodes. Adsorption describes the interaction of positive and negative ions. In contrast, desorption describes how ions at the surface begin to be ejected when the surface charge emerges due to the same charge sign (Wen et al., 2017).

Biochar is beneficial in water treatment as an electrode material because it has the potential to be employed as an abundant alternative catalyst material for hydrogen and oxygen synthesis (Rahman et al., 2020). The biochar unique properties mentioned earlier is a prospective electrode material for capacitive deionization applications (Q. S. Liu et al., 2010; Viglašová et al., 2018).

Graphene, carbon aerogels, carbon nanotubes, activated carbon and organized mesoporous carbon are the most prevalent electrode materials in CDI cells. It is difficult to prepare, and the increased cost of these materials makes it unfeasible. Different carbonaceous precursors, such as wood, coal, starch, coconut shells, and synthetic sources such as resins, can be used to make activated carbons (Zhuang et al., 2020). CDI is limited in the desalination of wastewater containing NaCl solution in many kinds of literature. For example, CDI can be applied to purify water streams containing ions such as Na^{+}, Cl^{-}, SO_4^{-}, and NO^{3-} and heavy and transitional metal ions (e.g., Zn^{2+}, Cu^{2+}, Cd^{2+}, and Cr^{6+}) in industrial wastewater treatment (Li & Wu, 2015; W. Zhao et al., 2016).

The CDI device is made up of one or more pairs of electrodes that produce positively and negatively charged poles when the potential is supplied to them. Electrostatic force draws cations to the negative electrode, whereas anions are attracted to the positive electrode by electrostatic force to ions separated from the water. Short circuit or reverse current can then be used to rejuvenate the electrodes by releasing ions back into concentrated solution (Hao Chen et al., 2015; Dehkhoda, 2016). Based on the desalination mechanism of CDI, the electrode material is the key to the performance of CDI. The ideal CDI electrode material should meet the following conditions: 1) large specific surface area, increasing ion adsorption sites; 2) high conductivity and ion mobility; 3) excellent hydrophilicity, which ensures the full utilization of electrode hole structure; 4) High electrochemical stability with pH and voltage variations to ensure operational persistence and system constancy; 5) Easily shaped according to design requirements (X. Zhao et al., 2020). CDI uses low direct current power (either constant current or constant voltage) to polarize a pair of porous electrodes allowing ion adsorption.

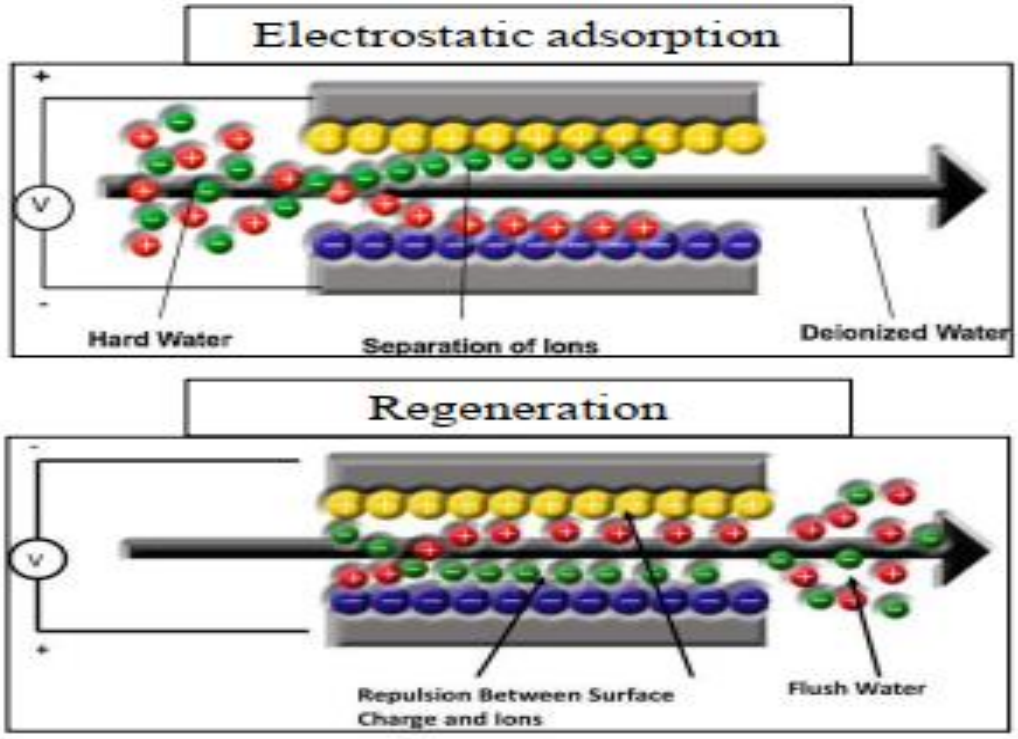

Figure 2-4: Diagram of capacitive deionization adapted from (Dehkhoda, 2016)

The essential effect in the CDI process is the capacitive storage of ions in the EDLC. The CDI method primarily employs two charge storage mechanisms: capacitive electrosorption and pseudocapacitive ion intercalation (W. Zhao et al., 2016). Capacitive electrosorption is a popular method for initiating adsorption on the surface of very porous carbon electrodes using an applied voltage. Charged ions in the salt solution are forced to flow toward oppositely charged electrodes, where an EDLC forms on their surfaces, thanks to an electric field produced between a pair of porous carbon electrodes. In the adsorption phase, charged ions are stored within the double layer. When the electric field is eliminated or the polarity of the electrodes is reversed, the ions are released back into the bulk solution (desorption), and the electrodes are regenerated (Elisadiki & King'ondu, 2020).

The addition of metal oxides to the carbon electrode (Pokharel, 2020; X. Zhao et al., 2020) and the use of thin polymeric ion exchange membrane sheaths for the anode (Li & Wu, 2015) have shown good results in inhibiting electrode oxidation reactions. Pseudocapacitive ion intercalation is a way in which ions from water reversibly mix with those of the electrode via faradaic reactions on the electrode's surface. Carbon compounds with tunable structural features, high electrical conductivity, and cheap are, in general, promising electrode materials for CDI, as they

can improve ion removal efficiency (Tsubota et al., 2018; Palagonia et al., 2019). Furthermore, electrode materials must have a high salt adsorption capacity, a high specific capacitance (high charge efficiency), and sufficient mechanical strength to withstand the cell's hydrodynamic forces. Materials should be resistant to bio fouling, can go through charging and discharging cycles, and have hydrophilic qualities, as well as be free of toxic chemicals and rust-causing compounds (Tsubota et al., 2018; Jothi Ramalingam et al., 2020).

Table 2-5: Difference between fossil fuel and biochar-based electrodes (C. Zhao & Chen, 2019)

Fossil fuel-based	**Biochar based electrode**
Slow ionic accessibility and small mass transfer	Fast ionic accessibility and high mass transfer
Expensive	Low cost
Low electrical conductivity	Large electrical conductivity
Consumes more energy	Consumes less energy
Rare occurrence	Easily available
High environmental issue	Low environmental concern

The one disadvantage of fossil fuel-based treatment is high energy consumption, as also shown in table 2.4. (Sundarapandiyan et al., 2010) Reported an energy consumption of 0.8 kWh/kg COD at a current density of 0.024A/cm^2 for achieving 81.03% COD reduction 30 g/l of NaCl electrolyte. (Asaithambi et al., 2020) Also got 3.10 kWh/m^3 energy consumption using photon as an oxidant for the electrochemical treatment. A 5.77 kWh was reported in (Aouni et al., 2009).

2.5.7. Biochar/Composite Formation in Electrode

Because of their huge surface area, outstanding electrical conductivity, and superior mechanical stability, biochar-based electrochemical materials have received a lot of attention, although they have a low specific capacitance. TMO, which is produced from reversible and quick faradaic processes, has recently been done to enhance electrochemical behavior when integrated with carbon-based materials (Aouni et al., 2009; Jothi Ramalingam et al., 2020). Low conductivity and surface area, as well as weak intrinsic conductivity and significant structural damage during cycling, severely limit ion/ electron movement and reduce cycling longevity, making it difficult for TMOs to achieve the high theoretical specific capacitance value. Many efforts were made to

construct hybrid materials due to the limitations of each substance (Y. Cheng et al., 2019) that optimize the electrodes' electrochemical performance. Because of their high theoretical specific capacitance from the faradaic charge transfer mechanism, ruthenium oxide (RuO_2), manganese oxide (MnO_2), and vanadium oxide (V_2O_5), tin oxide (SnO_2), and tungsten oxide (WO_3) are often used in supercapacitors (Seow et al., 2012; Gezahegn, 2020).

MnO_2 has emerged as an excellent faradaic material, which can be used as an alternative TMO due to its good environmental compatibility, high theoretical specific capacity up to 1370 F/g (B. H. Cheng et al., 2017), extended operating potential, and cost-effectiveness. It has poor ionic (10-13 S/cm) and electrical (10^{-5}-10^{-6} S/cm) conductivities restricting it to be practical. Porous carbons have therefore been used as conductive skeletons for the growth of MnO_2. The charge transfer is aided by carbon's good conductivity and strong structure. As a result, MnO_2/carbon nanocomposites may have better electrochemical performance (Y. Cheng et al., 2019; Gezahegn, 2020).

Fabrication of carbon nanofibers using disposable and low-cost bamboo chopsticks has been studied in (B. H. Cheng et al., 2017). The carbon-fiber sheets were electrodeposited with MnO_2, resulting in a high specific capacitance of 375 F/g and remarkable specific energy. The reported material can be attributed to the synergistic effect of faradic and capacitor charge storage mechanisms, as well as large electroactive sites that allow for fast electrolyte ion diffusion and migration (Dehkhoda, 2016; Gezahegn, 2020) shown maximum capacitance obtained for electrodeposited MnO_2 thin films is 345 F/g at a scan rate of 5 mV/s. It reported specific capacitance of MnO_2 is far below its theoretical value because of poor conductivity and low electrolyte solution accessible surface area**.**

(MnO_2) surface $+ C^+ + e^-$ ⟷ $([MnO_2]^-C^+)$ surface……2.12

The second one is based on the concept of intercalation of H^+ or alkali metal cations such as Na^+ in the electrode during reduction and deintercalation upon oxidation (Subramanian et al., 2005; Gezahegn, 2020). It is based on the intercalation/deintercalation of protons and cations on MnO_2.

$MnO_2 + C^+ + e^-$ ⟷ $([MnOO]^-C^+)$ intercalation……..2.13

Where, C^+ refers to protons (H^+) or alkaline cations (e.g. Na^+, Li^+, and K^+).

2.5.8. Ingredients in Electrode Preparation

Metals and metal oxides, carbonaceous materials, solvents, conductive agents, and electrode materials are among the materials used to make biochar electrodes. Binders are recognized as inactive components since they do not interact with the binding affinity of the cells. Binders are not passive materials and influence electrochemical performance. Binders have amazing properties such as stability, tensile strength flexibility, and viscosity. The main purpose of using a binder is to form stable networks of the solid electrode components, i.e., the active materials and conducting agents. Thus, the binder has to ensure close contact of the composite electrode toward the current collector (Priyono et al., 2019). Alkyd, acrylic, epoxy, polyurethane, and chlorinated rubber are the most widely used synthetic binders (Gide, 1967; Lema, 2021).

A solvent is a liquid that contains one or more volatile components under dry conditions that can dissolve a binder without causing a chemical reaction. The majority of the binder in the paint composition is solid or extremely viscous, and it must be diluted to a lower viscosity for easy processing and application. Paint processing, application, and film creation all benefit from solvent (Lema, 2021).

CHAPTER THREE

3. MATERIALS AND METHODS

3.1. Materials

Table 3-1: Ingredients used throughout the experiments

No.	Chemical	Application	Manufacturer
1.	Concentrated sulfuric acid 96% (H_2SO_4)	Bamboo activation, COD determination	Blulux laboratories Pvt. Ltd
2.	Hydrochloric acid 37% (HCl)	For Rinsing base activated bamboo	Blulux laboratories Pvt. Ltd
3.	Potassium hydroxide (KOH)	Bamboo activation	Carelabmed Pvt.Ltd
4.	Sodium hydroxide (NaOH)	Bamboo activation, for rinsing base activated bamboo	Alpha chemical Pvt.Ltd
5.	Phosphoric acid (H_3PO_4)	Bamboo activation	Uni-chem Pvt.Ltd
6.	Potassium permanganate ($KMnO_4$)	Oxidizing agent in MnO_2 formation	Labtech chemicals Pvt.Ltd
7.	Manganese sulfate monohydrate ($MnSO_4.H_2O$)	Reducing agent in MnO_2 formation	Alpha chemika Pvt.Ltd
8.	Potassium dichromate ($K_2Cr_2O_7$)	Oxidant in COD determination	Loba chemie Pvt. Ltd
9.	Ferrious ammonium sulfate ($Fe(NH_4)_2(SO_4)_2$)	Titrant in COD determination	Loba Chemie Pvt. Ltd
10.	Ferroin indicator	Endpoint detector in COD titration	Loba Chemie Pvt. Ltd
11.	Sodium chloride (NaCl)	Electrolyte in electrochemical treatment and cyclic voltammetry analysis	Neolab life science Co.
12.	Glucose powder	Source for synthetic wastewater preparation	Blulux laboratories Pvt. Ltd
13.	Chlorinated rubber	Binder in electrode preparation	Tarak Chemicals Pvt. Ltd
14.	Toluene	Solvent in electrode preparation	Loba chemie Pvt. Ltd

3.2. Equipment

Types of equipment used during the experimental work include digital mass balance, grinder, sieves, muffle furnace, oven, digital pH meter, hot plate, shaker, the crucible, beaker, mortar and pestle, burette, magnetic stirrer, measuring cylinder, desiccator, petri dish, filter pump, filter paper, DC power supply, copper wire, XRD, FTIR, SEM, and CV.

3.3. Overall framework of the experiments

Figure 3.1 illustrates the Overall framework of the experiments**.** The initial stage was to collect bamboo raw material from Meqi. After that, cutting and pretreatment of bamboo, activation with KOH, NaOH, H_2SO_4, and H_3PO_4 as detailed in the following section, drying in an oven, carbonizing activated bamboo at varying temperatures and times, cooling, grinding, washing to adjust pH, filtering and drying activated bamboo biochar, preparing activated biochar composite with MnO_2 by mixing, washing, filtering, and calcining, and preparing working electrode by making a mold, slurry, and FTIR characterization was done at analytical chemistry at Addis Ababa University, while XRD and CV analysis was done at School of Material, Chemical and Material Engineering at Department of Materials Engineering, ASTU. Synthetic wastewater prepared from glucose was treated using biochar based anode electrode in the electrochemical process. After the treatment COD using titration and energy consumption for each experiment have been determined.

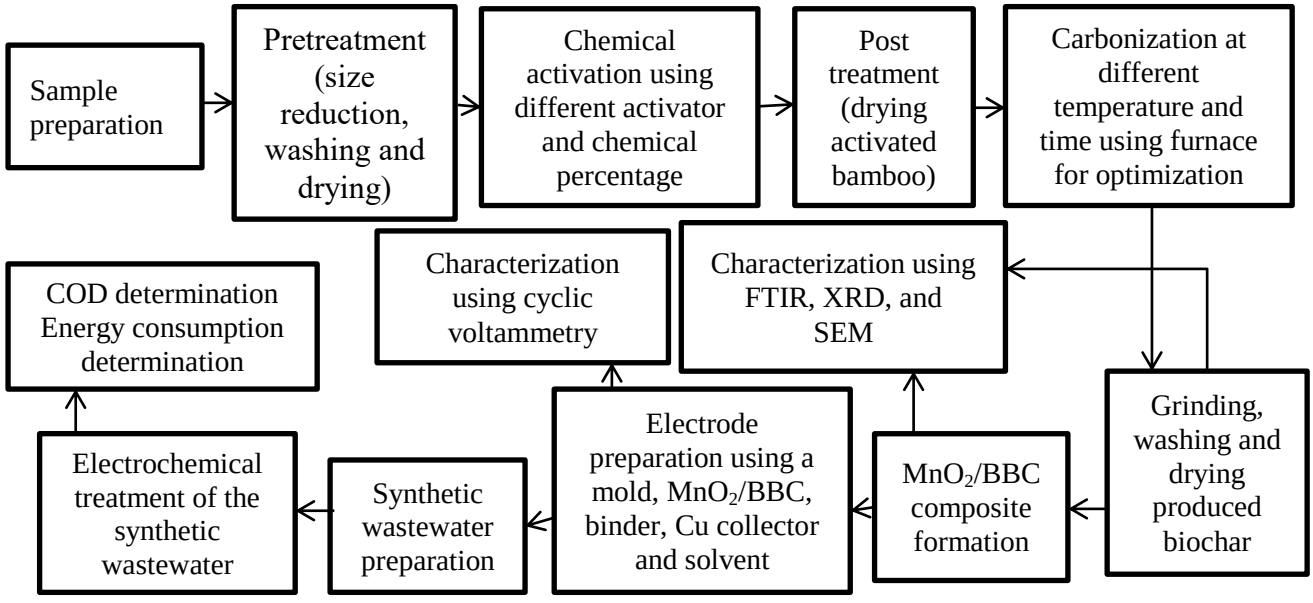

Figure 3-1: Experimental design

3.4. Method

3.4.1. Raw material collection and pretreatment

Bamboo biomass was transported from Meqi, a town 59 kilometers from Adama and 137 kilometers from Addis Ababa on the Hawassa route. The sample was collected and dried in the sun for 3-4 days. Then it was chopped to a uniform size of 2 cm x 2 cm x 1 cm. After washing with deionized water to remove exterior dust and drying for 6 hours at 105 °C while no mass change occurs. Moisture content is determined using equation 3.1 (Ji Zhang et al., 2017). Figure 3.2 indicates the bamboo pretreatment scheme.

$$\text{Moisture content} = \left(\frac{\text{initial mass} - \text{final mass}}{\text{initial mass}}\right) * 100\ \% \qquad 3.1$$

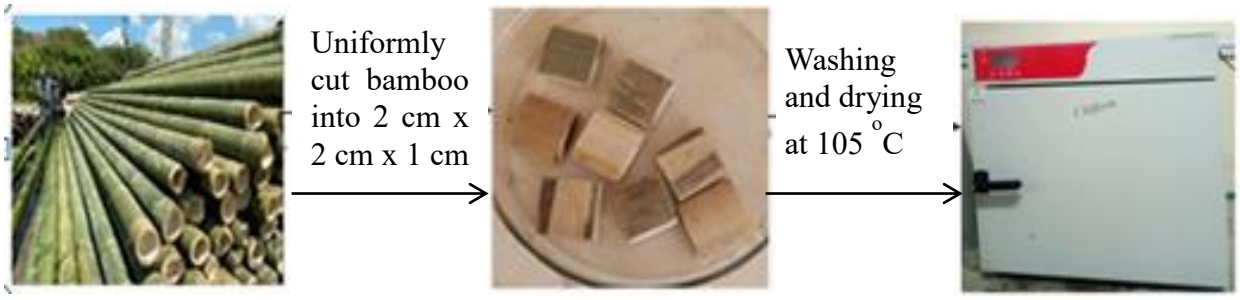

Figure 3-2: Preparation of raw bamboo

3.4.2. Raw Material Activation

To enhance biochar property like making pores surface, sustaining abundant functional groups and increase biochar yield to be economical, dried bamboo was soaked with chemical activators. Two alternative parameters, chemical activator, and chemical percentage composition were applied in soaking with a 3:1 ratio of activator to bamboo for 24 hours at room temperature for the entire soaking activities. H_2SO_4, KOH, H_3PO_4, and NaOH in a 30% solution were tested in the first soaking period to determine the optimal chemical activator based on biochar yield. The better chemical activator was chosen based on biochar yield, and it was then soaked in 35% and 40% solution to see what effect the variation in solution preparation had. To have a good biochar yield and performance, proper impregnation of the sample to the activator is crucial. Increasing

the impregnation ratio could cause micropores to develop into mesopores, but new micropores would nearly never emerge, reducing the surface area. As a result, the best impregnation ratio is 3:1; it produces the largest surface area and total pore volume (Tsubota et al., 2018). This was also supported by (Ji Zhang et al., 2017) shows that when the impregnation ratio KOH to bamboo increased from 3:1 to 5:1, the yield of biochar decreased. It was primarily because KOH encouraged dehydration and the development of cross-links during the heat treatment, resulting in the production of some volatile materials. It was mostly due to the possibility that too much KOH could clog activated chars pores, preventing volatiles from passing through the pore channel (Ji Zhang et al., 2017).

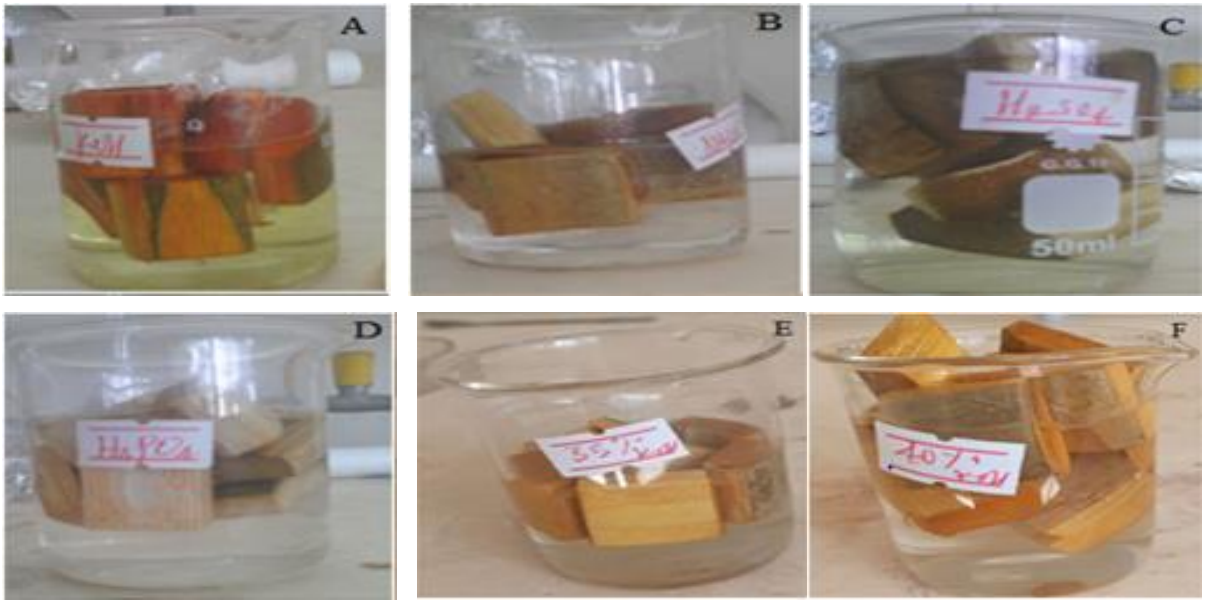

Figure 3-3: Shows the activation of bamboo by soaking in A). 30% KOH, B). 30% NaOH, C). 30% H_2S0_4, D). 30% H_3PO_4, E). 35% KOH and F). 40% KOH

3.4.3. Carbonization of Activated Bamboo

The carbonization of inactivated bamboo was first carried out at 600 ^{o}C for 60 minutes for samples before temperature variable carbonization was carried out (Ji Zhang et al., 2017). Different chemical activators, percentage composition, carbonization temperature, and carbonization duration were used in the bamboo biomass activation to find the best combination of these elements that yields high biochar yield explicitly. In other words, the effects of chemical activators were initially seen in 30% solutions of KOH, H_2SO_4, H_3PO_4, and NaOH next to the

inactivated bamboo carbonization. Second, as previously stated, the best chemical activator from category one was optimized at 35% and 40% solution at 600 ^{o}C. The change in carbonation temperature at 400 ^{o}C and 900 ^{o}C was measured for 60 minutes in category three, the best combination of the previous two. Finally, the influence of time has been examined at 30 and 90 minutes in addition to 60 minutes as before done. Optimization for bamboo carbonization is generally presented in Table 3.2. Carbonized activated bamboos were allowed to cool before being ground with a mortar and pestle. The pH of the biochar was then adjusted with 1% HCl solution for these activated with NaOH and KOH and deionized water repeatedly. Biochar made from H_2SO_4 and H_3PO_4 activation was rinsed with 6% NaOH before being cleaned with deionized water. Finally, the washed biochar was dried and stored for future analysis. Activated bamboo biochar with maximum yield is considered as economical way and assumed as insuring biochar property (Ji Zhang et al., 2017; Tsubota et al., 2018).

Table 3-2: Bamboo carbonization conditions

Serial no.	**Chemical activator**	**Chemical activator percentage composition (%)**	**Carbonization temperature (^{o}C)**	**Carbonization time (minute)**
1.	-	-	600	60
2.	KOH			
3.	H_2SO_4	30	600	60
4.	NaOH			
5.	H_3PO_4			
6.		30		
7.	KOH	35	600	60
8.		40		
9.			400	
10.	KOH	35	600	60
11.			900	
12.				30
13.	KOH	35	600	60
14				90

The biochar yield can be determined using equation 3.2 (Ahmad & Hameed, 2009).

$$\text{Yield } (\%) = \left(\frac{Wc}{Wo}\right) * 100 \qquad 3.2$$

Where Wc is the dry weight of final activated carbon after washing and drying while Wo is the dry weight of the initial sample.

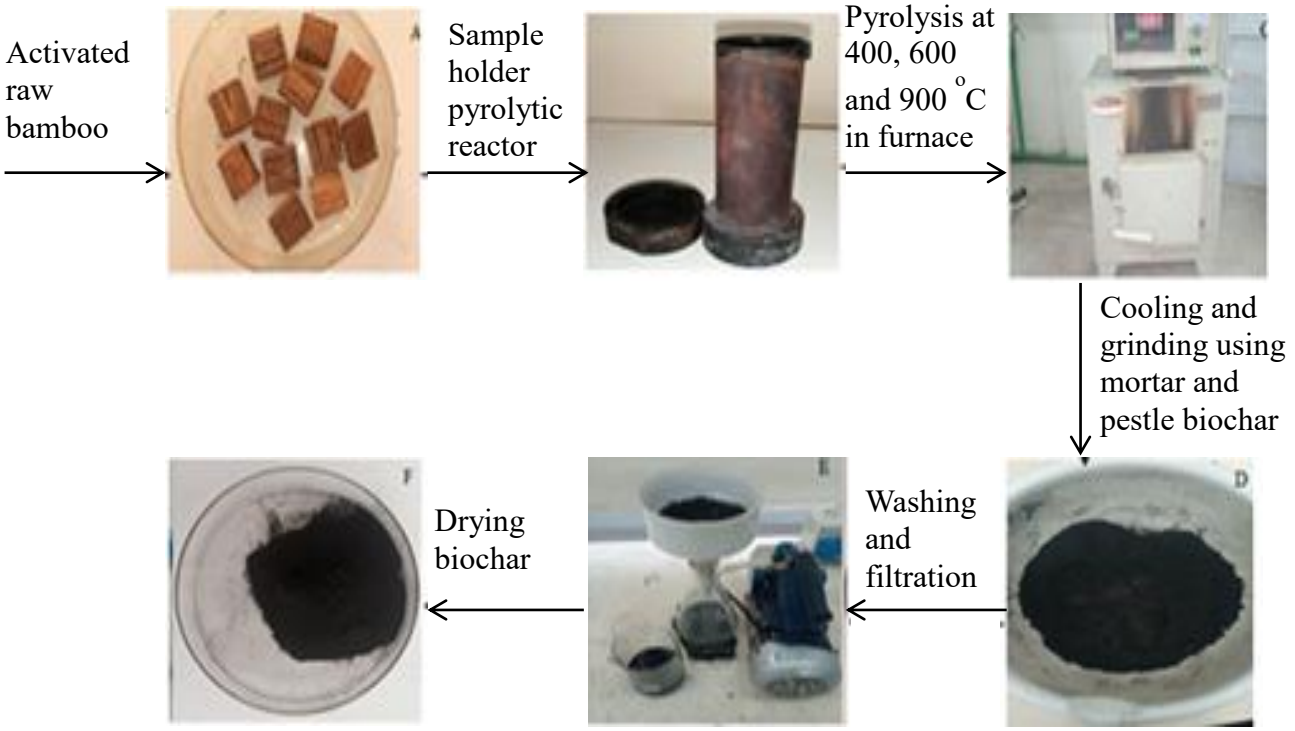

Figure 3-4: Activated bamboo carbonization flow diagrams

3.4.4. Activated Bamboo Biochar/MnO_2 Composite Formation

MnO_2 coating on bamboo biochar is carried out a procedure described in (Zhuang et al., 2020). 2 g activated biochar was mixed in a solution consisting of 80 mL H_2O and 27.6 mL 0.01 M $MnSO_4 \cdot H_2O$. 9.2 mL 0.01 M $KMnO_4$ was added for 3 hours stirring. After the reaction was completed, the solution was filtered and rinsed with deionized water. The sample was then calcined for 6 hours in a muffle furnace at 200 °C. Biochar produced from bamboo with 30% KOH at 600 °C in 60 minutes and 35% KOH at 600 °C in 60 minutes based on the biochar yield, and inactivated bamboo biochar (BBC) was used as a precursor with MnO_2 composite formation to cross-check the difference between chemical activation and no chemical activation. Equation

3.3 depicts the potential production of MnO_2 from the starting materials (Dehkhoda, 2016; Gezahegn, 2020). The coating step is shown schematically in Figure 3.5.

$$3MnSO_4 + 2KMnO_4 + 2H_2O \longrightarrow 5MnO_2 + K_2SO_4 + 2H_2SO_4 \quad \ldots\ldots 3.3$$

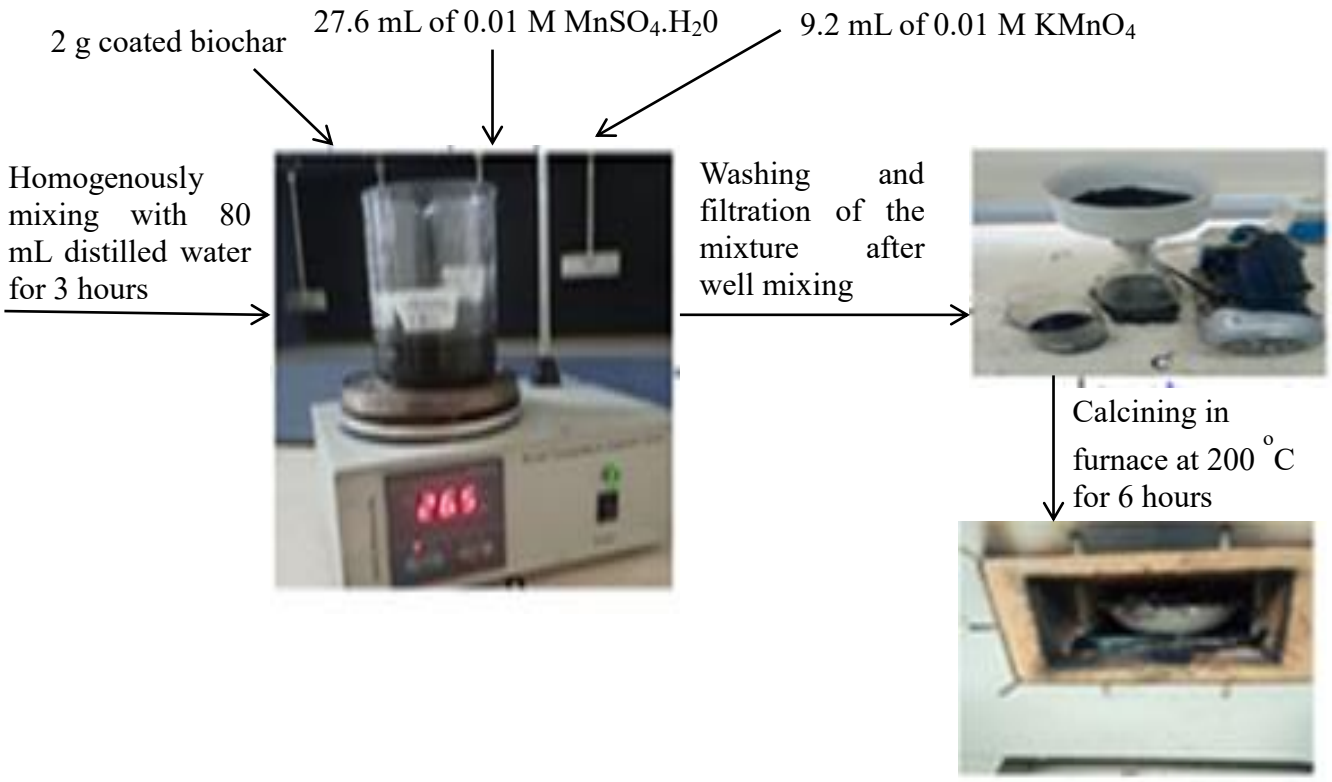

Figure 3-5: MnO_2/bamboo bio chars composite preparation

3.4.5. Characterization of Raw Bamboo and its Biochar Derivatives

To compare and check the effects of carbonization with and without activation and MnO_2 addition to the biochar on the raw bamboo different parameters are needed to be studied. The following analyses namely FTIR, XRD, and SEM have been selected for this study.

3.4.5.1. Fourier Transforms Infrared Spectroscopy (FTIR)

To investigate the presence of functional groups in biochar and its derivatives FTIR in the range of 4000-400 cm^{-1} at 4 cm^{-1} resolution and 64 scan rates were used.

3.4.5.2. X-Ray Diffraction (XRD)

To determine structural information and space between crystals of the bamboo and its biochar derivatives, XRD analysis of Shimadzu, Japan diffractometer model XRD-7000 with scanning area at a diffraction angle (2θ) was set at 10° to 50° at scanning range of $3^{o}\,min^{-1}$ was used. d-spacing the distance between the atomic layers of crystal was measured using the Bragg equation Eq. 3.4 (Qanytah et al., 2020):

$$n\lambda = 2d\sin\theta \qquad 3.4$$

Where n is an integer, λ is the wavelength of the X-ray used, d is the distance between a crystal, θ is the diffraction angle.

3.4.5.3. Scanning Electron Microscopy (SEM)

The surface morphology of selected MnO_2 modified biochar and its initial activated biochar were analyzed using a JEOL scanning electron microscope.

3.5. Electrode Preparation and Characterization

The outcome of MnO_2 modified biochar, which has good XRD, FTIR, and SEM qualities, was used to make an electrode for electrochemical purposes. The BBC/MnO_2 coated electrode was characterized using cyclic voltammetry (CV).

3.5.1. Working Electrode Preparation

The working electrode prepared from MnO_2 coated on bamboo biochar with the best performance, as determined by SEM, XRD, and FTIR analysis. Based on the procedure in (Yong Zhang et al., 2015), the electrode preparation is followed with little modification as described in Figure 3.6. According to the findings, MnO_2/35% KOH BBC outperformed MnO_2/30% KOH BBC and MnO_2/BBC. A mold was prepared from a glassy tube with a dimension that foot the port in cyclic voltammetry. A copper (Cu) current collector of uniform size was cut, having a length 10 cm and a diameter 2.5 mm was ready to be inserted after biochar slurry formation. Then, using aluminum (Al) foil, a 4.5 cm long glassy tube with a 4 mm small diameter and a 6 mm high diameter (conically shaped) was folded. This was followed by plastering the Al foil with the mold to ensure the stability of the mold size and shape.

After making a mold biochar-based electrode was prepared as follow. Chlorinated rubber is an effective binder, as mentioned in (Lema, 2021). The slurry was prepared with 75% biochar (active material) and 25% chlorinated rubber (binder) was dispersed in toluene (solvent). The formed slurry was added carefully into the prepared mold and the well rinsed Cu current collector was then immersed into it. Then the prepared electrode was dried in an oven at 80 ^{o}C overnight until toluene was evaporated (Yong Zhang et al., 2015). The dried electrode was used for further analysis using cyclic voltammetry.

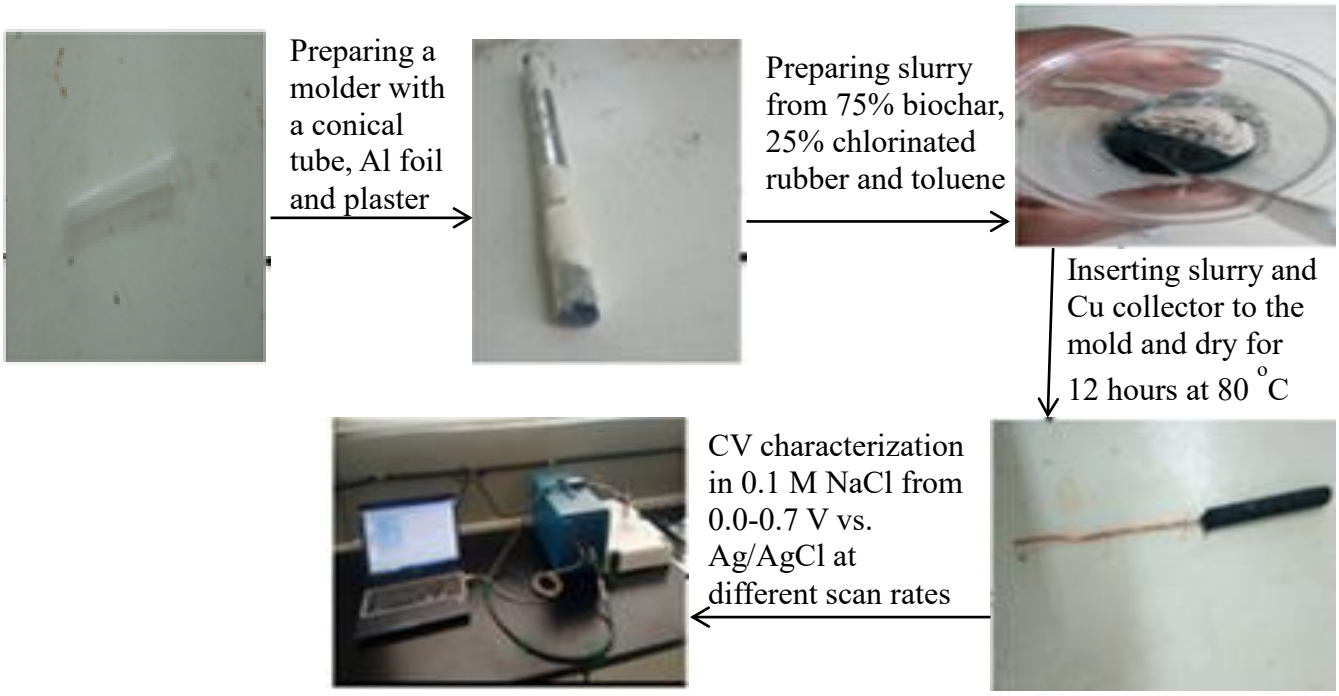

Figure 3-6: Working electrode preparation

3.5.2. Performance evaluation of Electrode using Cyclic Voltammetry (CV)

Cyclic voltammetry is an electrochemical measurement used to investigate an analyte's electrochemical property in solution. In CV the working electrode potential is scaled linearly vs. time in a cyclic voltammetry experiment, and the current versus the potential is recorded. Unlike linear sweep voltammetry, after reaching the specified potential, the working electrode's potential is ramped in the opposite direction to return to the initial potential in a CV experiment. These potential-ramping cycles can be performed as many times as necessary. The current at the working electrode potential is plotted Vs. the applied voltage to give the cyclic voltammogram trace (Zhuang et al., 2020).

In the three-electrode configuration, the prepared bio char electrode was used as a working electrode, Platinum (Pt) was used as a counter electrode, and Ag/AgCl as a reference electrode. A 0.1 M NaCl solution was as an electrolyte. On the SP-300 modeled cyclic voltammetry equipment, tests in the three-electrode configuration were performed with a potential of 0.0-0.7 V vs. SCE at 5, 10, 20, 50, 100, and 200 mV/s scan rates. Capacitance is the ability of a component or circuit to collect and store energy in the form of an electrical charge. By integrating the area under the CV curves, the specific capacitance (F/g), which shows the electrode's charge storage capacity per unit mass, is obtained (Elisadiki & King'ondu, 2020). The capacitance of the electrode material is calculated using equation 3.5 (Yong Zhang et al., 2015).

$$C = \frac{2I\Delta t}{m\Delta V} \qquad 3.5$$

Where ΔV is the potential operating window (V), Δt is the discharge time (s), I is the discharge current (A), and m is the total mass of the active material (g).

3.5.3. Energy Density and Power Density Calculation from Cyclic Voltammetry

Energy density is the measure of how much energy a battery contains in proportion to its weight. This measurement is typically presented in Watt-hours per kilogram (Wh/kg). A watt-hour is a measure of electrical energy that is equivalent to the consumption of one watt for one hour. Power density is the measure of how quickly the energy can be delivered, rather than how much-stored energy is available. The energy density (E) in Wh/kg and specific power (P) in W/kg were calculated according to the following equations 3.6 and 3.7 according to (Tsubota et al., 2018; Qanytah et al., 2020):

$$E = \left(\frac{C * 1000}{2 * 3600}\right) * (\Delta V)^2 \qquad 3.6$$

$$P = \frac{E * 3600}{\Delta t} \qquad 3.7$$

Where, where C (F/g) is the specific capacitance, ΔV (V) is the operating potential window, and Δt (s) is the discharge time.

3.6 Electrochemical wastewater treatment via biochar electrode

3.6.1. Synthetic Wastewater Sample Preparation

Synthetic COD-containing wastewater was prepared by diluting 2.811 g of glucose in 1 liter of distilled water using the stoichiometric relationship presented in the appendix to get an initial COD concentration of 3000 mg/L as a wastewater source. After that, the diluted sample was uniformly mixed and processed for treatment (Ivanova et al., 2016). A pH of 7.11 is measured in the prepared wastewater sample. Prepared wastewater samples are stored in a refrigerator at room temperature to reduce the affection that comes from the environment.

3.6.2 Electrochemical Setup

In an electrolytic reactor containing 75 mL of synthesized sample, the electrodes were arranged vertically and parallel to each other. The electrodes have a total surface area of 4.25 cm^2. Figure 3.7 shows setup for the electrochemical reactor. A DC power supply with a voltage and current reader, a cathode (Cu), anode (prepared electrode), an electrochemical 100 ml beaker, and NaCl electrolyte are included. The DC unit can provide a voltage of 15 V. The cathode and anode were separated by 2 cm. Then, using a combination of the electrochemical process parameters specified in Table 3.3, each process was conducted for two hours.

Table 3-3: Electrochemical treatment combination parameters

Run	**Operating parameters**	
	NaCl electrolyte concentration (g/L)	**Current density (mA/cm^2)**
1.	1	7.06
2.	2	7.06
3.	1	11.76
4.	2	11.76

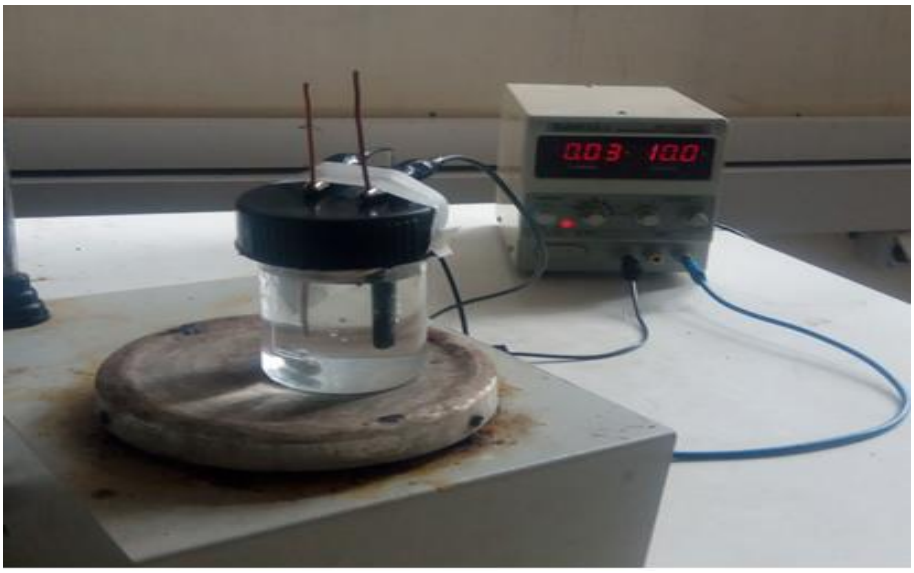

Figure 3-7: Electrochemical setup

3.6.3 Chemical Oxygen Demand (COD) Determination

Chemical Oxygen Demand is the amount of dissolved oxygen to oxidize and stabilize a sample when an organic or inorganic matter of a sample solution is responsive to a strong chemical agent. The COD value indicates the mass of oxygen consumed per liter of solution and expressed in mg/L. In COD, biodegradable and non-biodegradable will be oxidized chemically, which overestimates the biodegradable demand to consider it as one of the important parameters (Haixiu Chen et al., 2019).

The COD determination for this experiment (open titrimetric reflux) after treatment was carried out using according to the procedure (Korpe et al., 2019). To analyze the COD values for a particular sample, samples are added to the COD digestions tubes, which are kept in the digester block. 10 ml of wastewater sample and blank sample (distilled water) is individually mixed with 5.0 mL of 0.25 N potassium dichromate solution ($K_2Cr_2O_7$) followed by 15.0 mL of H_2SO_4. 0.2 g of mercuric sulfate ($HgSO_4$) is required to fix the interference of chlorine in the water sample, which gives incorrect COD estimation. The false COD estimation in wastewater occurs when Cl concentration is greater than 2000 mg/l (Costa et al., 2010). To minimize the miscalculation synthesizing wastewater samples with known Cl content is mandatory. The resultant mixture was mixed thoroughly using a magnetic stirrer. After attaining uniform mixing, the contents were

transferred to the COD cell tests, and then the cells were sealed with caps and placed in the COD digester, which was then allowed to get heated at 150 °C for 2 h. After cooling, the resulting solution was flushed into an Erlenmeyer flask and made up to 150 mL with distilled water. Then the solution was titrated with 0.1N ferrous ammonium sulfate (FAS) standard in the presence of Ferroin indicator.

The addition of 2–3 drops of Ferroin indicator to the digested sample changes the color of the digested sample into greenish-blue and the endpoint of titration being reddish-brown. Similarly, blank sample titration was carried out. Initial and final burette readings are noted before and after titration, and the COD value was calculated according to the formula. The formula used for the measurement of COD is given below.

$$\mathrm{COD}\ \left(\frac{\mathrm{mg}}{\mathrm{L}}\right) = \frac{(\mathrm{A} - \mathrm{B}) * \mathrm{N} * 8 * 1000}{\mathrm{V}} \qquad 3.8$$

Where, **A** = Volume of FAS required to achieve endpoint of titration for blank sample, **B** = Volume of FAS required to achieve endpoint of titration for wastewater sample, **N** = Normality of FAS, **8** = Milli equivalent weight of O_2 (1 mL of 1 N $K_2Cr_2O_7$ = 8 mg O_2), **1000** = Volume of solution in mL, and **V** = Volume of wastewater sample (ml).

3.6.4. Power Consumption

The operating cost of electrochemical is related to the power consumption, chemical and equipment cost. The power consumption of the electrochemical process was calculated using the following Equation 3.9 (Sundarapandiyan et al., 2010).

$$\text{Energy consumption} = \frac{\frac{\mathrm{tVA}}{\mathrm{Sv}}}{\left(\frac{\Delta\mathrm{COD}}{10^6}\right)} \left(\frac{\mathrm{KWh}}{\mathrm{m}^3}\right) \qquad 3.9$$

Where t is the time of electrolysis in (hour), V is the average cell voltage in (Volt), A is current I (ampere), Sv is sample volume in liters and ΔCOD is the difference in COD in time t in mg/L.

CHAPTER FOUR

4. RESULTS AND DISCUSSION

4.1. Moisture Content Determination

The moisture content of raw bamboo has been determined at 105 ^{o}C in three triplicates. After 6 hours, there was no noticeable weight change in the three samples, and it had an average moisture content of 8.702%. The moisture content of bamboo from different sources was 10.74% (Sahoo et al., 2021), 4.22% (R. Xu et al., 2020), 13.3% (Norakmalah Mohd Zawawi et al., 2017) and 17.02% (Qanytah et al., 2020). The obtained moisture content from this study falls in range with the assessed results earlier. Because a larger moisture content in the raw sample would absorb more heat during combustion, it needed to be reduced (R. Xu et al., 2020). When exposed to heat at a temperature of 105 ^{o}C, moisture is released after readily volatile oxygen and hydrogen release. The volatile matter skipped the precursor faster in the first three hours, but there was no change in mass in the last three hours, resulting in final moisture content of 8.702%.

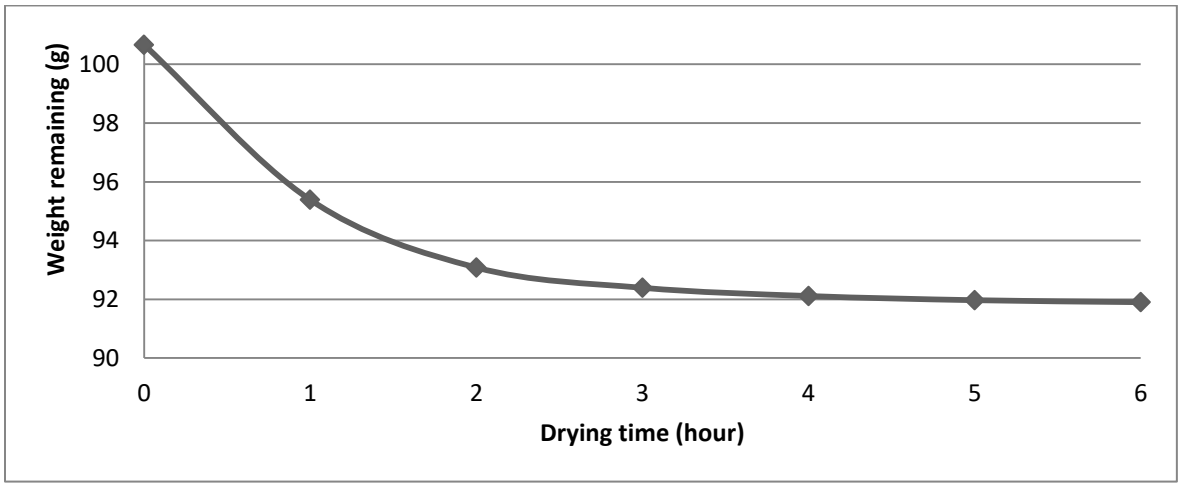

Figure 4-1: Drying curve of raw bamboo

4.2. Biochar Yield Production

From raw bamboo to have a sample with higher biochar yield four different factors such as chemical activator (KOH, NaOH, H_2SO_4, and H_3PO_4), activator chemical percentage (30, 35, and

40%), carbonization temperature (400, 600, and 900 ^{o}C), and carbonization time (30, 60 and 90 minutes) as mentioned in Table 3.2.

4.2.1. Effect of Chemical Activator

The above-mentioned parameters were used to step-by-step detect a high level of biochar. The influence of the first factor at various levels with high biochar yield is referred to as the local optimum value for that factor and the maximum value is used for the subsequent factors. Figure 4.2 shows the biochar derived by the chemical activator effect. Biochar made from inactivated bamboo produces an average biochar yield of 23.07%. The yields of the carbonization process from inactivated bamboo were from 20–25% in the range of 400–800 °C for the carbonization temperature (Tsubota et al., 2018). For bamboo, the biochar yield was obtained about 27% with an increase of the pyrolysis temperature at 600 ^{o}C (Sahoo et al., 2021). At 600 ^{o}C bamboo biochar yield was 25% (Hata et al., 2015) which agrees with the work. This signifies that activation is necessary for higher biochar yield production.

The first effect resulted in a greater biochar production of 27.51% from 30 % KOH than all the other chemical activators. It suggests that KOH may aid in the cracking of big molecular intermediates, resulting in smaller molecular gaseous products. The bamboo biochar produced a yield of 32.5% activated using KOH studied by (Qanytah et al., 2020). The higher biochar yield results from the dissociation of K and K_2CO_3 from KOH to intercalate the carbon matrix to create well-defined porosity and expand carbon lattice (Qanytah et al., 2020). This allows biochars readily to fit the application required.

H_3PO_4 treated bamboo yields 25.78% biochar yield. The phosphoric acid introduced into the interior of the precursor particle prohibited the production of tar as well as other liquids such as acetic acid and methanol during heat treatment and also prevented particle shrinkage or volume contraction according to the statement in (Ahmad & Hameed, 2009). The 25.78% bamboo biochar yield indicates that there was inadequate phosphoric acid participating in the activation than KOH used the same amount. The carbon precursor would be heavily consumed without effective development of the pore structure, implying that phosphoric acid also guarded the carbon skeleton, as opposed to the 40.2% reported by (J. Jiang et al., 2013).

A biochar yield from bamboo initiated with H_2SO_4 at 400 ^oC and 800 ^oC was 26.25 and 20.76%, respectively (Norakmalah Mohd Zawawi et al., 2017). The result from this work (22.69%) lies in between the results mentioned here. The low biochar yield (18.53%) from NaOH activated bamboo was an indication of the inadequate amount is used for the activation. Some study shows it is effective and better for activating mango, coconut residue as discussed in (Fujishige et al., 2017) giving a higher yield. Indeed, KOH significantly promoted the decomposition of biochar and volatile intermediates of bamboo (W. Chen et al., 2020) reported that KOH usually acts as a dehydrating agent that decreases oxygen and hydrogen content by increasing carbon content during activation. Comparison between biochar activation with sulfuric acid, phosphoric acid, and potassium hydroxide has shown that KOH activation resulted in a higher quantity of oxygen-containing functional groups and surface area. Here, it is observed that KOH can improve the bio char yields, which significantly improves the biomass use rate.

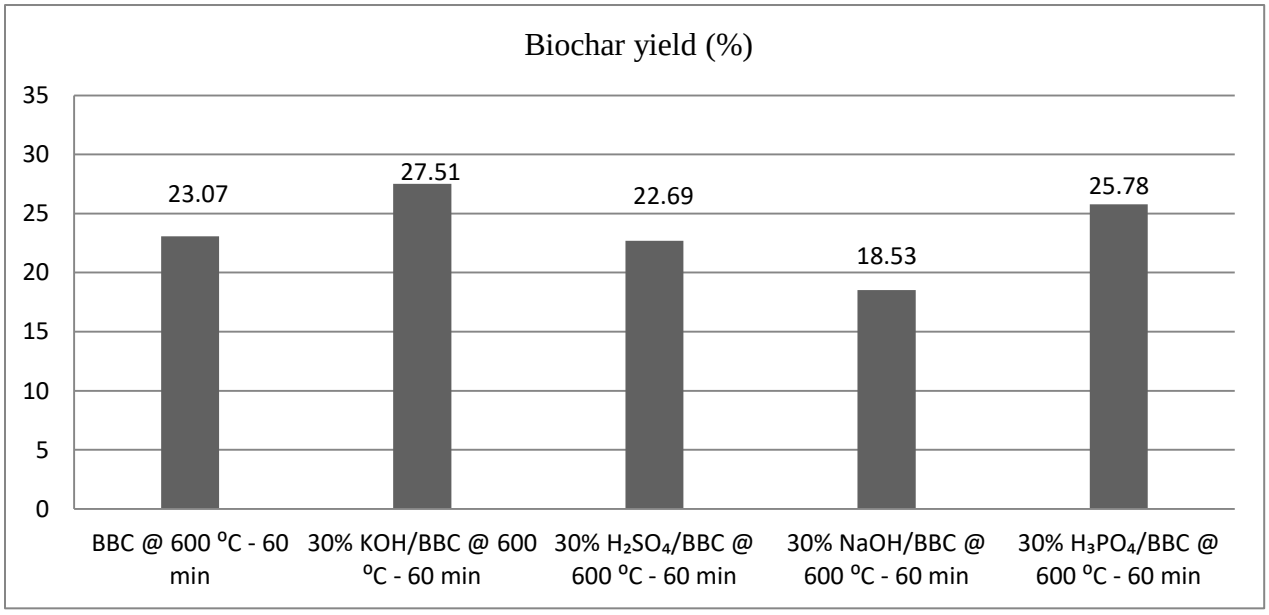

Figure 4-2: Biochar yield from chemical activator effect

4.2.2. Effect of Chemical Percentage

30% KOH yields maximum from the previously given activators, followed by biochar yield results from the chemical composition as shown in Figure 4.3with the same temperature and time as in Figure 4.2. The dosage of the activating agent is another factor that has significance on the activation process. With a KOH/biomass ratio of 2:1, the biochar yield of 17% was obtained in (W. Chen et al., 2020). This suggests that KOH may facilitate the breaking of large molecular

intermediates, resulting in smaller molecular gaseous products. The above concept reveals a high biochar result when the above ratio was increased to 3:1 of KOH/biomass fractions in this study listed in the table below. An impregnation ratio of 3:1 was also maximum biochar yield which produces the largest surface area and total pore volume as reported in (Tsubota et al., 2018). This was also stated in (Ji Zhang et al., 2017) showing that when the impregnation ratio KOH to bamboo increased from 3:1 to 5:1, the yield of biochar decreased.

The most suitable chemical percentage produces high yield biochar also as stated in (Ji Zhang et al., 2017). From this experiment optimum biochar yield at 35% KOH was obtained in case of chemical percentage variation. This was because KOH promoted the dehydrating effect and the formation of cross-links during the heat treatment, which led to some volatile matter, produced at 40% KOH/BBC and insufficient amount for activated in case of 30% KOH. The excessive chemical agent would break the framework in the activated carbon (Jubing Zhang et al., 2011). At high KOH concentration, the higher reactivity of KOH allows the biomass material to disintegrate its structure to produce low bio char yield. At lower concentrations, enough KOH is absent to activate the biomass properly to have a high yield.

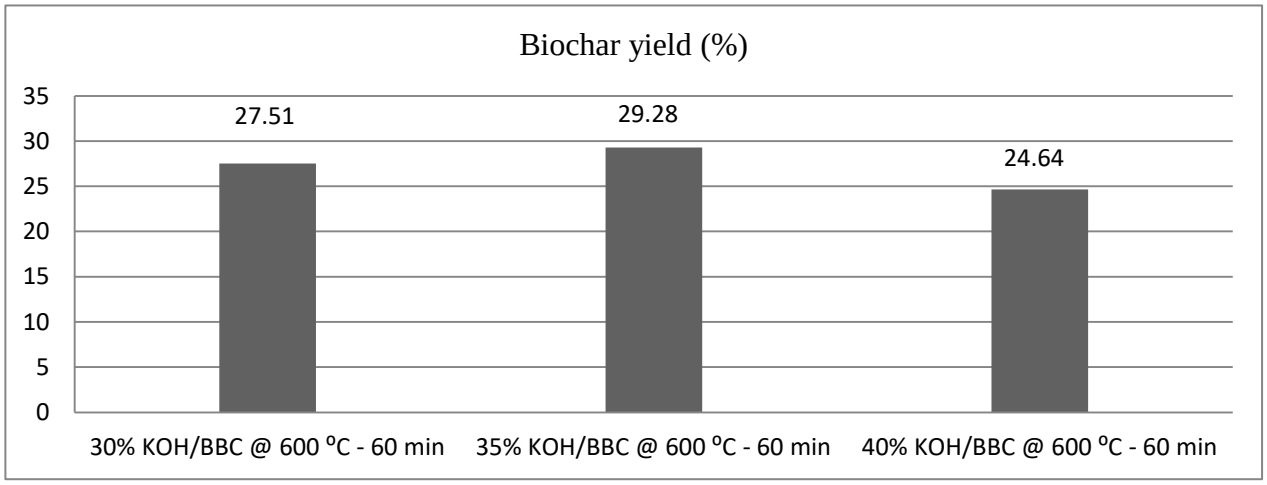

Figure 4-3: Biochar yield from chemical percentage effect

4.2.3. Effect of carbonization temperature

The goal of the study of this effect was to examine the interplay of bamboo biomass pyrolysis in 35% KOH activation at various temperatures. Carbonization with 35% KOH at 600 ^{o}C for 60 minutes yielded more biochar of 29.28% from the previous two effects. Figure 4.4 shows the biochar production from the third carbonization effect. From (Fujishige et al., 2017) in the

literature part, weight loss up to 70% from bamboo has been reported at the temperature of 600 ^{o}C activated using KOH. When the temperature rises over a certain point, potassium vapor is vigorously diffused into different carbon layers, forming a new porous structure. However, the carbon may react too much with the K_2CO_3, resulting in the micropores combining and the framework structure collapsing. This provides an adequate explanation for the decrease in activated carbon surface area as temperature rises (Jubing Zhang et al., 2011). The reason is that at high carbonization temperature, in which most of the disorganized carbon is removed (rupture of the pore structure). When the activation temperature increased above 800 °C, the particles were burned out completely due to very high gasification rates (Parthasarathy et al., 2021). Certain oxygen and potassium metals from KOH are transformed to gas products or bio-oil at high temperatures decreasing biochar yield formation (Sahoo et al., 2021). While at lower temperatures biomasses do not decompose easily.

At low temperature mostly about 100 ^{o}C, bamboo activated with KOH releases H_2O and CO_2 indicating that KOH is attached to the biomass that is converted to $KHCO_3$ by absorbing surrounding H_2O and CO_2. At a temperature reached around 200°C, $KHCO_3$ is rapidly decomposed, which coincided with the increase of weight loss due to the generation of H_2O and CO_2. As shown in the studies of (B. Xu et al., 2010; Zhou et al., 2012) the probable reaction between KOH and bamboo above a temperature of 580 ^{o}C are as follow:

$$6KOH + 2C \longrightarrow 2K + 3H_2 + 2K_2CO_3 \quad (1)$$

$$KOH + (- O - CH_3) \longrightarrow K_2CO_3 + K + H_2 + CH_4 \quad (2)$$

$$KOH + (C - H) \longrightarrow K_2CO_3 + K + H_2 \quad (3)$$

$$KOH + (- COOH) \longrightarrow K_2CO_3 + K + H_2 + CO_2 \quad (4)$$

$$K_2CO_3 \longrightarrow K_2O + CO_2 \quad (5)$$

$$CO_2 + C \longrightarrow 2CO \quad (6)$$

$$K_2CO_3 + 2C \longrightarrow 2K + 3CO \quad (7)$$

$$K_2O + C \longrightarrow 2K + CO \quad (8)$$

(Ji Zhang et al., 2017) Also mentioned that the proper temperature is required for carbon pore development; a higher temperature would result in excessive activation reactions, which would have adverse effects on the development of internal pores due to the overburn-off of lignin, as well as cellulose and hemicellulose, resulting in a lower yield. A low biochar yield (17.5%) from KOH activated bamboo obtained in (Mahanim et al., 2011) was due to the high volatile content and high pyrolysis temperature (600 ^{o}C). Organic chemicals become unstable at higher temperatures because heat supplies energy to the molecules, causing them to break their bonds and connections, which causes the substances to be released as gas and liquid products (Mahanim et al., 2011). Due to the boiling point of K (760 ^{o}C), activation with KOH at high temperatures gives only a limited amount of biochar, resulting in carbon burn-off (Sajjadi et al., 2019). At higher temperatures KOH has a small effect on biochar yield formation, since a burn-off, even the lignin component occurs at maximum heat supply.

And the yields decrease with the increase of the activation temperature. These were mainly because of C-KOH reaction resulted in pore formation and carbon atom consumption of activated carbon. While the pore development of carbon needs the appropriate temperature, a higher temperature would result in excessive activation reactions that cause adverse effects on the development of internal pores. Then some micropores, which account for the large specific surface area, could be converted to mesopores due to over burn-off and resulted in the reduction of yield.

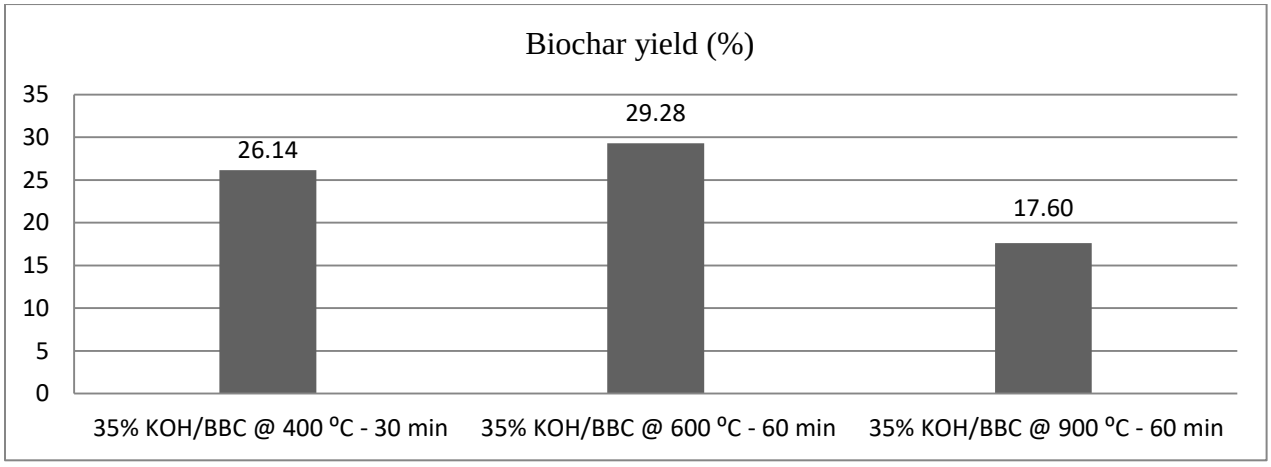

Figure 4-4: Biochar yield from carbonization temperature effect

4.2.4. Effect of Carbonization Time

In the biochar generation from the above three parameters investigated, from the effect of chemical activator with KOH, from chemical percentage concentration at 35%, and from carbonization temperature at 400 ^{o}C was considerably yielding high biochar yield. So, based on the previous study, three parameters were connected to the effect of carbonization time to produce a fourth that produces a large amount of biochar. Figure 4.5 shows the biochar yield due to the time effect. A long enough residence time changes the structure of carbon atoms, causing char particles to constrict. The collapse of microstructure is caused by the shrinking of pores, which diminishes the surface area (Parthasarathy et al., 2021). Pyrolysis did not have enough time to stimulate the creation of pores due to the shorter carbonization time, resulting in limited adsorption capacity. While a long carbonization period may result accelerates surface erosion also this statement is mentioned in (B. Xu et al., 2010; J. Jiang et al., 2013; Ivanova et al., 2016).

(Parthasarathy et al., 2021) When the pyrolysis period was prolonged from 1 h to 4 h under N_2 flowing inert gas, the biochar yield reduced from 23.2 to 20.22%. This stresses that increasing the holding period decreased the carbon, hydrogen, and nitrogen composition, which can be attributed to carbon burn-off. With activated bio char, the results from time variation match this hypothesis: 26.98% at 30 minutes, 26.24% at 90 minutes, and 35% KOH at 600 °C. At this point, the local maximum biochar output is 26.98% after 30 minutes of carbonization.

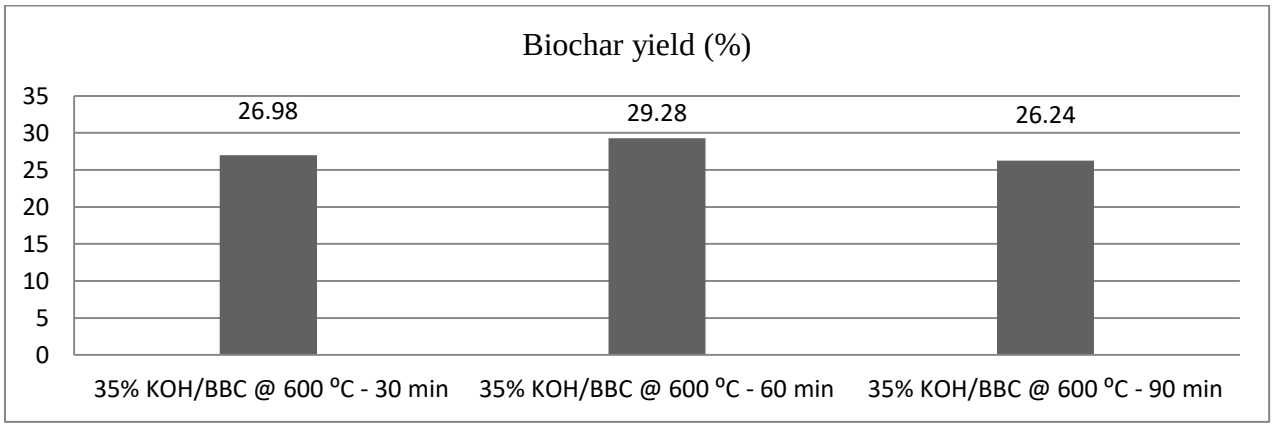

Figure 4-5: Biochar yield from carbonization time effect

The above Figures 4.2-4.5 show the activated bamboo biochar yield after all carbonization effects have been tested. The maximum yield of 29.28 and 27.51% was obtained from 35% KOH

and 30% KOH activated bamboo carbonized at 600 ^{o}C for 60 minutes. A 26.98% bamboo biochar yield was the third-highest yield obtained by activating 35% KOH and carbonizing at 400 ^{o}C for 30 minutes. Thus, for characterization and next application three samples were chosen. The samples with the top two highest biochar yields, namely 35% KOH/BBC and 30% KOH/BBC at 600 ^{o}C for 60 minutes for both, and for comparison BBC without activation, have been nominated and preceded. (W. Zhang et al., 2019) stated that biochar produced at lower carbonization temperatures has low conductivity and is not usually used for energy storage material. According to this hypothesis even better yield is obtained at 400 ^{o}C from this work, it should be rather skipped in addition to its lower biochar yield than at 600 ^{o}C. Biochars from the pyrolysis at a lower temperature are usually applied in soil amendment improvement. Also mentioned that (Karnan et al., 2017) carbonization at higher (> 800 ^{o}C) when biochar is used in electrode preparation, does not enhance the electrode stability. From this study, even if the biochar yield at 900 ^{o}C is lower, it would hinder ensuring electrode stability to select as a base for electrode preparation. The experiments at 400 ^{o}C and 900 ^{o}C are performed for checking any significance change in biochar yield and property and assess their applicability in electrode preparation.

4.3. Characterization of biochar and its derivative

The next three sub-topics discuss results obtained from Fourier transforms infrared spectroscopy (FTIR), X-ray diffraction (XRD), and scanning electron microscopy (SEM) for raw bamboo and its biochar derivatives.

4.3.1. Fourier Transforms Infrared Spectroscopy (FTIR) Analysis

For raw bamboo, the peak at 3407 cm^{-1} indicates O-H vibration in hydroxyl groups. The location of hydrogen-bonded O-H groups usually at range 3200 – 3750 cm^{-1} for alcohol and phenol which involve in hydrogen bonding, may be due to adsorbed water (B. Xu et al., 2010; Ivanova et al., 2016). The chemical bonds of C≡C, C=O, and C=C are represented by peaks at 2135, 1720, and 1613 cm^{-1}, respectively. The small peaks represent C-O at 1360, and 1045 cm^{-1}, C=C is described in the range of 1436 cm^{-1}, while C-C is represented by the large peaks at 1253 cm^{-1}. The presence of a C-H bond can now be seen at 2916 and 594 cm^{-1}. It indicates the O-H group and C-H bond at 594 cm^{-1} wave length (Norakmalah Mohd Zawawi et al., 2017).

The above functional groups show minor alterations after being inactivated bamboo carbonized at 600 ^{o}C for 60 minutes. The loss of hydrogen and oxygen atoms due to the broken link from the O-H group is indicated by a minor peak with low intensity at 3391 cm^{-1}. This is signifying that hydrophilic groups are highly decreased. Even though the intensity at 2916 cm^{-1} decreases, the presence of C-H in aliphatic methyl and methylene groups after carbonization is ensured by a newly generated peak at 2847 cm^{-1}. This mainly came from aliphatic $–CH_2$ and alkanes $–CH_3$ as also reported in (W. Zhao et al., 2016). The reduced intensity at this peak implies the hydrogen element has been removed in large amounts after carbonization. Stretching in the C≡C bond at 2081 cm^{-1} has been observed (Armynah et al., 2019). The stretching of alkyne compounds is observed at this bond. A deforming peak at 1720 cm^{-1} attributes the disappearance of carboxylic groups a disappearing, indicating they were oxidized. It is observed due to C=O stretching vibration in ketone, carboxylic acid, or ester (Zhuang et al., 2020). The peak shift of C=C bond from 1613 to 1560 cm^{-1} having lower intensity is associated with benzene skeleton disappearance also indicated in (Ji Zhang et al., 2017). It is attributing the presence of C=C in cyclic alkene or unsaturated ketone indicating the diminishing of the hydrophilic group. The C=C bond is also visible in a newly created peak at 1452 cm^{-1} are benzenes. After carbonization, which was also reported at (Armynah et al., 2019), the C-C stretching bond is visible at 1253 cm^{-1} recommends either aliphatic or aromatic (ester and phenol). At 1154 cm^{-1} is attributed to the C-O stretching vibration of alcoholic and phenolic groups (Hata et al., 2015). Here is a highly structurally deformed BBC an indication of maximum temperature is applied to carbonize raw bamboo. The smaller presence of functional group indicates the lower involvement in mitigating pollutants from wastewater due the limited participants in the adsorption process.

When 0.01 M MnO_2 was coated into the initial biochar few changes have been observed. One of the changes was a peak shift in O-H to 3383 cm^{-1} with low intensity than the initial biochar. In addition to the above a slight shift from 1154 to 1191 cm^{-1} associating C-O groups and O-H bending (Lam et al., 2019). The last observed difference from biochar was a new small peak that appeared at 615 cm^{-1} is associated with the stretching vibration of Mn-O. This is also reported in (Gao et al., 2008) indicating the manganese presence in biochar. As previously indicated, the carbonization and activation processes had a substantial impact on the surface properties of activated materials since they destroyed aromatic rings and functional groups, resulting in the reduction and even removal of these peaks following carbonization (W. Zhao et al., 2016). The

weak attachment of Mn on the biochar surface describes the lower potential to be used in electrode preparation since its owns small energy storage capability.

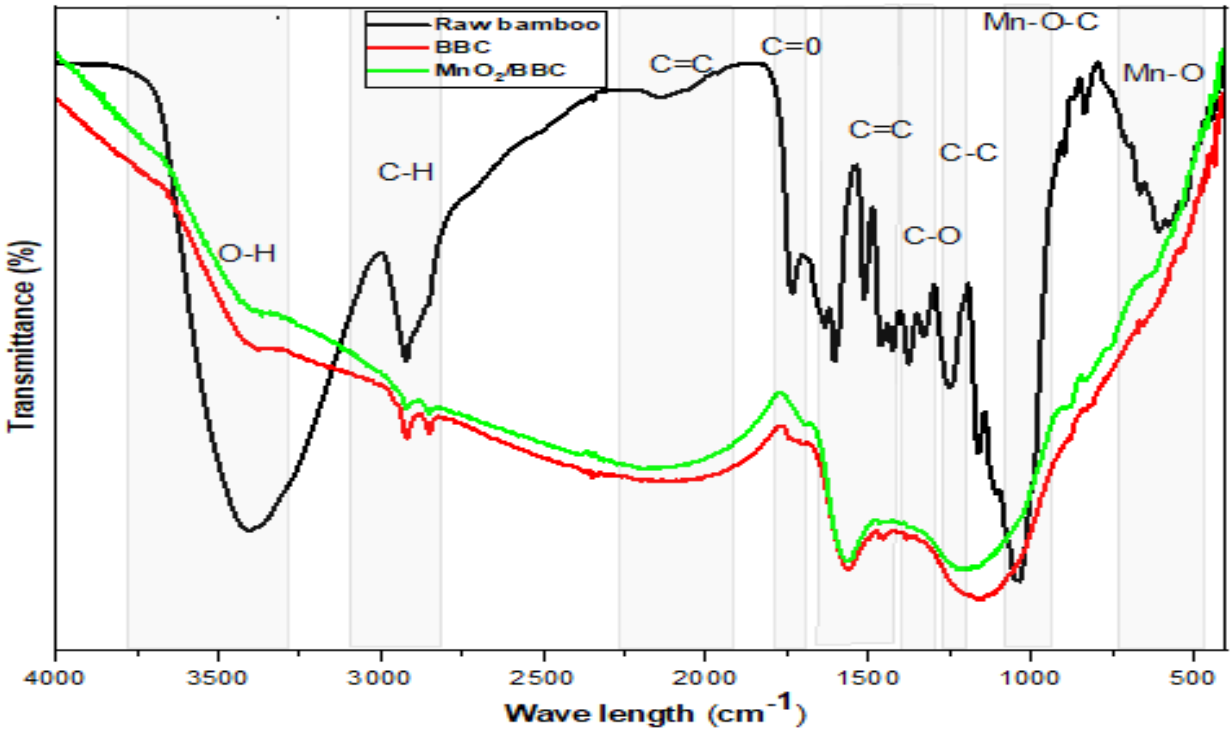

Figure 4-6: FTIR of raw bamboo, BBC, and MnO_2/BBC

Raw bamboo activated with 30% KOH and carbonized at 600 ℃ has numerous bond forms and moves. The loss of hydrogen and oxygen atoms due to the broken link from the hydroxyl group is indicated by a low-intensity peak at 3391 cm^{-1}. Because KOH has lower ionization energy when dissolved in water, it signifies that the ionic relationship between a metal atom (i.e. K) and the hydroxyl ion (OH^-) is weaker, and thus the bond can be simply broken when dissolved in water to produce an aqueous solution. In the aqueous solution of KOH, this results in the release of additional hydroxyl (O-H) ions (Qanytah et al., 2020). The peak spectrum at 2924 and 2847 cm^{-1} show the existence of C-H in aliphatic methyl and methylene groups after carbonization which came from aliphatic $–CH_2$ and alkanes $–CH_3$ also confirmed in (W. Zhao et al., 2016). Stretching in the C≡C bond at 2081 cm^{-1} has been observed also in (Armynah et al., 2019) representing the alkyne compound.

A deforming peak at 1736 cm^{-1} attributes the disappearance of carboxylic groups a disappearing, indicating they were oxidized to evolve CO and CO_2. It is also observed due to C=O stretching

vibration in ketone, organic acid, or ester (Zhuang et al., 2020). The peak shift of the C=C bond from 1613 to 1576 cm^{-1} showed C-C stretching because of the newly formed aromatic ring (Qanytah et al., 2020). Showed it could be due to corresponded to hydrophilic group remarkably decreased. At 1360 cm^{-1} shift to merged peak at 1375 cm^{-1} to indicate the C-O strength also shown in (Yimeng Zhang et al., 2017). This is representing the C–O stretching vibrations from glycosidic linkages from cellulose as indicated in (H. Lyu et al., 2019). At 1252 cm^{-1} indicates the C-C group of the either aliphatic or aromatic (Armynah et al., 2019). At 1169 cm^{-1} a stretching vibration band of C-O groups and O-H bending in alcohols (Lam et al., 2019). The newly formed peak at 877 cm^{-1} implies the C-H stretching because of the hydrogen attachment from KOH (Viglašová et al., 2018; W. Chen et al., 2020).

When 0.01 M MnO_2 was coated on 30% KOH activated biochar, a change in bonds occurred including Mn-O bond formation, which was likewise substantial compared to 0.01 M MnO_2 coated to inactivated BBC. The rise in the hydroxyl group after the injection of MnO_2 is indicated at 3636 cm^{-1}. This is due to the activated biochars free oxyl group, which easily attaches to H ions. Tiny intensity peaks show the C-H attachment at 3046 and 2832 cm^{-1} in the presence of alkene and alkanes, respectively. As shown by the result obtained at 3636 cm^{-1}, the reduction is related to the attachment of the H atom to a freely moving O-H to increase the hydroxyl group. (Qanytah et al., 2020) mentioned it as well. A deformation in C=O and C≡C bond at1720 and 2135 cm^{-1} has been obtained instead of noisy peaks appearing to show unknown bond formation in the region of 2750 to 1650 cm^{-1}. At 1552, 1386, 1207 cm^{-1} shows the presence of C=C, C-O, and C-C functional groups, respectively. At 1091 cm^{-1} shows the C-O and O-H also as reported in (Lam et al., 2019). At 992 $cm^{-1,}$ denoting the presence of the alkoxy C-O became weak significantly and attributed to the formation of Mn-O-C (Zhuang et al., 2020). In addition, a slight new band appeared at 625 and 547 cm^{-1} that is associated with the stretching vibration of Mn-O. This Mn-O formation at this peak is reported in (Gao et al., 2008; Gezahegn, 2020). This implies the insertion of MnO_2 to the biochar is more tangible than in the inactivated bamboo biochar which is has an impact on increasing energy storing ability of materials. This result shows better enhancement of abundant functional groups and Mn attachment which is favorable for adsorption of contaminants in wastewater sample than MnO_2/BBC.

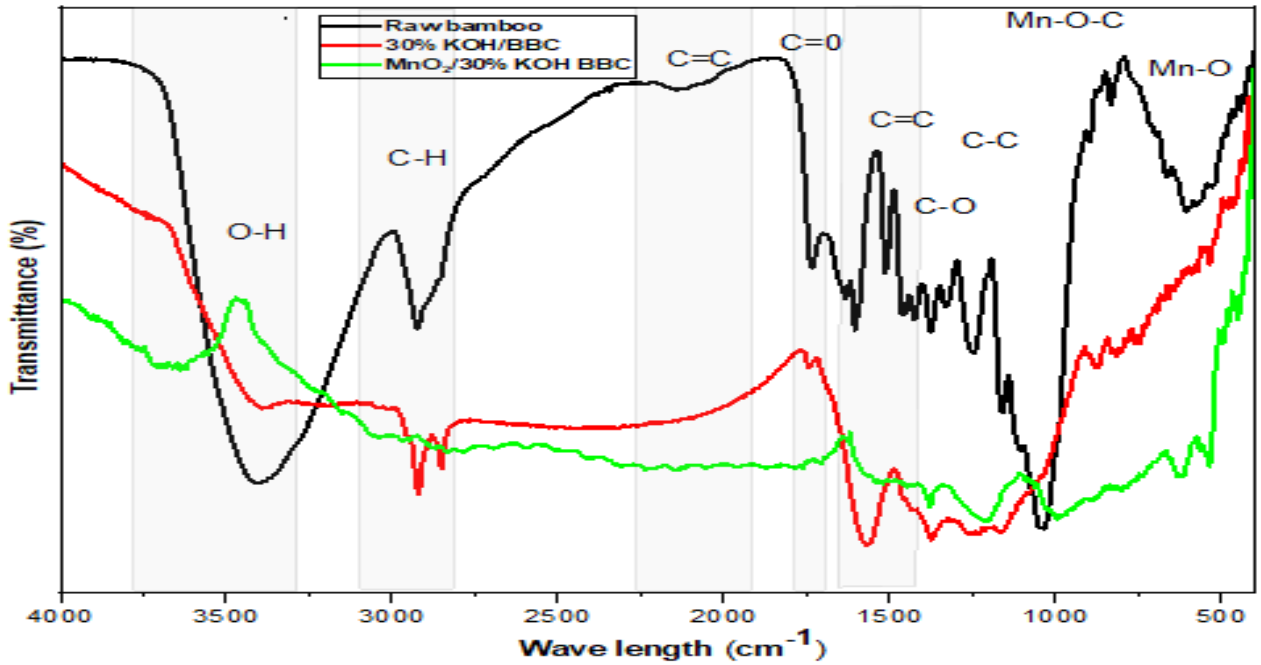

Figure 4-7: FTIR of raw bamboo, 30% KOH BBC and MnO_2/30% KOH BBC

Activated raw bamboo by 35% KOH carbonized at 600 ^{o}C effect using biochar is as indicated in Figure 4.8. A peak with low intensity at 3437 cm^{-1} indicates the increased hydroxyl group. Meaning that the added O-H group directly increases the O-H group concentration (Jubing Zhang et al., 2011). The peak spectrum at 2931 and 2854 cm^{-1} show the existence of C-H in aliphatic methyl and methylene groups after carbonization, which came from aliphatic $–CH_2$ and alkanes $–CH_3$ also shown in (W. Zhao et al., 2016). A stretching peak at 2135 cm^{-1} attributes the chemical bond of C≡C expansion of alkynes in hemicellulose being pronounced clearly at the highest temperature (Armynah et al., 2019). A deforming peak at 1744 cm^{-1} attributes the presence of C=O stretching vibration in ketone, carboxylic acid or ester also stated in (Zhuang et al., 2020). This is an indication that these groups are oxidized to evolve CO_2 and CO. The peak shift of the C=C bond from 1613 to 1576 cm^{-1} showed C-C stretching because of the newly formed aromatic ring. This is also an implication in the decrement of hydrophilic groups. (Viglašová et al., 2018; W. Chen et al., 2020) Showed it could be due to corresponded to hydrophilic group remarkably decreased. The C=C from the benzene bond appears at 1460 cm^{-1}, while the C-O strength appears at 1375 cm^{-1} from glycosidic linkages from cellulose, as indicated in (H. Lyu et al., 2019). This bond has obtained a shift from 1161 cm^{-1} after raw bamboo pyrolysis was reported at (Yong Zhang et al., 2015; Viglašová et al., 2018).

Changes happened when 0.01 M MnO_2 was coated to 35% KOH activated bamboo biochar. A decrease in the hydroxyl group at 3383 cm^{-1} attributes to the shift of hydrogen ions to increase the C-H at 2977 and 2924 cm^{-1}. A deforming peak at 1744 cm^{-1} attributes the presence of C=O stretching vibration in ketone, organic acid, or ester (Zhuang et al., 2020). At 1375 cm^{-1} to indicate the C-O strength describes the symmetric deformation vibration of -CH_3 in lignin. This represents the C–H stretching vibrations from alcohol and phenol structures or corresponding to carboxyl O=C–O (H. Lyu et al., 2019). At 1069 $cm^{-1,}$ denoting the presence of the alkoxy C-O became weak significantly and attributes the formation of Mn-O-C (Zhuang et al., 2020). In addition, new stretching peaks appeared at 655, 594, and 532 cm^{-1} that are associated with the stretching vibration of Mn-O. This Mn-O formation at this peak is reported in (Gao et al., 2008; Gezahegn, 2020). The FTIR results obtained compared with the above two; MnO_2/35% KOH BBC shows favorable Mn-O formation in its infrared spectrum. The bold Mn-O formation and presence of abundant functional groups in MnO_2/35% KOH BBC is an implication for the applicability in adsorption.

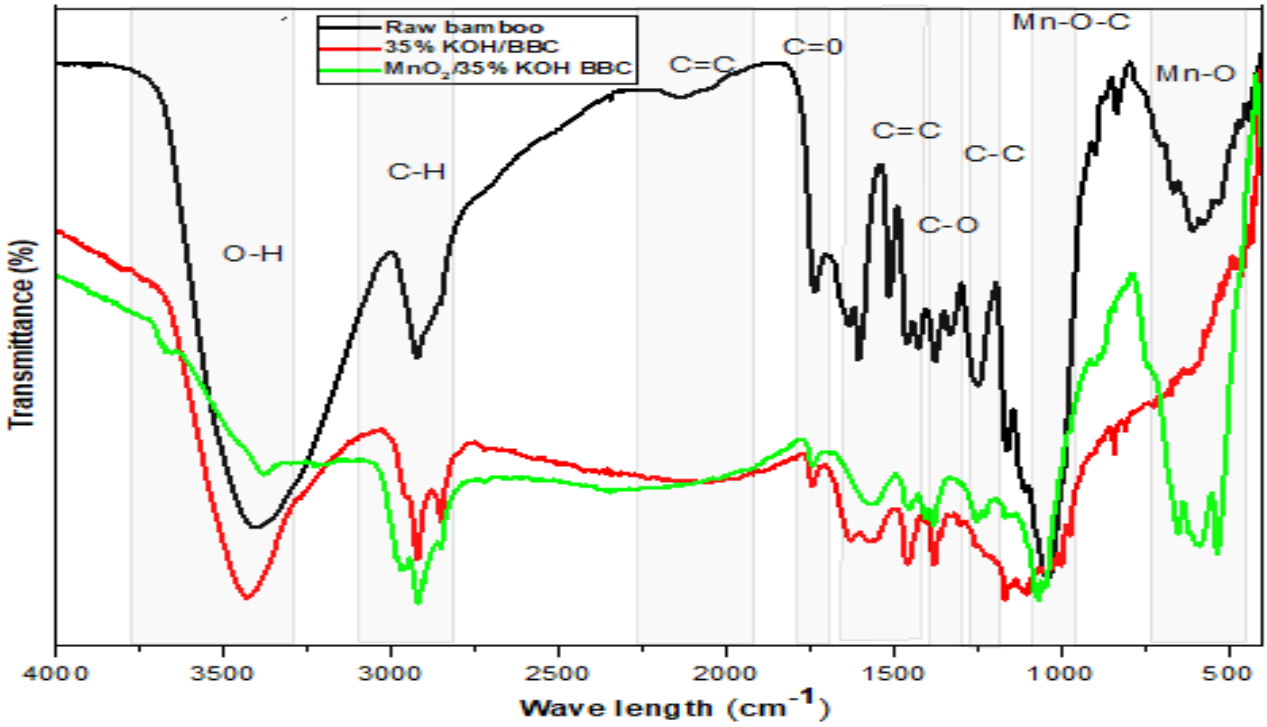

Figure 4-8: FTIR of raw bamboo, 35% KOH BBC and MnO_2/35% KOH BBC

4.3.2. X-ray Diffraction (XRD) Analysis

For raw bamboo sharp peaks at 16.29 and 21.92^{o} and weak peak at 44.05^{o} has been obtained after XRD analysis. Raw bamboo has a strong crystalline structure, as evidenced by the sharpness of the peaks. The two strong peaks at 16.29 and 21.92^{o}, representing the usual crystalline structure of cellulose (triclinic) and cellulose (monoclinic) in raw bamboo, were visible. The existence of these peaks and the crystallinity has been also mentioned in (Wen et al., 2017; W. Chen et al., 2020). The other peak at 44.05^{o} indicates the graphite band (Yimeng Zhang et al., 2017).

The carbonization of raw bamboo at 600 ℃ changes the structure by displacing the first two peaks. The two sharp peaks at 16.29 and 21.92^{o} merged into a single dispersion peak over time. The heat decomposition of cellulose resulted in amorphous carbon and aliphatic side chain formation. Carbonized bamboo's crystalline structure was reduced to 23.4^{o}, indicating an amorphous structure. This implied that the loss of the crystalline structure of cellulose in the precursor. This amorphous structure agreement is also confirmed by (Guoxiong Zhang et al., 2018). With insignificant peak shift in the strong peak at 44.05^{o} to 43.98^{o} in biochar describes graphite-like atomic order. These findings reveal that following carbonization, bamboo biochar maintained its crystalline carbon structure in this zone. This also suggests that BBC had a higher degree of graphitization, resulting in the production of a graphite monocrystalline structure, it is a sign of a good electrode material (Yimeng Zhang et al., 2017).

In the case of MnO_2 addition to the biochar one major change that occurred was a new peak formation at 37.81^{o}. This peak is an illustration of the presence of MnO_2 existence following coating. MnO_2 occurs in small quantities. The formation of MnO_2 at this point is in agreement with (Wen et al., 2017; Gezahegn, 2020). Due to the breakdown of cellulose structure, a slight peak shift from 23.4^{o} to 23.53^{o} increased the amorphous structure found in BBC. In MnO_2 coated bamboo biochar, the prominent peak at 44.04^{o} characterizes graphite-like atomic order. Based on the X-ray diffraction patterns, it can be assumed that the bamboo biochar with and without MnO_2 coating produced under various conditions has both an amorphous and crystalline structure.

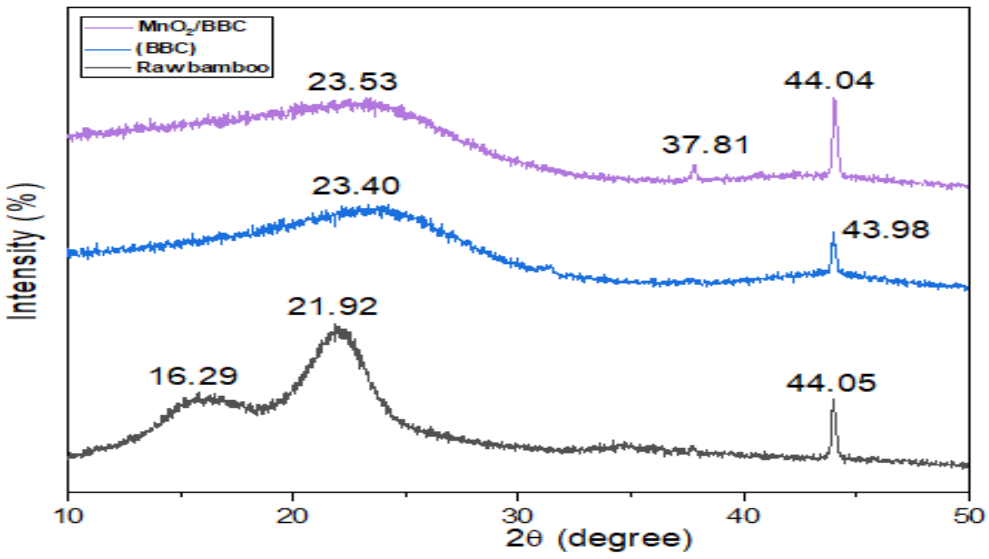

Figure 4-9: XRD of raw bamboo, BBC and 0.01 M MnO_2/BBC

30% KOH activated bamboo biochar showed at 23.8^o emphasizes the amorphous structure which implies that the loss of the crystalline structure of cellulose in chars which is visible at 16.29 and 21.92^o gradually turned into one dispersing peak. The broadening peak at 23.8° in activated BBC indicated that the atom bond gradually disappeared and established the hexagonal structures. The activation process causes inter-aromatic layers that are not symmetrical so that the degree of crystallinity decreased (Qanytah et al., 2020). At 44.04^o, the atomic order is similar to that of graphite. This result suggested that as KOH activation increased, the microcrystalline structure of cellulose gradually diminished, while crystallites gradually developed and evolved (R. Xu et al., 2020). KOH activation makes the peaks in raw bamboo sample less significant due to the breakdown of the hexagonal symmetry of the carbon lattice during the KOH activation leading to defects in the lattice in the form of layer structure defects caused by potassium intercalation from the crystalloids and the evaporation of carbon (W. Zhao et al., 2016; W. Chen et al., 2020).

Following MnO_2 coating the broad peak close to 23.13° emphasizes the amorphous structure which implies that the loss of the crystalline structure of cellulose in the raw sample (Aouni et al., 2009; W. Chen et al., 2020). After injecting MnO_2, A raises the strength of the peak at 43.73^o to show a crystalline structure. With the addition of MnO_2, the microcrystalline structure of cellulose decreased substantially, whilst crystallites gradually developed and evolved also supported by (Haixiu Chen et al., 2019; Gezahegn, 2020). In the addition of MnO_2 to the 30%

KOH activated biochar one big change that occurred was a new peak formation at 37.81°. This peak is an illustration of the presence of MnO_2 existence following coating. MnO_2 occurs in small quantities more in agreement. The formation of MnO_2 at this was also reported in (Wen et al., 2017; Haixiu Chen et al., 2019; Gezahegn, 2020). This amorphous structure facilitates the electrolyte's capability to insert into/expel from the MnO_2 matrix, resulting in a larger contact area between electrode and electrolyte, which is ideal for optimizing capacitance performance (Yong Zhang et al., 2015). From the XRD results, it can be thought that the produced bamboo biochar activated using 30% KOH with and without MnO_2 addition at different conditions owns both amorphous and crystalline structures collectively.

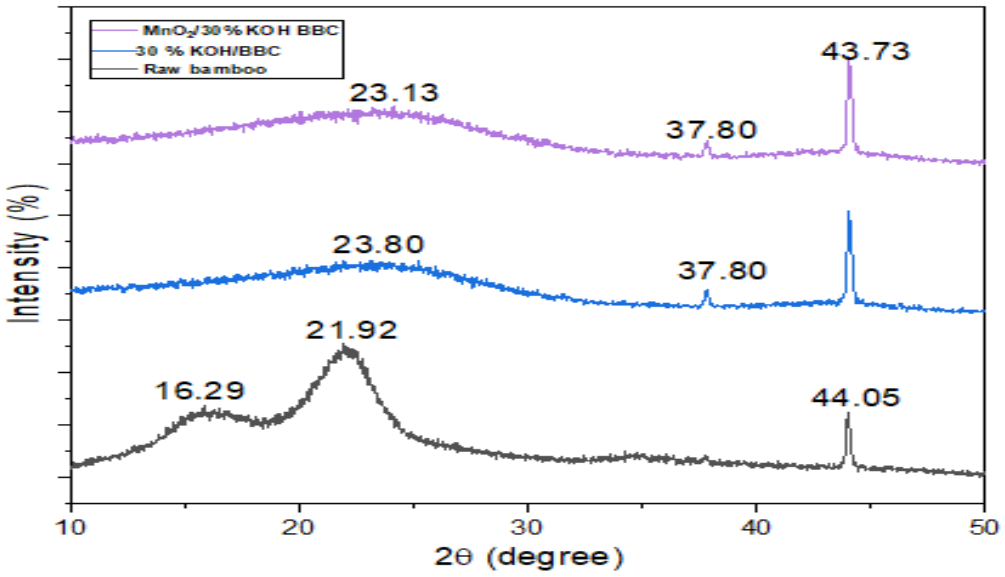

Figure 4-10: XRD of raw bamboo, 30 % KOH BBC and 0.01 M MnO_2/30 % KOH BBC

Bamboo activated by 35% KOH a shift in peak to 23.53° emphasizes the amorphous structure which implies that the loss of the crystalline structure of cellulose in the biochars. The characteristic peak at 16.29 and 21.92° of the activated biomass carbons significantly decreases in intensity and broadens in width, indicating the orderliness in the atomic arrangement has been increasingly destroyed after the KOH activations the same as in (Aouni et al., 2009; W. Chen et al., 2020). This is due to the formation of high levels of in-plane condensation, which should greatly enhance the electrical conductivity (Li & Wu, 2015). At 43.98° represents graphite-like atomic order. This result indicated that the microcrystalline structure of cellulose gradually decreased, while the crystallites gradually formed and evolved with the increase in KOH

activation (R. Xu et al., 2020). KOH activation makes the peaks in raw bamboo sample less significant due to the breakdown of the hexagonal symmetry of the carbon lattice during the KOH activation leading to defects in the lattice in the form of layer structure defects caused by potassium intercalation from the crystalloids and the evaporation of carbon (W. Zhao et al., 2016).

In the case of MnO_2 coating broad peak close to 23.43° emphasizes the amorphous structure, which implies that the loss of the crystalline structure of cellulose in chars (Qanytah et al., 2020). A increases the intensity of peak at 44.05^o after MnO_2 addition to representing crystalline structure. This result indicated that the microcrystalline structure of cellulose gradually decreased, while the crystallites gradually formed and evolved with MnO_2 addition (Wen et al., 2017; Gezahegn, 2020). I n the addition of MnO_2 to the activated biochar one big change that occurred was a new peak formation at 37.81^o. This peak is an illustration of the presence of MnO_2 existence following coating. MnO_2 occurs in small quantity more in agreement with (Wen et al., 2017; Gezahegn, 2020). This amorphous structure is beneficial to the electrolyte to insert into or expel out from the MnO_2 matrix, leading to an increased contact area between electrode and electrolyte, which is much favorable for enhancing their capacitance performance (Yong Zhang et al., 2015). From the XRD analysis, 30% KOH activated bamboo biochar and coated by MnO_2 at different conditions owns both amorphous and crystalline structures.

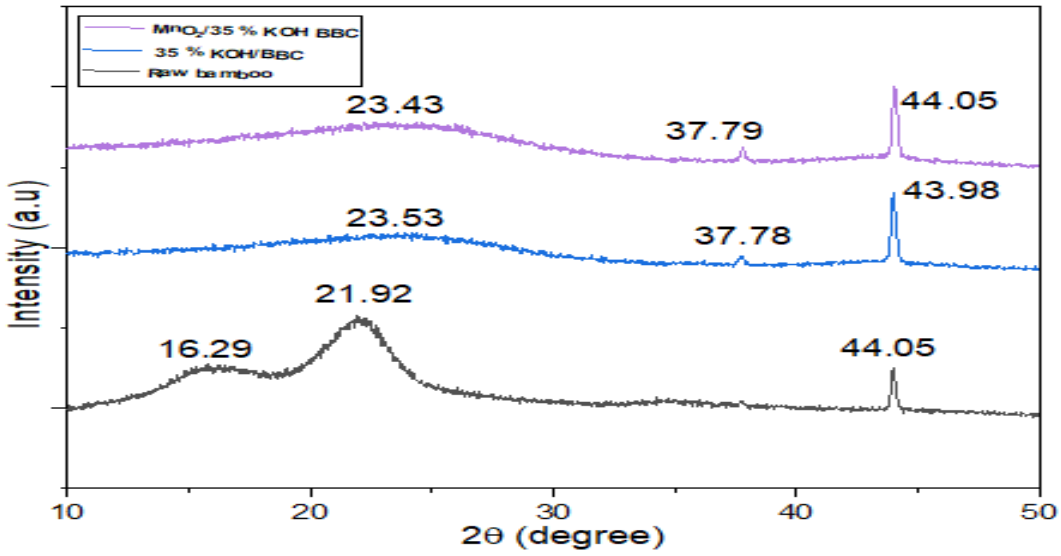

Figure 4-11: XRD of raw bamboo, 35% KOH BBC and 0.01 M MnO_2/35% KOH BBC

Table 4.1 shows the average d-spacing of activated and coated bamboo biochar and in comparison with its precursor. (Qanytah et al., 2020) Reported that porosity creation is directly associated with widening the space between the crystals in samples. This notion is supported by findings from this study, which show that the distance between crystals in the precursor is less than that of activated and coated biochars. As shown in the table, the d-spacing value of bamboo biochar after activation is lower than that of activated biochar after coating. D-spacing is greater in MnO_2/35% KOH BBC, indicating maximum pore formation. The pore structure is established when the gap between basic crystals is cleansed of tar and other components during the coating and activation process. (Qanytah et al., 2020) Also, the minimum space between crystals, the more crystalline material is less effective in penetrating electrolytes, which is less effective in electrochemical application and adsorption/desorption.

Table 4-1: Average d-spacing and average crystal size from XRD analysis

Sample	Average d-spacing (nm)
Raw bamboo	0.022
BBC	0.296
MnO_2/BBC	0.310
30% KOH/BBC	0.304
MnO_2/30% KOH BBC	0.326
35% KOH/BBC	0.318
MnO_2/35% KOH BBC	0.340

4.3.3. Scanning Electron Microscopy (SEM) Analysis

Even though amorphous structure appears in all inactivated bamboo biochar, 30% KOH and 35% KOH/BBC, 35% KOH/BBC show more functional groups in its spectrum and visible Mn-O attachment after MnO_2 coating. For another comparison, 35% KOH/BBC and MnO_2 coated 35% KOH/BBC was analyzed their morphological structure using SEM analysis. The SEM micrograph of the samples is shown in Figures 4.12 and 4.13. After chemical activation, pores of various shapes and sizes are readily visible on the 35% KOH/BBC surface. Pore developments were induced by the breakup of some material in the precursor due to thermal expansion during the activation stage, as can be seen in figure 4.12. When the precursor is exposed to a high

activation temperature, the reaction rate between the activating agent, KOH, and carbon increases, resulting in the creation of pores (Hao Chen et al., 2015; W. Chen et al., 2020). In Figure 4.9, there are several nano-sized holes in the skeleton of activated carbon, which may have been caused by KOH etching during the activation process. The 35% KOH/BBC electrolyte's hierarchical porous structure improves ion movement and permeability. Carbon gasification and potassium metal intercalation are involved in KOH activation, which is short-lived. The creation of macropores on the carbon surface is driven by gasification as also reported in (Qanytah et al., 2020).

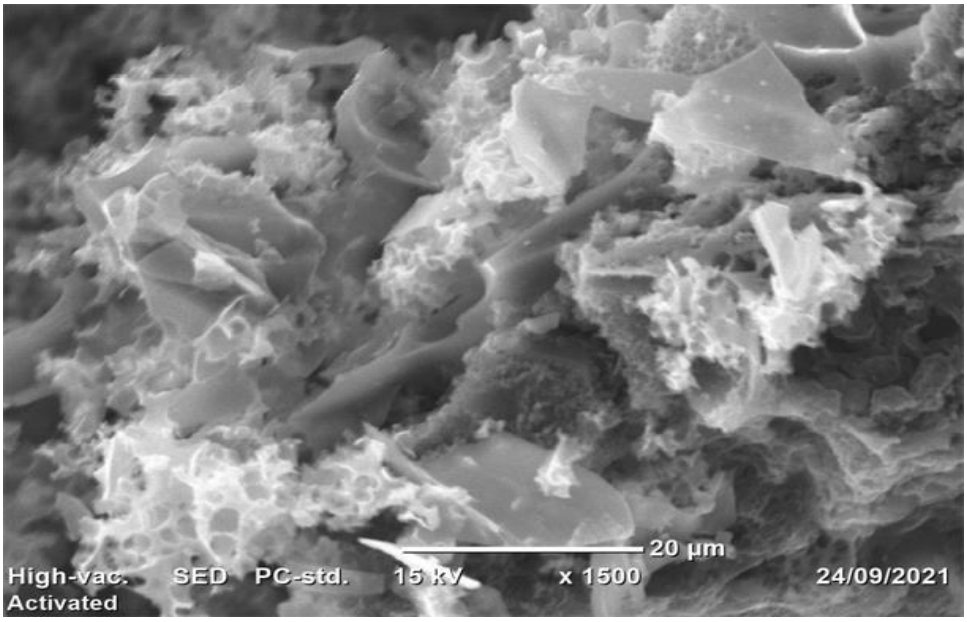

Figure 4-12: SEM image for 35% KOH BBC

As shown in Figure 4.13, MnO_2 particles affection can be seen on the 35% KOH BBC surface, which proves that MnO_2 particles were successfully anchored on the activated carbon due to the chemical coprecipitated method. On the surface of MnO_2 coated activated bamboo biochar, rough particles and big pores in a honeycomb form. The MnO_2 particles with large channels will help enhance the overall electrolyte penetration, which has been reflected also in (Gezahegn, 2020) and provide high specific capacitance critical to the capacitive materials. The activated carbon's enormous surface area and porous structure are due to its well-developed pores and distributed particles. Both things have a consolidated mesoporous structure. The effect of MnO_2

addition on porosity improvement is also witnessed in XRD analysis using d-spacing and amorphous structure formation.

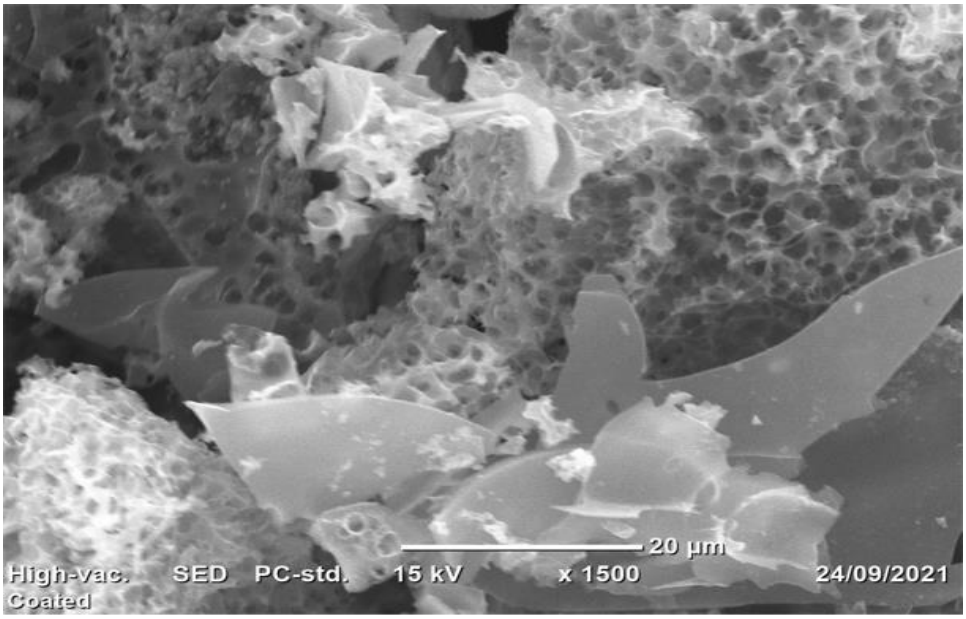

Figure 4-13: SEM image for MnO_2/35% KOH BBC

4.4. Electrode Performance Analysis

4.4.1. Cyclic Voltammetry (CV)

The CV characterization for the prepared working electrode was conducted with 0.01 M of NaCl electrolyte at 0.0-0.7 V versus SCE reference electrode different improvement under 0.01 M, 0.1 M, and 0.2 M MnO_2/35% KOH BBC concentration. The main purpose of using different MnO_2 doses is to check out the effect on the electrochemical property of the electrode. Figure 4.14 shows the CV profile for 35% KOH/BBC electrode was first assessed without MnO_2 addition. The graph appears to be shaped like a narrow leaf structure, with a smaller integrated surface area and lower specific capacitance. The best electrochemical supercapacitor electrodes have a rectangular shape and a high specific capacitance, as well as a greater integrated surface area (Zhou et al., 2012; Wen et al., 2017; Armynah et al., 2019).

The capacitance for 35% KOH/BBC electrode was 1.761, 0.301, 0.092, 0.038, 0.067, and 0.053 F/g at 5, 10, 20, 50, 100, and 200mV/s respectively. The maximum specific capacitance was obtained at a scan rate of 5mV/s; while the minimum capacitance was recorded at a scan rate of

50 mV/s. Lower scan rates have a higher specific capacitance than higher scan rates. This could be owing to the biochars property, as well as the presence of pores, which could lead to the formation of a bulk layer that blocks and reduces electrical conductivity, and hence capacity (Sofyan et al., 2018). The CV profile of 35% KOH/BBC shows a smaller surface area throughout the given scan rates. This attributes that it has low reactivity and electrochemical performance (Wen et al., 2017; Hui Chen et al., 2020) agreed with this statement that the higher surface area in cyclic voltammetry graph, the higher electrochemical activity to ensure the free movement of ions that is beneficiation in contaminant mitigation like in CDI technology. The lower specific capacitance registered from the prepared electrode suggests that bio char owns low energy storing ability to be used as electrode material.

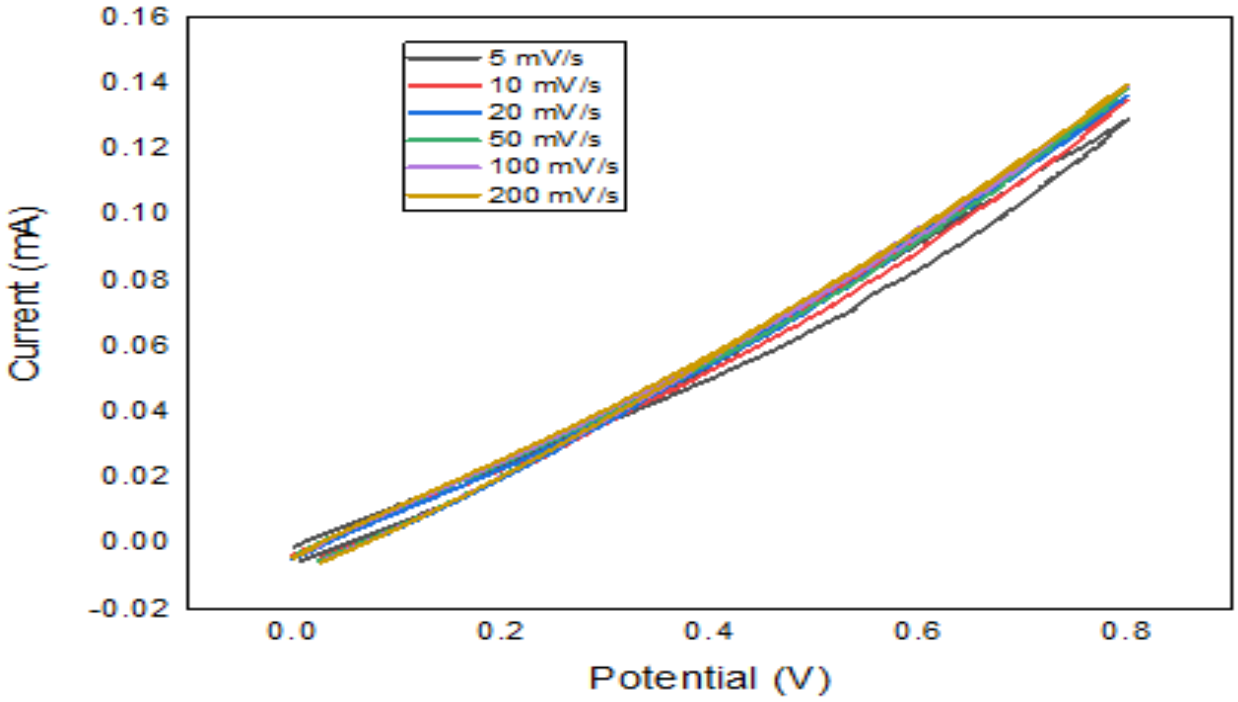

Figure 4-14: CV profile of 35% KOH/BBC with a potential difference of 0.0-0.7 V vs. SCE in 0.1 M NaCl at different scan rates

Figure 4.15 demonstrates the CV profile for 0.01 M MnO_2/35% KOH BBC electrode. The CV profile for 0.01 M MnO_2/35% KOH BBC demonstrates a quasi-rectangular-like structure. It approaches an imaginary CV profile structure, which is maximum electrode performance (Zhou et al., 2012; Hao Chen et al., 2015; Armynah et al., 2019). It should be noted that a perfect rectangular-shaped CV curve can only be found in an ideal supercapacitor. In real systems,

electrolyte ion diffusion may be obstructed by migration force and polarized resistance is expected to be produced so that the CV curve deviates from the ideal rectangle. Furthermore, heteroatoms such as MnO_2 present in carbon may undergo faradic redox reaction and the CV curves deviate from the rectangular shape, the approximately rectangular shaped CV curve is retained even at higher scan rates, which is an indication of rapid electrolyte ion diffusion even at higher scan rates (Shrestha et al., 2016).

0.01 M MnO_2/35% KOH BBC electrode has a greater integrated surface area and higher specific capacitance than the 35% KOH/BBC electrode seen above. The large areas encompassed by the CV curves verify the strong capacitive response of the as-fabricated electrode. The asymmetry of the CV curves at 0.01 M MnO_2/35% KOH BBC verifies the presence of a capacitive effect endowed by MnO_2 coating (Hao Chen et al., 2015). The greater surface area of 0.01 M MnO_2/35% KOH BBC than 35% KOH/BBC implies that 35% KOH BBC is only served as the substrate to provide a large specific surface area and good electrical conductivity for the active MnO_2 coating (Wen et al., 2017). The resulting higher surface area results in better electrolyte access and ion diffusion. The specific capacitance of 0.01 M MnO_2/35% KOH BBC electrode was 75.281, 68.624, 45.546, 37.346, 12.708 and 3.823 F/g at 5, 10, 20, 50, 100, and 200mV/s respectively. Maximum specific capacitance (75.281 F/g) is achieved at a 5 mV/s scan rate, while minimum capacitance was obtained at 200 mV/s scan rate which is 3.823 F/g. The justification for the specific capacitance being higher at lower scan rates than at higher scan rates is due to the uneven presence of manganese and carbon, which may begin to create a bulk layer that blocks and reduces electrical conductivity and, therefore capacity (Sofyan et al., 2018). This is supported by the fact that (Zhuang et al., 2020) specific capacitance falls as the scan rate rises, since ions do not have enough time to flow into electrode material at high scan rates, and hence some internal active MnO_2 cannot be fully exploited. These results reveal that the 0.01 M MnO_2/35% KOH BBC has good cycling stability and reversibility compared with 35% KOH/BBC. A larger area of the CV curve, which is due to the incorporation of MnO_2 improving the overall specific capacitance.

The CV of 35% KOH/BBC electrode presented separately in Figure 4.14 was much lower than that of 0.01 M MnO_2/35% KOH BBC electrode as plotted in Figure 4.15. Compared to the 35% KOH/BBC electrode, 0.01 M MnO_2/35% KOH BBC electrode revealed a larger integral CV.

The approximately rectangular cyclic voltammetry structure indicates maximum electrochemical stability and low polarization effect. This confirmed that the 0.01 M MnO_2/35% KOH BBC electrode exhibited excellent electrocatalytic activity. These improved properties could enhance the electron transfer kinetics of 0.01 M MnO_2/35% KOH BBC electrode via the reactive defects on graphitic structure, the larger surface area the appropriate pore system, and the abundant functional groups (H. Lyu et al., 2019).

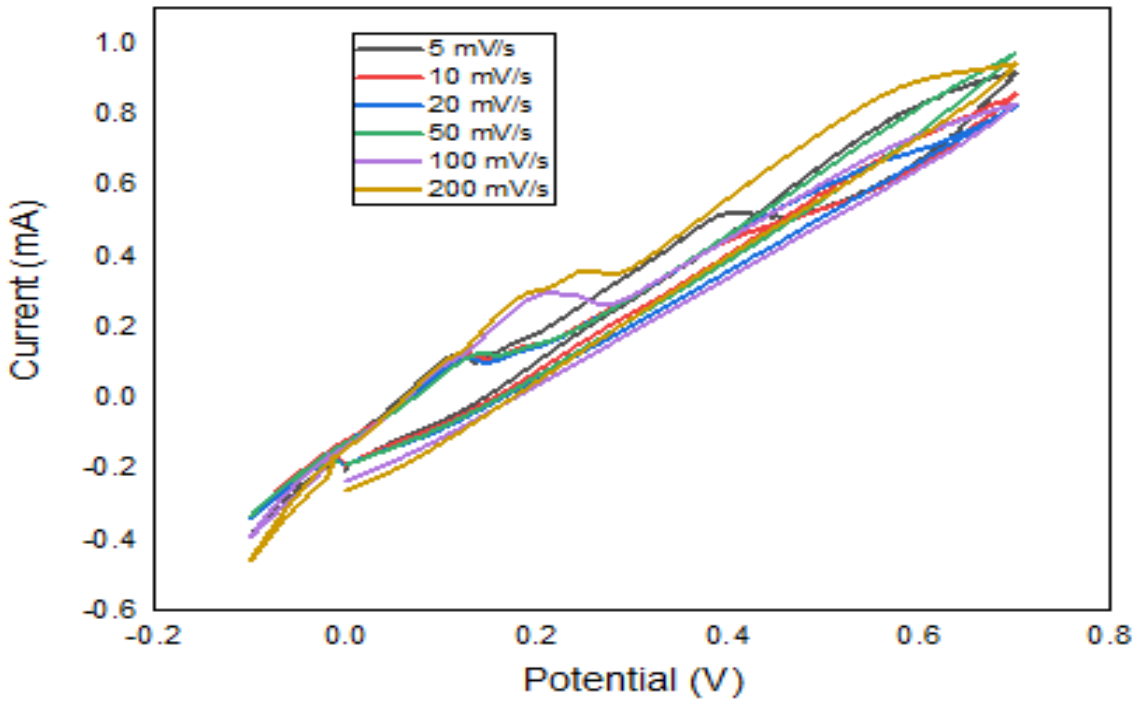

Figure 4-15: CV profile of 0.01 M MnO_2/35% KOH BBC composite with a potential difference of 0.0-0.7 V vs. SCE in 0.1 M NaCl at different scan rates

Figure 4.16 shows the CV profile for 0.1 M MnO_2/35% KOH BBC electrode. The CV profile for 0.1 M MnO_2/35% KOH BBC looks leaf-like structure with smaller integrated surface area and lower specific capacitance than 0.01 M MnO_2/35% KOH BBC electrode and higher than 35% KOH/BBC electrode. The specific capacitance of 0.1 M MnO_2/35% KOH BBC electrode was 8.192, 4.935, 3.088, 1.071, 0.422 and 0.145 F/g at 5, 10, 20, 50, 100 and 200mV/s respectively. The maximum specific capacitance of 8.192 F/g is achieved at a 5 mV/s scan rate, while minimum capacitance (0.145 F/g) was obtained at a 200 mV/s scan rate. As mentioned above, the high specific capacitance at lower scan rates is due to the uneven presence of

manganese and carbon and the presence of pores might start forming a bulk layer that blocks and decreases the electrical conductivity and thus the capacity (Sofyan et al., 2018). In practical systems, migration force may hinder electrolyte ion diffusion, and polarization resistance is expected to result, causing the CV curve to diverge from the ideal rectangle. Carbon heteroatoms can undergo faradic redox reactions, causing CV curves to vary from a rectangular shape (Shrestha et al., 2016). However, within the studied potential window, we did not observe such faradic redox reactions from the oxygen heteroatom. The minimum specific capacitance from 0.1 M MnO_2 coated bio char than 0.01 M MnO_2/35% KOH BBC is that when excess manganese is used in bio chars its lower conductivity affects the movement of ions. In addition to its poor conductivity, the smaller electrolyte concentration could be the other factor and inappropriate MnO_2 incorporation.

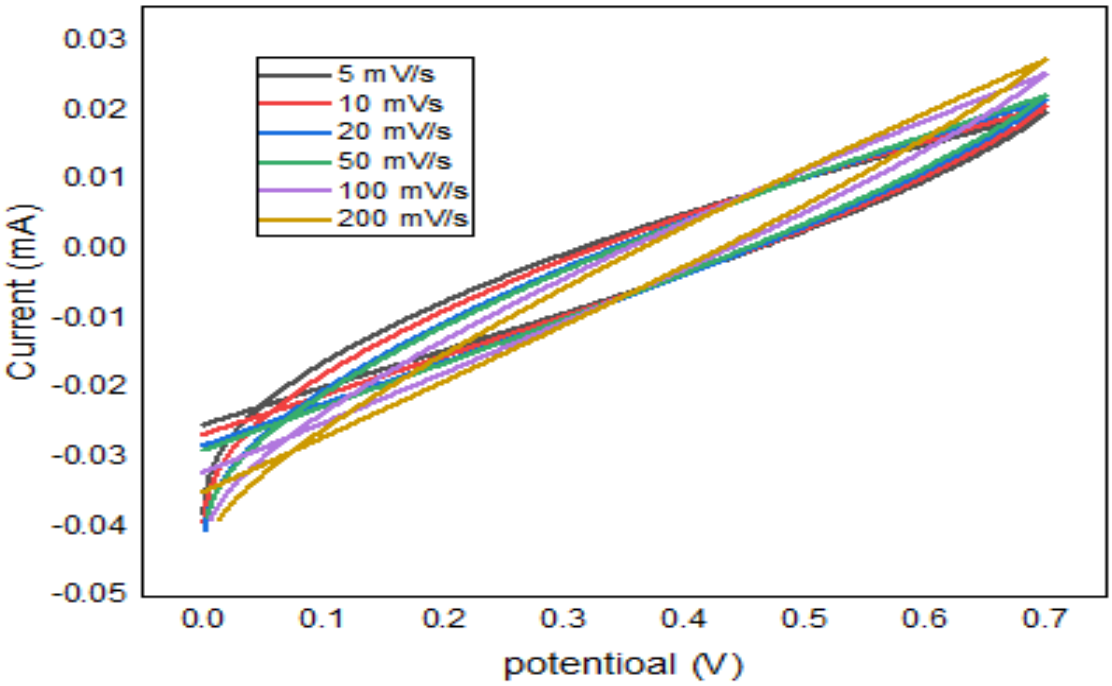

Figure 4-16: CV profile of 0.1 M MnO_2/35% KOH BBC composite with a potential difference of 0.0-0.7 V vs. SCE in 0.1 M NaCl at different scan rates

Figure 4.17 shows the CV profile for 0.2 M MnO_2/35% KOH BBC electrode. Compared to 0.01 M MnO_2/35% KOH BBC-based electrode the CV profile for 0.2 M MnO_2/35% KOH BBC looks leaf-like structure with smaller integrated surface area and low capacitance but greater than 0.1 M MnO_2/35% KOH BBC electrode and 35% KOH/BBC electrodes. The specific capacitance of

0.2 M MnO_2/35% KOH BBC electrode was 16.523, 16.781, 21.419, 8.413, 6.995 and 4.597 F/g at 5, 10, 20, 50, 100, and 200mV/s respectively. Maximum specific capacitance (21.419 F/g) is achieved at a 20 mV/s scan rate, while a minimum capacitance of 4.597 F/g was obtained at a 200 mV/s scan rate. The electrochemical characteristics of 0.2 M MnO_2/35% KOH BBC electrode are higher than 35% KOH/BBC and 0.1 M MnO_2/35% KOH BBC electrode in terms of the specific capacitance obtained at different scan rates and the total integrated surface area. Compared to the 0.01 M MnO_2/35% KOH BBC electrode, it has a lower specific capacitance and total integrated surface area and a leaf-like structure that is far from optimal. The vast areas covered by the CV curves demonstrate the electrode's robust capacitive response as-fabricated. This is because increasing the specific surface area improves electrolyte availability and ion diffusion (Hao Chen et al., 2015). The same reason is applied as for 0.1 M MnO_2 coated biochar electrode for the low capacitance recording.

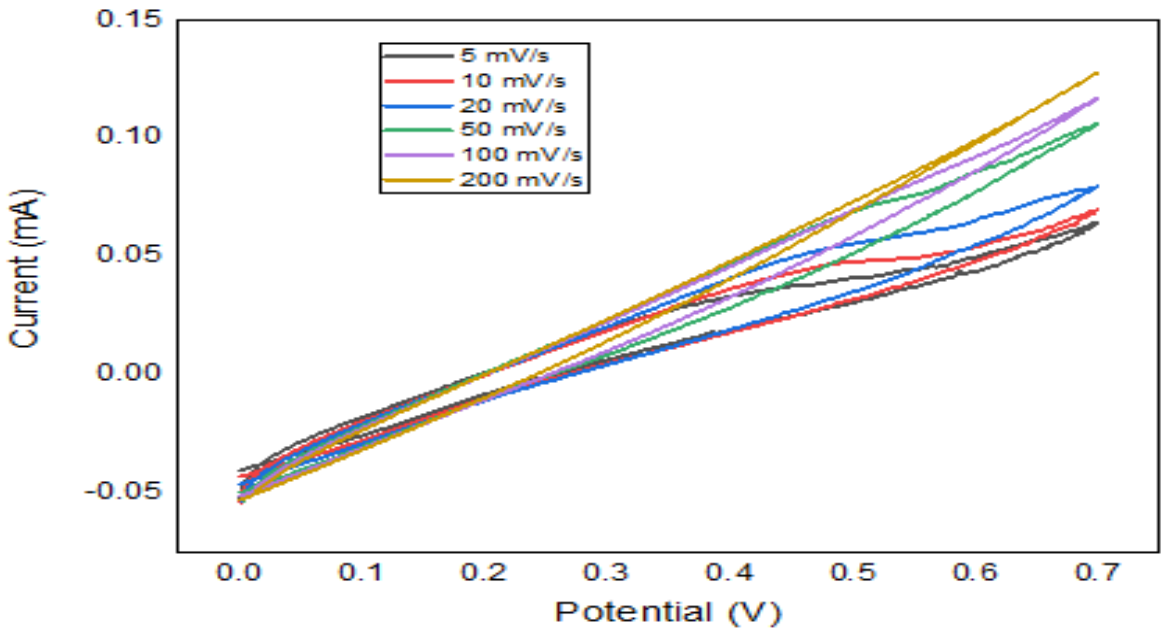

Figure 4-17: CV profile of 0.2 M MnO_2/35% KOH BBC composite with a potential difference of 0.0-0.7 V vs. SCE in 0.1 M NaCl at different scan rates

From Figure 4.18 the maximum specific capacitance of the as-prepared electrodes from 35% KOH/BBC, 0.01 M MnO_2, 0.1 MnO_2 and 0.2 M MnO_2/35% KOH BBC composites are 1.761, 75.281, 8.192 and 21.419 F/g, respectively. A higher MnO_2 loading does not facilitate the achievement of high capacitance. 0.01 M MnO_2 gives a high specific capacitance than 35%

KOH/BB, 0.1 M MnO_2, and 0.2 M MnO_2 loadings. This indicates that the optimal 35% KOH/BBC doping amount is achieved at 0.01 M MnO_2, which is consistent with the CV results. This is supported by (Yong Zhang et al., 2015) higher MnO_2 amount coating does not enhance the specific capacitance due to its weak side (conductivity and low surface area) dominating the surface to lower the electrochemical activity. To verify whether the increased specific capacitance value of the 0.01 M MnO_2/35% KOH BBC electrode was caused by the capacitive behavior of 35% KOH/BBC in the electrode, pure 35% KOH/BBC electrode was also measured under the same condition. The specific capacitance of pure 35% KOH/BBC calculated is 1.761 F/g, which is so small that it may be negligible as compared to the composite. The superior electrochemical capacitive performance of 0.01 M MnO_2/35% KOH BBC composite material can be attributed to the combined contribution of the partly EDLCs of 35% KOH/BBC and the main redox pseudocapacitance of MnO_2 material. A high specific capacitance could be attributed to the large surface area, porous structure, good conductivity, and high degree of Mn distribution in the activated biochar. But, the specific capacitance of MnO_2 is far below its theoretical value because of poor conductivity and low electrolyte solution accessible surface area.

It can be observed that there is no presence of significant redox peak 35% KOH/BBC, 0.1 M MnO_2/35% KOH BBC and 0.2 M MnO_2/35% KOH BBC, indicating that non-faradaic reaction was involved during charging and discharging of carbon fiber (i.e. weak transfer of charges). Redox peak is a peak derived from a faradaic reaction. (Guoxiong Zhang et al., 2018; Haixiu Chen et al., 2019) also reported the good electrochemical performance of the composite electrode can be attributed to the unique network (i.e. 35% KOH/BBC in this study) with porosity and interconnectivity, which facilitates the penetration of the electrolyte into the electrode. As a result, in addition to specific capacitance surface area as a major factor for electrochemical activity, 0.01 M MnO_2/35 % KOH BBC-based electrode material ensures it is better and higher than the others described. Because of its large surface area and abundance of micropores are less distorted, encouraging ion transport into the inner pores. Among the studied results, the pore structure of 0.01 M MnO_2/35% KOH BBC is more suitable for ions of electrolytes transfer and adsorption than the other three samples, indicating that it was the promising electrode for electrochemical application than the other. (Zhou et al., 2012; Armynah et al., 2019; Haixiu Chen et al., 2019) All agreed with the relation that the high electrochemical performance of electrodes is the reflection of high surface area and high capacitance. The CV

data reveal that 0.01 M MnO_2 enhanced the current response of the 0.01 M MnO_2 toward 0.1 M NaCl, indicating increased electrochemical active sites by 35% KOH/BBC surface modification.

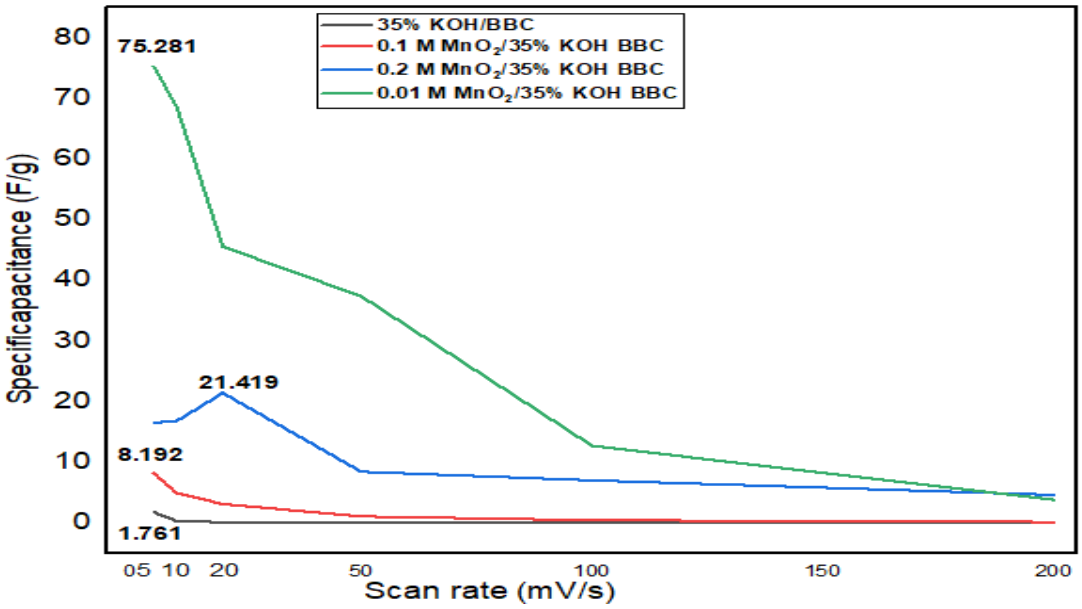

Figure 4-18: Specific capacitance from CV for 35% KOH/BBC, 0.01 M MnO_2/35% KOH BBC, 0.1 M MnO_2/35% KOH BBC and 0.2 M MnO_2/35% KOH BBC electrode with a potential difference of 0.0 - 0.7 V vs. SCE in 0.1 M NaCl at 5, 10, 20, 50, 100, and 200mV/s scan rates

4.4.2. Energy Density and Power Density Determination

The electrochemical performance of electrode materials can be also determined based on the energy density and power density of the fabricated electrode. The higher energy indicates much more energy is stored in the electrode proportional to its weight. In the case of biochar electrodes, as a biochar slurry is added to the current collector, more energy is expected to be stored. When more energy is contained in an electrode, then more ions will participate during the electrochemical process. Based on this study, a maximum energy density of 0.1199, 5.1266, 0.5578, and 1.4586 Wh/kg from 35% KOH/BBC, 0.01 M MnO_2/35% KOH BBC, 0.1 M MnO_2/35% KOH BBC, and 0.2 M MnO_2/35% KOH BBC respectively was obtained as shown in Appendix. the same biochar weight used for electrode preparation shown that 0.01 M MnO_2/35% KOH BBC stored more energy in comparison with the others. The higher energy density from 0.01 M MnO_2/35% KOH BBC favors the electron transportation inside the electrodes and ion transportation in the porous channels within the electrodes and at the electrode-electrolyte

interface. The lower energy density of 35% KOH/BBC, 0.1 M MnO_2/35% KOH BBC and 0.2 M MnO_2/35% KOH BBC than in 0.01 M MnO_2/35% results in slow ion diffusion and high viscosity and poor kinetics in the electrolyte. The energy density of the electrode can be increased by using other composites with high conductivity, maximum specific capacitance, and higher surface area as support and other porous carbon materials. The rate of delivery of energy designated by power density is also the determinant of ion movement in a solution/wastewater. From this study, the maximum power density was 14.388, 615.192, 66.936 and 175.032 W/kg from 35% KOH/BBC, 0.01 M MnO_2/35% KOH BBC, 0.1 M MnO_2/35% KOH BBC and 0.2 M MnO_2/35% KOH BBC respectively. The same biochar weight used for electrode preparation showed that 0.01 M MnO_2/35% KOH BBC increased energy/ions movement, facilitating a faster electrochemical feature. As shown in figure 4.19, the higher energy density-power density of 0.01 M MnO_2/35% KOH BBC signifies that 0.01 M MnO_2 is the proportional concentration for maximum energy storage. This result has also been confirmed by specific capacitance, as discussed before. An electrode with a high energy density has a longer run time. In addition to these points, it tells the well-designed MnO_2/35% KOH BBC composite has impressive electrochemical features.

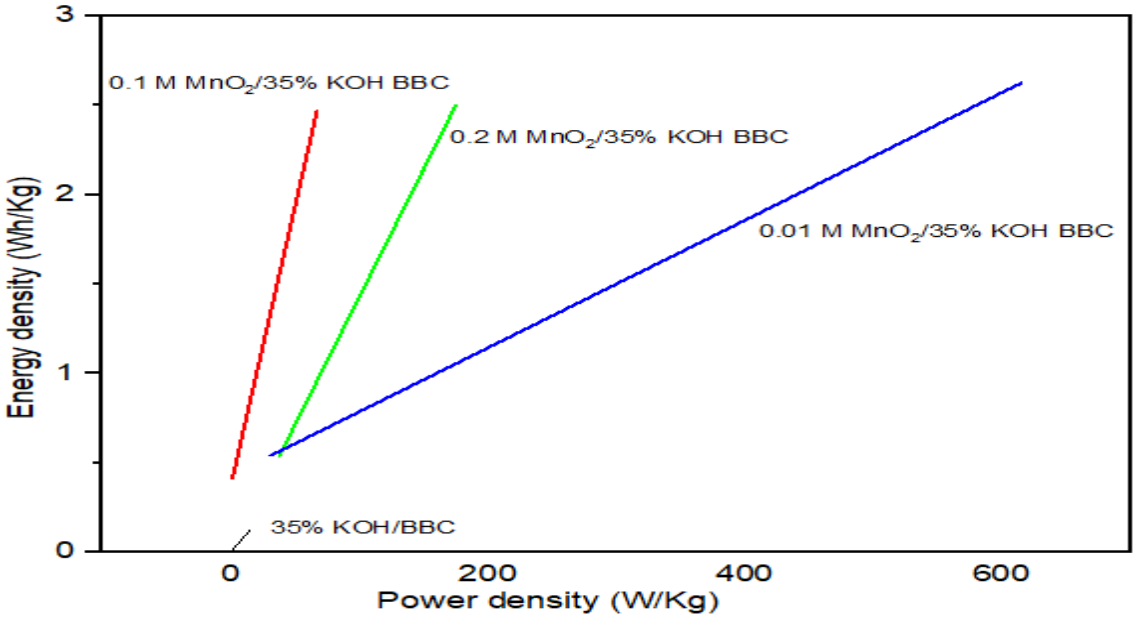

Figure 4-19: Energy density Vs power density profile from CV profile

4.5. Results from Biochar Electrode-Based Electrochemical Treatment

4.5.1. Chemical Oxygen Demand (COD) of Treated wastewater sample

The COD removal findings shown here were obtained after electrochemical treatment of synthetic tannery wastewater with a 0.01 M MnO_2/35 % KOH BBC produced electrode as anode and a Cu electrode as cathode material in a two-electrode configuration. The oxidation part's bio char-based electrode has remarkable removal efficiency. With an initial COD concentration of 3000 mg/L, an applied voltage of 10 V, an initial COD concentration feed of 75 mL for treatment, 4.25 cm^2 total surface areas of electrodes, and a 2 hour treatment time, Figures 4.20 and 4.21 displays COD removal efficiency. The COD value drops from 3000 mg/l to 1021.64 mg/L in run one with 1 g/L NaCl electrolyte concentration and 7.06 mA/cm^2 current density, a 65.94% reduction. The COD value declines by 68.92% from 3000 mg/L to 932.41 mg/L in run 3 when the NaCl electrolyte concentration is 1 g/L and the current density is 11.76mA/cm^2. Run 2 eliminate 70.83% of COD from 3000 mg/L to 874.97 mg/L COD concentration using 2 g/L NaCl and 7.06 mA/cm^2 current density. The final treatment conducted at high NaCl concentration (2 g/L) and high current density 11.76 mA/cm^2 compared with the above combination decreases to 703.22 mg/L from 3000 mg/L COD concentration with COD reducing the efficiency of 76.56%. These findings suggest that incorporating biomass-based materials into water treatment applications could lower the cost of operating materials used in other systems as mentioned in the next topic (energy consumption), minimize pollutant release and sludge development, and provide additional benefits. This work's maximum result (76.56%) is at maximum electrolyte concentration; however, it might be higher if more NaCl salt would be used. When the Cl_2 amount in a water sample surpasses 2000 mg/L, the COD reading may be inaccurate (Costa et al., 2010). 2 g of NaCl in 1-liter water contains 1440 mg/l of COD, which will pass 2000 mg/L when increased to 3 g NaCl and this will interfere the COD determination. For runs one, two, three, and four, the treated synthetic wastewater has a pH of 7.10, 7.07, 7.08, and 7.08, respectively, confirming the neutral wastewater sample. The role of NaCl as an electrolyte increased the conductivity of the process to move ions towards their opposite charges to reduce the concentration of complex ions. The effect can be seen in run 1, 2 and run 3, 4, when the NaCl salt is increased the removal efficiency for COD. It also works in case of current density increment, means of increasing the ion movement.

The increased COD reduction is attributed to the hydroxyl radical-mediated oxidation of organic molecules. Because of the excellent adsorption property of this generated electrode material, hydroxyl radicals are mostly adsorbed on the prepared anode electrode surface. The addition of the composite to the biochar electrode results in a greater adsorption property. The higher the specific capacitance obtained through CV analysis, the greater the removal efficiency. As shown in the literature (Abera, 2020) illustrated the reaction mechanisms of the redox reaction using NaCl electrolytes. When the current density is low, it takes a long time to eliminate the contaminants. The creation of an increased amount of OH group in the solution was attributable to increasing the current density from 7.06 to 11.76mA/cm^2 to accelerate decontamination. The generation of OH radicals through oxidation is done when a potential is applied to the anode electrode. In addition the generation from potential used to the electrode, biochars forms OH radicals to participate in the electrochemical combined with adsorption process. The presence of NaCl helps in generating H^+ reactive components by the interaction of H_2O and Cl_2. Hyperchloreous acid (HOCl) generated from the above reaction also forms reactive H^+. MnO_2 coated biochar anode (MOx) when reacting with H_2O forms reactive radicals MOx(OH) and H^+. These reactive radicals are the active participant in pollutant mitigation from wastewater sample.

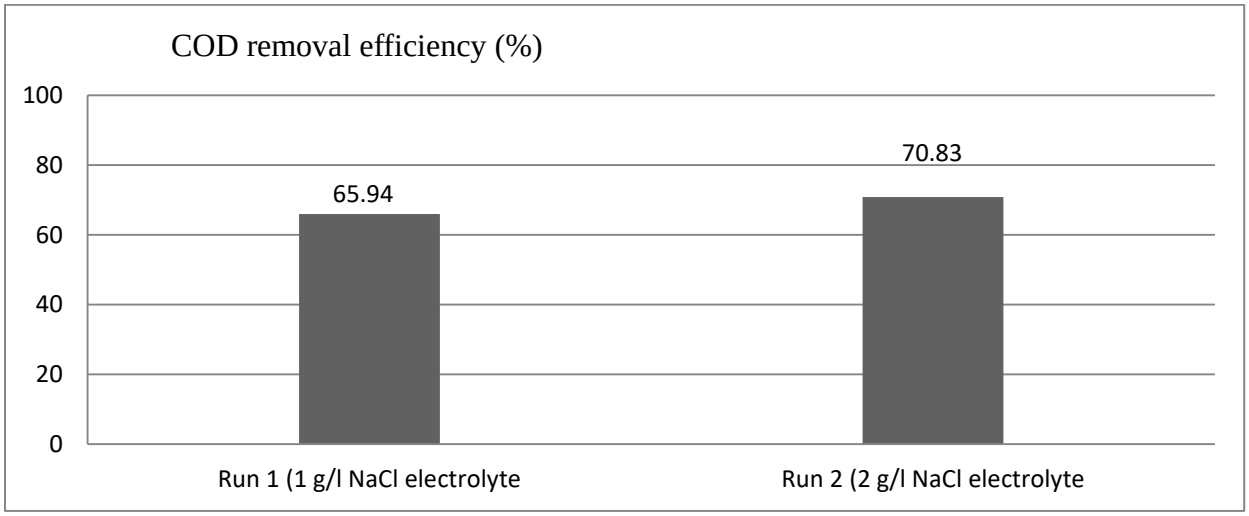

Figure 4-20: COD removal at different electrolyte concentrations at a constant low current density (7.06mA/cm^2)

In the case of the bamboo biochar adsorption section, the COD removal effectiveness is comparable to previous efforts. (Hata et al., 2015) Reported a COD removal rate of 42% utilizing

bamboo biochar as an adsorbent, which is significantly lower than any of the runs performed in this study with the same treatment duration. According to the (Ahmad & Hameed, 2009) report, wastewater using bamboo biochar adsorbent has 75.21% COD after 10 hours. From this, it can be said that the bamboo biochar electrode has greater removal effectiveness while using less biochar and taking less time to be applicable for real wastewater decontamination. One cause could be the introduction of MnO_2, which aids the redox reaction by creating capacitive electrode materials. The genuine image of what is obtained in the treatment is that MnO_2 increased the specific capacitance after its addition. Incomplete decontamination could be caused by a low electrolyte concentration, a short reaction time, inadequate MnO_2 incorporation with biochar, or an undetected reaction inside the reactor.

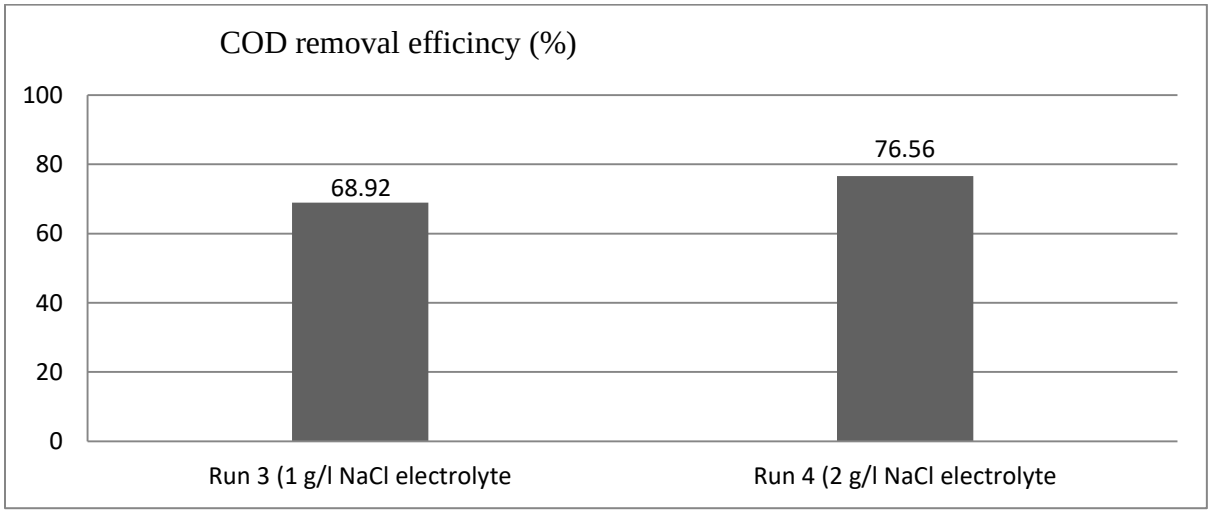

Figure 4-21: COD removal at different electrolyte concentrations at a constant high current density (11.76mA/cm^2)

4.5.2. Energy Consumption Determination

As illustrated in Tables 4.2 and 4.3, the amount of energy consumed for each treatment is reported. Low electrolyte concentration and high current density resulted in the highest energy consumption (6.43 kWh), while low current density and high electrolyte concentration resulted in the lowest energy consumption (3.76 kWh). The reason behind this is that the addition of NaCl reduces power usage due to an increase in conductivity. (Sundarapandiyan et al., 2010) Discussed that when the concentration of electrolytes gets increased the redox reaction performance increases due to the ions participation will evolve at a higher edge. Energy consumption was 5.79 kWh with the highest COD reduction attained at greater current density

and electrolyte content. Due to partial electrical energy heating and increased energy consumption, high current density wastes energy. Increased current density supplies, especially at low electrolyte concentration, result in higher energy usage. It is supported by (Sundarapandiyan et al., 2010) that increasing electrolyte concentration increases the conductivity of wastewater, meaning decreasing the cell potential. The amount of energy required decreases as the cell potential decreases. When we return to this topic, consider runs 3 and 4, which have lower and higher salt concentrations, but both have high current density. When NaCl concentrations are increased from 1 g/L to 2 g/L with maximum COD removal, the energy required for treatment drops from 6.43 kWh to 5.79 kWh. This also works with lower current density supplies at runs 1 and 2, resulting in a reduction in energy consumption from 4.04 kWh to 3.76 kWh with the same salt increments, as well as a higher COD reduction at the lower energy need. This indicates that the energy consumption can be reduced by adjusting the NaCl concentration or making a more capacitive biochar-based electrode.

Table 4-2: Energy consumption at low current density (7.06mA/cm^2) with varying electrolyte concentration.

Run	Current density (mA/cm^2)	Electrolyte concentration (NaCl g/L)	Energy consumption (kWh/kg)
1.	7.06	1	4.04
2.	7.06	2	3.76

The porous carbon material derived from MnO_2 coated bamboo biochar as electrode material makes it applicable in electrochemical systems because of its maximum pollutant removal efficiency with lower energy consumption.

Table 4-3: Energy consumption at high current density (11.76mA/cm^2) with varying electrolyte concentration.

Run	Current density (mA/cm^2)	Electrolyte concentration (NaCl g/L)	Energy consumption (kWh/kg)
3.	11.76	1	6.43
4.	11.76	2	5.79

CHAPTER FIVE

5. CONCLUSION AND RECOMMENDATION

5.1. Conclusion

Starting with the industrial revolution, wastewater has become a global vital concern, intending to transform agriculture's dominant economic structure into an industrial-based economy while simultaneously releasing dangerous toxins. In recent years, biomass-based solutions have been used to minimize and eliminate hazardous components found in these effluents. As a response, this research focuses on developing a modified bamboo biochar-based electrode as an anode material for electrochemical treatment of COD of synthetic wastewater. The effect of chemical activator (KOH, NaOH, H_2SO_4, and H_3PO_4), the percentage composition of activators (30%, 35%, and 40%), carbonization temperature (400, 600, and 900 ^oC), and carbonization time (30, 60, and 90 minutes) has been performed when producing bamboo biochar. A biochar yield of 29.28% and 27.51% from 35% KOH and 30% KOH activated bamboo activated at 600 ^oC for 60 minutes, respectively, has been recorded from the above combination. This illustrates KOH is the most effective activator in forming pores and initiating biomasses for carbonization. Based on biochar yield both 35% KOH/BBC and 30% KOH/BBC, inactivated biochar was selected to make a composite with MnO_2 separately for comparison. 0.01 M MnO_2 was synthesized from a 1:3 of 0.01 M $MnSO_4.H_2O$ to 0.01 M $KMnO_4$ with 0.01 M of NaOH and 2 g of biochar in 80 mL distilled water calcined at 200 ^oC. Bamboo biochar from 35% KOH activation shows better MnO_2 formation on the surface of the biochar identified from FTIR, XRD, and SEM analysis.

As a result of their interesting characteristics, 35% KOH BBC and MnO_2/35% KOH BBC were used to synthesize biochar-based electrodes. In addition to 0.01 M, 0.1 M, and 0.2 M of MnO_2 coatings were performed to check the manganese effect on the electrode characteristics. After the slurry was loaded into a cylindrically molded material, an electrode was made using a Cu current collector, chlorinated rudder binder, and toluene solvent. The electrode performance was checked by cyclic voltammetry, which revealed that the 0.01 M MnO_2 coated biochar electrode performed better electrochemically. The electrode had a rectangular-like form, a larger integrated area, and the highest capacitance. Due to the manganese inclusion with the biochar possess a

large surface area and the greatest specific capacitance was around 75 F/g. A maximum energy density of 5.1266 Wh/kg and power density of 615.192 W/kg was also achieved in 0.01 M MnO_2/35% KOH BBC-based electrode. MnO_2 coated biochar electrode showing maximum electrochemical performance was obtained in removing pollutants in synthetic wastewater by electrochemical mechanism. A maximum COD removal of 76.56% was achieved at 11.76 mA/cm^2 current density and 2 g/L salt concentration after 2 hour treatment. When manganese dioxide is added to activate bamboo biochar, it increases the removal efficiency and reduces longer electrolysis time. The combined action of biochar, the introduction of MnO_2, and the effect of parameters from the electrochemical system result in decreased energy usage. Overall, the electrochemical approach combined with coated biochar can be considered an appealing alternative that can be successfully implemented for synthetic wastewater treatment, specifically COD, according to this study.

5.2. Recommendation

Based on the results of the present study, the following recommendations are forwarded;

- The effect of activation and carbonization parameters is impartial in finding maximum biochar yield other than the effects discussed here. Parameters like heating rate, pyrolysis mediums, i.e. microwave reactors, should be considered.
- The incorporation of transitional metal oxides for better performance may differ with various biochar sources, preparation conditions, target application ensures an effort.
- It is imperative to mention that further research is deemed necessary to increase the specific capacity of biochar electrodes through the optimization of capacitive metal and transitional metal oxides for owning better electrochemical performance.
- For better biochar electrode, electrode properties like galvanostatic charge/discharge test, electrochemical impedance spectroscopy, and cyclic stability requires deep analysis.
- The effect of pH, initial concentration effluents, electrolyte concentration, synthetic wastewater makeup, current density, contact time others needed to be investigated when testing such technologies in synthetic wastewater to prefer for real samples.
- Based on the applicability of biochar-based electrodes for synthetic wastewater treatment, further studies in real wastewater samples and other industrial and municipal effluents should be practical.

Reference

Abera, M. (2020). Treatment of Tannery Soaking Wastewater Using Advanced Electro Oxidation. Http://hdl.handle.net/123. http://hdl.handle.net

Agnieszka Kapałka, Helmut Baltruschat, and C. C. (2011). Electrochemical Oxidation ofOrganic Compounds Induced by Electro-Generated Free Hydroxyl Radicals on BDD Electrodes. June. https://doi.org/10.1002/9781118062364.ch10

Ahmad, A. A., & Hameed, B. H. (2009). Reduction of COD and color of dyeing effluent from a cotton textile mill by adsorption onto bamboo-based activated carbon. Journal of Hazardous Materials, 172(2–3), 1538–1543. https://doi.org/10.1016/j.jhazmat.2009.08.025

Ahmad, A. A., & Hameed, B. H. (2010). Effect of preparation conditions of activated carbon from bamboo waste for real textile wastewater. Journal of Hazardous Materials, 173(1–3), 487–493. https://doi.org/10.1016/j.jhazmat.2009.08.111

Alemu, T., Mekonnen, A., & Leta, S. (2019). Integrated tannery wastewater treatment for effluent reuse for irrigation: Encouraging water efficiency and sustainable development in developing countries. Journal of Water Process Engineering, 30(November 2017), 100514.

Ambaye, T. G., Vaccari, M., van Hullebusch, E. D., Amrane, A., & Rtimi, S. (2021). Mechanisms and adsorption capacities of biochar for the removal of organic and inorganic pollutants from industrial wastewater. International Journal of Environmental Science and Technology, 18(10), 3273–3294. https://doi.org/10.1007/s13762-020-03060-w

Aouni, A., Fersi, C., Ben Sik Ali, M., & Dhahbi, M. (2009). Treatment of textile wastewater by a hybrid electrocoagulation/nanofiltration process. Journal of Hazardous Materials, 168(2–3), 868–874. https://doi.org/10.1016/j.jhazmat.2009.02.112

Armynah, B., Tahir, D., Tandilayuk, M., Djafar, Z., & Piarah, W. H. (2019). Potentials of Biochars Derived from Bamboo Leaf Biomass as Energy Sources: Effect of Temperature and Time of Heating. International Journal of Biomaterials, 2019, 12–18.

Asaithambi, P., Govindarajan, R., Yesuf, M. B., & Alemayehu, E. (2020). Removal of color, COD and determination of power consumption from landfill leachate wastewater using an

electrochemical advanced oxidation processes. Separation and Purification Technology, 233(April 2019), 115935. https://doi.org/10.1016/j.seppur.2019.115935

Ashish Chauhan, R. K. (2015). Screening the Effect of Ultrasonic Wave on Effluent Treatment. Journal of Bioremediation & Biodegradation, 06(03), 6–10.

Bakhtiari, A., Berberashvili, T., & Kervalishvili, P. (2017). Water Treatment Improvement by Ultrasonic Approach. American Journal of Condensed Matter Physics, 7(4), 81–86.

Bashir, M. J. K., Isa, M. H., Kutty, S. R. M., Awang, Z. Bin, Aziz, H. A., Mohajeri, S., & Farooqi, I. H. (2009). Landfill leachate treatment by electrochemical oxidation. Waste Management, 29(9), 2534–2541. https://doi.org/10.1016/j.wasman.2009.05.004

Bhagawan, D., Chandan, V., Srilatha, K., Shankaraiah, G., Rani, M. Y., & Himabindu, V. (2018). Industrial wastewater treatment using electrochemical process. IOP Conference Series: Earth and Environmental Science, 191(1).

Birhanie, M., Leta, S., & Khan, M. M. (2017). Treatment of Tannery Wastewater to Remove Hazardous Pollutants by Scoria (Volcanic ash) a Low cost Adsorbent. International Journal of Environment, Agriculture and Biotechnology, 2(6), 2841–2849.

Bosnic, M., Buljan, J., Daniels, R. P. (2000). Pollutants in tannery effluents. United Nations Industrial Development Organization, August, 26. https://leatherpanel.org/sites/default/files/publications-attachments/pollutants in tannery effluents.pdf

Chaplin, B. P. (2014). Critical review of electrochemical advanced oxidation processes for water treatment applications. Environmental Sciences: Processes and Impacts, 16(6), 1182–1203.

Chen, Haixiu, Xue, H., Liu, J., Li, Z., & Hou, Y. (2019). Research on COD detection method based on UV-Vis spectroscopy. November 2019, 41. https://doi.org/10.1117/12.2548522

Chen, Hao, Liu, D., Shen, Z., Bao, B., Zhao, S., & Wu, L. (2015). Functional Biomass Carbons with Hierarchical Porous Structure for Supercapacitor Electrode Materials. Electrochimica Acta, 180, 241–251. https://doi.org/10.1016/j.electacta.2015.08.133

Chen, Hui, Hu, H., Han, F., Liu, J., Zhang, Y., & Zheng, Y. (2020). CoMoO4/bamboo charcoal hybrid material for high-energy-density and high cycling stability supercapacitors. Dalton Transactions, 49(31), 10799–10807. https://doi.org/10.1039/d0dt00147c

Chen, W., Gong, M., Li, K., Xia, M., Chen, Z., Xiao, H., Fang, Y., Chen, Y., Yang, H., & Chen, H. (2020). Insight into KOH activation mechanism during biomass pyrolysis: Chemical reactions between O-containing groups and KOH. Applied Energy, 278(June), 115730.

Chen, W., Yang, H., Chen, Y., Chen, X., Fang, Y., & Chen, H. (2016). Biomass pyrolysis for nitrogen-containing liquid chemicals and nitrogen-doped carbon materials. Journal of Analytical and Applied Pyrolysis, 120, 186–193. https://doi.org/10.1016/j.jaap.2016.05.004

Cheng, B. H., Zeng, R. J., & Jiang, H. (2017). Recent developments of post-modification of biochar for electrochemical energy storage. Bioresource Technology, 246, 224–233.

Cheng, F., & Li, X. (2018). Preparation and application of biochar-based catalysts for biofuel production. Catalysts, 8(9), 1–35. https://doi.org/10.3390/catal8090346

Cheng, Y., Hao, Z., Hao, C., Deng, Y., Li, X., Li, K., & Zhao, Y. (2019). A review of modification of carbon electrode material in capacitive deionization. RSC Advances, 9(42), 24401–24419. https://doi.org/10.1039/c9ra04426d

Costa, C. R., Montilla, F., Morallón, E., & Olivi, P. (2010). Electrochemical oxidation of synthetic tannery wastewater in chloride-free aqueous media. Journal of Hazardous Materials, 180(1–3), 429–435. https://doi.org/10.1016/j.jhazmat.2010.04.048

Deepa, A., Prakash, P., & Mishra, B. K. (2021). Performance of biochar-based filtration bed for the removal of Cr(VI) from pre-treated synthetic tannery wastewater. Environmental Technology (United Kingdom), 42(2), 257–269.

Dehkhoda, A. M. (2016). Development and characterization of activated biochar as electrode material for capacitive deionization. In Revista Brasileira de Ergonomia (Vol. 9, Issue August).https://www.infodesign.org.br/infodesign/article/view/355%0Ahttp://www.abergo.org.br/revista/index.php/ae/article/view/731%0Ahttp://www.abergo.org.br/revista/index.php/ae/article/view/269%0Ahttp://www.abergo.org.br/revista/index.php/ae/article/view/106

Demir, M., Ashourirad, B., Mugumya, J. H., Saraswat, S. K., El-Kaderi, H. M., & Gupta, R. B. (2018). Nitrogen and oxygen dual-doped porous carbons prepared from pea protein as electrode materials for high performance supercapacitors. International Journal of Hydrogen Energy, 43(40), 18549–18558. https://doi.org/10.1016/j.ijhydene.2018.03.220

Du, Z., Tian, W., Qiao, K., Zhao, J., Wang, L., Xie, W., Chu, M., & Song, T. (2020). Improved chlorine and chromium ion removal from leather processing wastewater by biocharcoal-based capacitive deionization. Separation and Purification Technology, 233(September 2019), 116024. https://doi.org/10.1016/j.seppur.2019.116024

Elisadiki, J., & King'ondu, C. K. (2020). Performance of ion intercalation materials in capacitive deionization/electrochemical deionization: A review. Journal of Electroanalytical Chemistry, 878, 114588. https://doi.org/10.1016/j.jelechem.2020.114588

Frolova, L., & Kharytonov, M. (2019). Synthesis of Magnetic Biochar for Efficient Removal of Cr(III) Cations from the Aqueous Medium. Advances in Materials Science and Engineering, 2019. https://doi.org/10.1155/2019/2187132

Fujishige, M., Yoshida, I., Toya, Y., Banba, Y., Oshida, K. ichi, Tanaka, Y. suke, Dulyaseree, P., Wongwiriyapan, W., & Takeuchi, K. (2017). Preparation of activated carbon from bamboo-cellulose fiber and its use for EDLC electrode material. Journal of Environmental Chemical Engineering, 5(2), 1801–1808. https://doi.org/10.1016/j.jece.2017.03.011

G/cherkos, B. (2019). Addis Ababa Institute of Technology School of Chemical and Bio Engineering Chromium Removal from Tannery Wastewater using Calcinated Eggshells as an Adsorbent : A Case study of Ethiopian Tannery Share. July.

Gao, T., Glerup, M., Krumeich, F., Nesper, R., Fjellvâg, H., & Norby, P. (2008). Microstructures and spectroscopic properties of cryptomelane-type manganese dioxide nanofibers. Journal of Physical Chemistry C, 112(34), 13134–13140. https://doi.org/10.1021/jp804924f

Genawi, N. M., Ibrahim, M. H., El-Naas, M. H., & Alshaik, A. E. (2020). Chromium removal from tannery wastewater by electrocoagulation: Optimization and sludge characterization. Water (Switzerland), 12(5). https://doi.org/10.3390/W12051374

Gezahegn, S. (2020). Wood and Bamboo Biochars and Their Application in Soils and Biocomposites Wood and Bamboo Biochars and Their Application in Soils and Biocomposites.

Ghani, W. A. W. A. K., Fernandez, P. S., Halele, M. Q., Sobri, S., & Jasni, J. (2016). Physical and electrochemical characterization of Palm Kernel Shell Biochar (PKSB) as supercapacitor. MATEC Web of Conferences, 62.

Gide, A. (1967). Some Organic Solvents, Resin Monomers and Related Compounds, Pigments and Occupational Exposures in Paint Manufacture and Painting. Angewandte Chemie International Edition, 6(11), 951–952., 5–24.

Halilovic, N., Krdzalic, E., Basic, A., Dacic, M., Avdic, N., Halilovic, N., Krdzalic, E., Basic, A., Dacic, M., & Avdic, N. (2017). Electrochemical treatment of leather industry wastewater. Glasnik Hemicara I Tehnologa Bosne I Hercegovine, 48, 15–20.

Hashem, M. A., Hasan, M., Momen, M. A., Payel, S., & Nur-A-Tomal, M. S. (2020). Water hyacinth biochar for trivalent chromium adsorption from tannery wastewater. Environmental and Sustainability Indicators, 5(February), 100022.

Hata, M., Amano, Y., Thiravetyan, P., & Machida, M. (2015). Preparation of Bamboo Chars and Bamboo Activated Carbons to Remove Color and COD from Ink Wastewater. Water Environment Research, 88(1), 87–96. https://doi.org/10.2175/106143015x14362865227751

Hoislbauer, C., & Siebenhofer, M. (2008). Photochemical and electrochemical advanced oxidation processes. AIChE Annual Meeting, Conference Proceedings, 58(3), 256–275.

Isarain-Chávez, E., De La Rosa, C., Godínez, L. A., Brillas, E., & Peralta-Hernández, J. M. (2014). Comparative study of electrochemical water treatment processes for a tannery wastewater effluent. Journal of Electroanalytical Chemistry, 713, 62–69.

Ivanova, N., Gugleva, V., Dobreva, M., Pehlivanov, I., Stefanov, S., & Andonova, V. (2016). Valorization of Glucose-Based Wastewater Through Production of Hydrogen, Volatile Fatty Acids and Alcohols. Intech, i(tourism), 13.

Jiang, H., Liu, J., & Han, W. (2016). The status and developments of leather solid waste

treatment: A mini-review. Waste Management and Research, 34(5), 399–408.

Jiang, J., Zhang, L., Wang, X., Holm, N., Rajagopalan, K., Chen, F., & Ma, S. (2013). Highly ordered macroporous woody biochar with ultra-high carbon content as supercapacitor electrodes. Electrochimica Acta, 113, 481–489.

Jothi Ramalingam, R., Sivachidambaram, M., Vijaya, J. J., Al-Lohedan, H. A., & Muthumareeswaran, M. R. (2020). Synthesis of porous activated carbon powder formation from fruit peel and cow dung waste for modified electrode fabrication and application. Biomass and Bioenergy, 142(May), 105800.

Karnan, M., Subramani, K., Srividhya, P. K., & Sathish, M. (2017). Electrochemical Studies on Corncob Derived Activated Porous Carbon for Supercapacitors Application in Aqueous and Non-aqueous Electrolytes. Electrochimica Acta, 228, 586–596.

Korpe, S., Bethi, B., Sonawane, S. H., & Jayakumar, K. V. (2019). Tannery wastewater treatment by cavitation combined with advanced oxidation process (AOP). Ultrasonics Sonochemistry, 59(August), 104723. https://doi.org/10.1016/j.ultsonch.2019.104723

Kouchachvili, L., & Entchev, E. (2017). Ag/Biochar composite for supercapacitor electrodes. Materials Today Energy, 6, 136–145. https://doi.org/10.1016/j.mtener.2017.09.002

Kuppusamy, S., Jayaraman, N., Jagannathan, M., Kadarkarai, M., & Aruliah, R. (2017). Electrochemical decolorization and biodegradation of tannery effluent for reduction of chemical oxygen demand and hexavalent chromium. Journal of Water Process Engineering, 20(September), 22–28. https://doi.org/10.1016/j.jwpe.2017.09.008

Lam, S. S., Azwar, E., Peng, W., Tsang, Y. F., Ma, N. L., Liu, Z., Park, Y. K., & Kwon, E. E. (2019). Cleaner conversion of bamboo into carbon fibre with favourable physicochemical and capacitive properties via microwave pyrolysis combining with solvent extraction and chemical impregnation. Journal of Cleaner Production, 236, 1–11.

Lema, Y. A. (2021). Formulation of chlorinated rubber-based traffic marking paint and evaluation of Nano-TiO2 / AMRS composite for its photocatalytic self- cleaning property By Yordanos Abay Lema Office of Graduate Studies Adama Science and Technology

University Adama , Eth. Astu.

Li, J., & Wu, Q. (2015). Water bamboo-derived porous carbons as electrode materials for supercapacitors. New Journal of Chemistry, 39(5), 3859–3864.

Liu, C., Wang, W., Wu, R., Liu, Y., Lin, X., Kan, H., & Zheng, Y. (2020). Preparation of Acid-And Alkali-Modified Biochar for Removal of Methylene Blue Pigment. ACS Omega, 5(48), 30906–30922. https://doi.org/10.1021/acsomega.0c03688

Liu, Q. S., Zheng, T., Wang, P., & Guo, L. (2010). Preparation and characterization of activated carbon from bamboo by microwave-induced phosphoric acid activation. Industrial Crops and Products, 31(2), 233–238. https://doi.org/10.1016/j.indcrop.2009.10.011

Lyu, H., Yu, Z., Gao, B., He, F., Huang, J., Tang, J., & Shen, B. (2019). Ball-milled biochar for alternative carbon electrode. Environmental Science and Pollution Research.

Lyu, L., Seong, K. D., Ko, D., Choi, J., Lee, C., Hwang, T., Cho, Y., Jin, X., Zhang, W., Pang, H., & Piao, Y. (2019). Recent development of biomass-derived carbons and composites as electrode materials for supercapacitors. Materials Chemistry Frontiers, 3(12), 2543–2570.

Mahanim, S. M. A., Wan Asma, I., Rafidah, J., Puad, E., & Shaharuddin, H. (2011). Production of activated carbon from industrial bamboo wastes. Journal of Tropical Forest Science, 23(4), 417–424.

Mani Tripathi, S., & Chaurasia, S. R. (2020). Detection of Chromium in surface and groundwater and its bio-absorption using bio-wastes and vermiculite. Engineering Science and Technology, an International Journal, 23(5), 1153–1161.

Mohammed, K., & Dabai, A. I. (2020). Chromium Removal From Tannery Wastewater: a Review. PLATFORM-A Journal of Science & Technology, 3(1), 63–71.

Mohd Abdah, M. A. A., Azman, N. H. N., Kulandaivalu, S., & Sulaiman, Y. (2020). Review of the use of transition-metal-oxide and conducting polymer-based fibres for high-performance supercapacitors. Materials and Design, 186, 108199.

Moradi, M., Vasseghian, Y., Khataee, A., Kobya, M., Arabzade, H., & Dragoi, E. N. (2020).

Service life and stability of electrodes applied in electrochemical advanced oxidation processes: A comprehensive review. Journal of Industrial and Engineering Chemistry, 87, 18–39. https://doi.org/10.1016/j.jiec.2020.03.038

Norakmalah Mohd Zawawi, Fazlena Hamzah, Mahanim Sarif, Shareena Fairuz Abdul Manaf, A. I. (2017). Characterization of Activated Carbon Using Chemical Activation Via Microwave Ultrasonic System. Malaysian Journal of Analytical Science, 21(1), 159–165.

Nur-E-Alam, M., Abu Sayid Mia, M., & Mafizur Rahman, M. (2017). COD Removal of Tannery Wastewater using Spent Tea Leaves. International Research Journal of Engineering and Technology, 11, 2395–56.

Palagonia, M. S., Erinmwingbovo, C., Brogioli, D., & La Mantia, F. (2019). Comparison between cyclic voltammetry and differential charge plots from galvanostatic cycling. Journal of Electroanalytical Chemistry, 847(November 2020), 113170.

Parthasarathy, P., Mackey, H. R., Mariyam, S., Zuhara, S., Al-Ansari, T., & McKay, G. (2021). Char Products From Bamboo Waste Pyrolysis and Acid Activation. Frontiers in Materials, 7(January), 1–15. https://doi.org/10.3389/fmats.2020.624791

Pokharel, A. (2020). Application of Biochar for Efficient Municipal Wastewater. August.

Priyono, S., Sari, T. D., Ramlan, Subhan, A., & Prihandoko, B. (2019). Effect of polymer binders on the electrochemical Performance of Al-doped lithium titanate electrode. Journal of Physics: Conference Series, 1282(1). https://doi.org/10.1088/1742-6596/1282/1/012056

Qanytah, Syamsu, K., Fahma, F., & Pari, G. (2020). Characterization of ball-milled sago pith waste-based activated carbon treated with KOH and KMnO4 as activating agent. IOP Conference Series: Materials Science and Engineering, 935(1).

Qu, W. H., Xu, Y. Y., Lu, A. H., Zhang, X. Q., & Li, W. C. (2015). Converting biowaste corncob residue into high value added porous carbon for supercapacitor electrodes. Bioresource Technology, 189, 285–291. https://doi.org/10.1016/j.biortech.2015.04.005

Rafique, M. I., Usman, A. R. A., Ahmad, M., & Al-Wabel, M. I. (2021). Immobilization and mitigation of chromium toxicity in aqueous solutions and tannery waste-contaminated soil

using biochar and polymer-modified biochar. Chemosphere, 266.

Rahman, M. Z., Edvinsson, T., & Kwong, P. (2020). Biochar for electrochemical applications. Current Opinion in Green and Sustainable Chemistry, 23, 25–30.

Saad, M. J., Sajab, M. S., Busu, W. N. W., Misran, S., Zakaria, S., Chin, S. X., & Chia, C. H. (2020). Comparative adsorption mechanism of rice straw activated carbon activated with NaOH and KOH. Sains Malaysiana, 49(11), 2721–2734.

Sahoo, S. S., Vijay, V. K., Chandra, R., & Kumar, H. (2021). Production and characterization of biochar produced from slow pyrolysis of pigeon pea stalk and bamboo. Cleaner Engineering and Technology, 3(April), 100101. https://doi.org/10.1016/j.clet.2021.100101

Sajjadi, B., Chen, W. Y., & Egiebor, N. O. (2019). A comprehensive review on physical activation of biochar for energy and environmental applications. Reviews in Chemical Engineering, 35(6), 735–776. https://doi.org/10.1515/revce-2017-0113

Sawalha, H., Al-Jabari, M., Elhamouz, A., Abusafa, A., & Rene, E. R. (2020). Tannery wastewater treatment and resource recovery options. In Waste Biorefinery. Elsevier B.V.

Senthil, C., & Lee, C. W. (2021). Biomass-derived biochar materials as sustainable energy sources for electrochemical energy storage devices. Renewable and Sustainable Energy Reviews, 137(xxxx), 110464. https://doi.org/10.1016/j.rser.2020.110464

Seow, T. W., Lim, C. K., Nor, M. H. M., Mubarak, M. F. M., Lam, C. Y., Yahya, A., & Zaharah Ibrahim. (2012). Review on wastewater treatment technologies Jayashree Dhote. International Journal of Engineering Research & Technology (IJERT), 1(5), 1–10.

Shrestha, L. K., Adhikari, L., Shrestha, R. G., Adhikari, M. P., Adhikari, R., Hill, J. P., Pradhananga, R. R., & Ariga, K. (2016). Nanoporous carbon materials with enhanced supercapacitance performance and non-aromatic chemical sensing with C1/C2 alcohol discrimination. Science and Technology of Advanced Materials, 17(1), 483–492.

Sivagami, K., Sakthivel, K. P., & Nambi, I. M. (2018). Advanced oxidation processes for the treatment of tannery wastewater. Journal of Environmental Chemical Engineering, 6(3), 3656–3663. https://doi.org/10.1016/j.jece.2017.06.004

Sofyan, N., Alfaruq, S., Zulfia, A., & Subhan, A. (2018). Characteristics of Vanadium Doped And Bamboo Activated Carbon Coated LiFePO4 And Its Performance For Lithium Ion Battery Cathode. Jurnal Kimia Dan Kemasan, 40(1), 9.

Subramanian, V., Zhu, H., Vajtai, R., Ajayan, P. M., & Wei, B. (2005). Hydrothermal synthesis and pseudocapacitance properties of MnO 2 nanostructures. Journal of Physical Chemistry B, 109(43), 20207–20214. https://doi.org/10.1021/jp0543330

Sudarsan, J. S., & Srihari, V. (2019). Evaluation of adsorption capacity of biochar mixed substrate to treat tannery wastewater by constructed wetland. AIP Conference Proceedings, 2112(June 2019). https://doi.org/10.1063/1.5112361

Sundarapandiyan, S., Chandrasekar, R., Ramanaiah, B., Krishnan, S., & Saravanan, P. (2010). Electrochemical oxidation and reuse of tannery saline wastewater. Journal of Hazardous Materials, 180(1–3), 197–203. https://doi.org/10.1016/j.jhazmat.2010.04.013

Tsubota, T., Ishimoto, K., Kumagai, S., Kamimura, S., & Ohno, T. (2018). Cascade use of bamboo as raw material for several high value products: production of xylo-oligosaccharide and activated carbon for EDLC electrode from bamboo. Journal of Porous Materials, 25(5), 1541–1549. https://doi.org/10.1007/s10934-018-0567-6

Viglašová, E., Galamboš, M., Danková, Z., Krivosudský, L., Lengauer, C. L., Hood-Nowotny, R., Soja, G., Rompel, A., Matík, M., & Briančin, J. (2018). Production, characterization and adsorption studies of bamboo-based biochar/montmorillonite composite for nitrate removal. Waste Management, 79, 385–394. https://doi.org/10.1016/j.wasman.2018.08.005

Wen, Y., Qin, T., Wang, Z., Jiang, X., Peng, S., Zhang, J., Hou, J., Huang, F., He, D., & Cao, G. (2017). Self-supported binder-free carbon fibers/MnO2electrodes derived from disposable bamboo chopsticks for high-performance supercapacitors. Journal of Alloys and Compounds, 699, 126–135. https://doi.org/10.1016/j.jallcom.2016.12.330

Xu, B., Chen, Y., Wei, G., Cao, G., Zhang, H., & Yang, Y. (2010). Activated carbon with high capacitance prepared by NaOH activation for supercapacitors. Materials Chemistry and Physics, 124(1), 504–509. https://doi.org/10.1016/j.matchemphys.2010.07.002

Xu, R., Deng, S., Wang, W., Schenk, J., & Wang, F. (2020). Structural Features and Combustion Behaviour of Waste Bamboo Chopstick Chars Pyrolysed at Different Temperatures. Bioenergy Research, 13(2), 439–451. https://doi.org/10.1007/s12155-020-10095-x

Yaqub, A., Ajab, H., Isa, M. H., Jusoh, H., Junaid, M., & Farooq, R. (2012). Effect of ultrasound and electrode material on electrochemical treatment of industrial wastewater. Journal of New Materials for Electrochemical Systems, 15(4), 289–292.

Yuan, C., Lin, H., Lu, H., Xing, E., Zhang, Y., & Xie, B. (2016). Synthesis of hierarchically porous MnO2/rice husks derived carbon composite as high-performance electrode material for supercapacitors. Applied Energy, 178, 260–268.

Zhang, C., He, D., Ma, J., Tang, W., & Waite, T. D. (2018). Faradaic reactions in capacitive deionization (CDI) - problems and possibilities: A review. Water Research, 128, 314–330. https://doi.org/10.1016/j.watres.2017.10.024

Zhang, Guoxiang, Chen, H., Liu, W., Wang, D., & Wang, Y. (2016). Bamboo chopsticks-derived porous carbon microtubes/flakes composites for supercapacitor electrodes. Materials Letters, 185(September 2016), 359–362.

Zhang, Guoxiong, Chen, Y., Chen, Y., & Guo, H. (2018). Activated biomass carbon made from bamboo as electrode material for supercapacitors. Materials Research Bulletin, 102(March), 391–398. https://doi.org/10.1016/j.materresbull.2018.03.006

Zhang, Ji, Gao, J., Chen, Y., Hao, X., & Jin, X. (2017). Characterization, preparation, and reaction mechanism of hemp stem based activated carbon. Results in Physics, 7, 1628–1633. https://doi.org/10.1016/j.rinp.2017.04.028

Zhang, Jubing, Zhong, Z., Shen, D., Zhao, J., Zhang, H., Yang, M., & Li, W. (2011). Preparation of bamboo-based activated carbon and its application in direct carbon fuel cells. Energy and Fuels, 25(5), 2187–2193. https://doi.org/10.1021/ef200161c

Zhang, W., Zou, Y., Yu, C., & Zhong, W. (2019). Nitrogen-enriched compact biochar-based electrode materials for supercapacitors with ultrahigh volumetric performance. Journal of Power Sources, 439(August), 227067. https://doi.org/10.1016/j.jpowsour.2019.227067

Zhang, Yimeng, Ma, Z., Zhang, Q., Wang, J., Ma, Q., Yang, Y., Luo, X., & Zhang, W. (2017). Comparison of the physicochemical characteristics of bio-char pyrolyzed from moso bamboo and rice husk with different pyrolysis temperatures. BioResources, 12(3), 4652–4669. https://doi.org/10.15376/biores.12.3.4652-4669

Zhang, Yong, Yao, Q. Q., Gao, H. L., Zhang, L. Sen, Wang, L. Z., Zhang, A. Q., Song, Y. H., & Wang, L. X. (2015). Synthesis and electrochemical performance of MnO2/BC composite as active materials for supercapacitors. Journal of Analytical and Applied Pyrolysis, 111, 233–237. https://doi.org/10.1016/j.jaap.2014.11.002

Zhao, C., & Chen, W. (2019). A review for tannery wastewater treatment: some thoughts under stricter discharge requirements. Environmental Science and Pollution Research, 26(25), 26102–26111. https://doi.org/10.1007/s11356-019-05699-6

Zhao, N., Zhao, C., Lv, Y., Zhang, W., Du, Y., Hao, Z., & Zhang, J. (2017). Adsorption and coadsorption mechanisms of Cr(VI) and organic contaminants on H3PO4 treated biochar. Chemosphere, 186(Vi), 422–429. https://doi.org/10.1016/j.chemosphere.2017.08.016

Zhao, W., Luo, L., Wang, H., & Fan, M. (2016). Synthesis of Bamboo-Based Activated Carbons with Super-High Specific Surface Area for Hydrogen Storage. BioResources, 12(1), 1246–1262. https://doi.org/10.15376/biores.12.1.1246-1262

Zhao, X., Wei, H., Zhao, H., Wang, Y., & Tang, N. (2020). Electrode materials for capacitive deionization: A review. Journal of Electroanalytical Chemistry, 873, 1327–1356.

Zhou, X., Li, L., Dong, S., Chen, X., Han, P., Xu, H., Yao, J., Shang, C., Liu, Z., & Cui, G. (2012). A renewable bamboo carbon/polyaniline composite for a high-performance supercapacitor electrode material. Journal of Solid State Electrochemistry, 16(3), 877–882.

Zhuang, R., Xu, L., Li, D., Muhammad, N., Chen, J., Yu, Y., Song, H., Ma, J., Liu, X., & Chen, X. (2020). Acidified bamboo-derived activated carbon/manganese dioxide composite as a high-performance electrode material for capacitive deionization. International Journal of Electrochemical Science, 15, 3104–3118. https://doi.org/10.20964/2020.04.23

Appendixes

Appendix A: Bamboo biochar yield calculation

Table 1: Biochar yield from bamboo at different effect combination

Biochar	Trial 1			Trial 2			Average biochar yield (%) = (trial 1 + trial 2)/2
	Bamboo before carbonized (g)	Bamboo after carbonized (g)	Biochar yield (%)	Bamboo before carbonized (g)	Bamboo after carbonized (g)	Biochar yield (%)	
BBC @ 600 ^{o}C - 60 min	20.08	4.54	**22.62**	20.04	4.71	23.52	23.07
30% KOH/BBC @ 600 ^{o}C – 60 min	20.06	5.54	27.63	19.95	5.46	27.39	27.51
30% H_2SO_4/BBC @ 600 ^{o}C – 60 min	20.08	4.48	22.31	19.98	4.61	23.07	22.69
30% NaOH/BBC @ 600 ^{o}C – 60 min	20.03	3.77	18.83	20.05	3.65	18.23	18.53
30% H_3PO_4/BBC @ 600 ^{o}C – 60 min	20.09	5.26	26.21	20.02	5.07	25.35	25.78
35% KOH/BBC @ 600 ^{o}C – 60 min	20.11	5.83	29.03	20.07	5.92	29.53	29.28
40% KOH/BBC @ 600 ^{o}C – 60 min	19.97	4.95	24.80	20.03	4.90	24.48	24.64
35% KOH/BBC @ 400 ^{o}C – 60 min	20.02	5.26	26.27	19.96	5.19	26.01	26.14
35% KOH/BBC @ 900 ^{o}C – 60 min	20.03	3.35	16.75	19.99	3.69	18.45	17.6
35% KOH/BBC @ 600 ^{o}C-30 minute	19.99	5.36	26.84	20.03	5.43	27.12	26.98
35% KOH/BBC @ 600 ^{o}C-90 minute	20.04	5.22	26.06	20.07	5.30	26.42	26.24

Biochar yield from bamboo is obtained from equation 3.2 as follow:

$$\text{Yield (\%)} = \left(\frac{\text{Wc}}{\text{Wo}}\right) * 100 \qquad 3.2$$

Where Wc is the dry weight of final activated carbon and Wo is the dry weight of the initial sample. For instance, yield = (4.54/20.08)*100% = **22.62%**.

Appendix B: Synthetic wastewater preparation

Wastewater sample targeting to contain specified COD content was prepared from glucose.

$C_6H_{12}O_6$ (glucose) + $6O_2$ (oxygen) $\longrightarrow$ $6CO_2 + 6H_2O$

(6-mole O_2/1 mole of glucose)*(32 g/mole O_2/180 g/mole of glucose) = 1.067 g O_2/g glucose. Since Mw of glucose ($C_6H_{12}O_6$) = 180 g/mole. In 1 g of glucose,

1000 mg glucose * 1.067 g O_2/g glucose = 1067 mg O_2/g glucose.

1 g glucose = 1067 mg O_2/g glucose

X = 3000 mg O_2/g glucose,

X = (1 g glucose * 3000 mg O_2/g glucose)/1067 mg O_2/g glucose,

X = 2.811 g glucose. This implies that to prepare synthetic wastewater containing 3000 mg O_2/g glucose we have to dissolve 2.811 g of glucose in 1 liter of distilled water.

Appendix C: Specific capacitance (C) calculation

Table 2: Specific capacitance of electrode obtained from cyclic voltammetry.

Electrode material	**Specific capacitance (F/g) at a scan rate of () mV/s**					
	5	**10**	**20**	**50**	**100**	**200**
35% KOH/BBC	**1.761**	0.301	0.092	0.038	0.067	0.053
0.01 M MnO_2/35% KOH BBC	75.281	68.624	45.546	37.346	12.708	3.823
0.1 M MnO_2/35% KOH BBC	8.192	4.935	3.088	1.071	0.422	0.145
0.2 M MnO_2/35% KOH BBC	16.523	16.781	21.419	8.413	6.995	4.597

Using equation 3.5, to determine the specific capacitance of electrode

$$C = \frac{2I\Delta t}{m\Delta V} \qquad 3.5$$

To drive an equation that fits with the integrated surface area of the CV profile, divide equation 3.5 by t both sides:

$$C = \frac{\frac{2 * I * t}{t}}{\frac{mV}{t}} \text{ which leads to } C = \frac{2 * I}{m * k}$$

Also can be written as $I = \frac{C*m*k}{2}$, Where V/t designated by k is scan rate of CV,

In the CV curve, the current changes by changing the potential from V_1 to V_2. Therefore, the above equation can be written in its integral form as:

$$\int_{v1}^{v2} I(v)dv = \int_{v1}^{v2} \left(\frac{C * m * k}{2}\right) dv$$

The left-hand side term from the above equation represents the area of the CV curve. Therefore the above equation can be written as:

$$\text{Area} = \int_{v1}^{v2} \left(\frac{C * m * k}{2}\right) dv$$

For the specific material, the value of C, m, and k is constant. Therefore the above equation can be solved as:

$$\text{Area}(A) = (V_2 - V_1) * \frac{C * m * k}{2}$$

The CV curve contains three areas. The larger area up to the upper curves from the baseline denoted by A_1 is given by: $A_1 = (V_2 - V_1) * \frac{C*m*k}{2}$

While the area from the base line up to the bottom curve designated by A_2 is given as:

$$A_2 = (V_1 - V_2) * \frac{C * m * k}{2}$$

The area of the between two curves, area of the CV profile is denoted by A is given as:

$$A = A_1 - A_2 = [(V_2 - V_1) * \frac{C * m * k}{2} - (V_1 - V_2) * \frac{C * m * k}{2}]$$

$$A = [(V_2 - V_1) * \frac{C * m * k}{2} + (V_2 - V_1) * \frac{C * m * k}{2}]$$

$A = [(V_2 - V_1) * C * m * k]$, written as $C = \frac{A}{(V_2 - V_1)*m*k}$ Or,

$$C = \frac{A}{m * k * (V_2 - V_1)}$$

It is the total specific capacitance of electrode material from the CV curve. Where C is the specific capacitance in F/g, A is the area inside the CV curve having units in an arbitrary unit, k, the scan rate of CV in mV/s, and (V_2-V_1) is the potential window of CV (total voltage range).

From the CV characterization V_2 = 0.7 V, V_1 = 0.0 V i.e. V_2-V_1 = 0.7 V, k = 5 mV/s (in case a calculation done here), m = 1.981 x10^3 mg and A is below screen shot from CV profile for 35% KOH BBC at 5 mV/s scan rate and A = 0.01221 from CV area for 35% KOH/BBC.

$$C = \frac{A}{m * k * (V_2 - V_1)} = \frac{0.01221}{5 * 1.981 * 10^3 * 0.7} = \mathbf{1.761\ F/g}$$

Table 3: Energy density from cyclic voltammetry

Electrode material	**The energy density (Wh/kg) at a scan rate of () mV/s**					
	5	**10**	**20**	**50**	**100**	**200**
35% KOH/BBC	**0.1199**	0.0205	0.0062	0.0026	0.0045	0.0036
0.01 M MnO_2/35% KOH BBC	5.1266	4.6733	3.1016	2.5432	0.8654	0.2603
0.1 M MnO_2/35% KOH BBC	0.5578	0.3360	0.2103	0.0729	0.0287	0.0098
0.2 M MnO_2/35% KOH BBC	1.1252	1.1427	1.4586	0.5729	0.4763	0.3130

Energy density was determined using the equation below,

$$E = \left(\frac{C * 1000}{2 * 3600}\right) * (\Delta V)^2 \qquad 3.6$$

For example, $E = \left(\frac{1.761*1000}{2*3600}\right) * (0.7)^2 = \mathbf{0.1199}\ \frac{\mathbf{Wh}}{\mathbf{kg}}$ Where, ΔV = 0.7 V, C = 1.761 F/g.

Table 4: Power density from cyclic voltammetry

Electrode material	**Power density (W/kg) at a scan rate of () mV/s**					
	5	**10**	**20**	**50**	**100**	**200**
35% KOH/BBC	**14.388**	2.460	0.744	0.312	0.540	0.432
0.01 M MnO_2/35% KOH BBC	615.192	560.796	372.192	305.184	103.848	31.236
0.1 M MnO_2/35% KOH BBC	66.936	40.320	25.236	8.748	3.444	1.176
0.2 M MnO_2/35% KOH BBC	135.024	137.124	175.032	68.748	57.156	37.560

The power density was determined using,

$$P = \frac{E * 3600}{\Delta t} \qquad 3.7$$

For example, $P = \frac{0.1199*3600}{30} = \mathbf{14.388}\ \frac{\mathbf{W}}{\mathbf{kg}}$ Where, Δt = 30 minute, E = 0.1199 Wh/kg.

Appendix D: COD and energy consumption calculation

Table 5: COD concentration and energy consumption determinations

Run	Initial COD concentration (mg/L)	COD concentration after treatment (mg/L)	COD removal (%)	Energy consumption (kWh/kg COD)
1.	3000	**1021.64**	**65.945**	**4.04**
2.	3000	932.41	68.919	6.43
3.	3000	874.97	70.834	3.76
4.	3000	703.22	76.559	5.79

To find COD concentration using the equation:

$$\text{COD}\left(\frac{\text{mg}}{\text{L}}\right) = \frac{(\text{A} - \text{B}) * \text{N} * 8 * 1000}{\text{V}} \qquad 3.8$$

Where A = Volume of FAS required to achieve endpoint of titration for blank sample, B = Volume of FAS required to achieve endpoint of titration for wastewater sample, N = Normality of FAS, 8 = Milli equivalent weight of O_2 (1 mL of 1 N $K_2Cr_2O_7$ = 8 mg O_2), 1000 = Volume of solution in mL, and V = Volume of wastewater sample (ml).

For instance for run 1:

A = 15.64 ml, B = 2.87 ml, N = 0.1 and volume of sample = 10 mL.

$\text{COD}\left(\frac{\text{mg}}{\text{L}}\right) = \frac{(15.64-2.87)*0.1*8*1000}{10} = \mathbf{1021.64}\,\frac{\mathbf{mg}}{\mathbf{L}}$, And the energy consumption for a process is determined using:

$$\text{Energy consumption} = \frac{\frac{\text{tVA}}{\text{Sv}}}{\frac{10^3}{\left(\frac{\Delta\text{COD}}{10^6}\right)}}\left(\frac{\text{KWh}}{\text{m}^3}\right) \qquad 3.9$$

Where t is the time of electrolysis in (hour), V is the average cell voltage in (Volt), A is current I (ampere), Sv is sample volume in liters and ΔCOD is the difference in COD in time t in mg/L. For example for run 1: t = 2 hour, V = 10 V, A = 0.03 A, Sv = 10 ml and$\Delta\text{COD} = 3000 - 1021.64 = 1974.36$ mg/L, Energy consumption $= \left(\frac{\frac{(2*10*0.03)}{10}}{\frac{\frac{1000}{1978.36}}{10^6}}\right) = \mathbf{4.04}\ \left(\frac{\mathbf{kWh}}{\mathbf{m}^3}\right)$